REPORT DOCUMENTATION PAGE

AFRL-SR-BL-TR-00-

0643

1. AGENCY USE ONLY (*Leave Blank*)	2. REPORT DATE 28 AUG 2000	3. REPORT TYPE AND DATES COVERED FINAL 01 AUG 1999 – 30 JUN 2000

4. TITLE AND SUBTITLE	5. FUNDING NUMBERS
NONLINEAR REDUCED ORDER MODELING OF LIMIT CYCLE OSCILLATIONS OF AIRCRAFT WINGS STTR PHASE I, FINAL REPORT	C F49620-99-C-0050 PE 65502F PR STTR

6. AUTHOR(S)
P. C. Chen and D. D. Liu, ZONA Technology;
K.C. Hall and E.H. Dowell, Duke University

7. PERFORMING ORGANIZATION NAME(S) AND ADDRESS(ES)	8. PERFORMING ORGANIZATION REPORT NUMBER
ZONA Technology, Inc. 7434 E. Stetson Drive, Suite 205 Scottsdale, AZ 85251 Tel 480-945-9988 / Fax 480-945-6588	ZONA 00-30

9. SPONSORING/MONITORING AGENCY(S) AND ADDRESS(ES)	10. SPONSORING/MONITORING AGENCY REPORT NUMBER
USAF, AFMC Air Force Office of Scientific Research 801 N. Randolph Street, Room 732 Arlington, VA 22203-1977 POC: Major Brian Sanders, 703-696-7259	

11. SUPPLEMENTARY NOTES

12a. DISTRIBUTION/AVAILABILITY STATEMENT	12b. DISTRIBUTION CODE
APPROVED FOR PUBLIC RELEASE; DISTRIBUTION UNLIMITED.	

13. ABSTRACT (*Maximum 200 words*)

This report documents the result of an STTR Phase I on the investigation in the use of a frequency–domain proper orthogonal decomposition (POD) / Reduced Order Modeling (ROM) procedure in conjunction with a harmonic balance nonlinear scheme for the prediction and analysis of limit cycle oscillations (LCO) of aircraft wings/airfoils in transonic flow regimes. A significant milestone has been reached in the phase I work. With four related cases studied in LCO and flutter, the result is that our frequency-domain method producing highly accurate solutions over a wide ranges of frequencies is potentially two orders of magnitude faster than conventional time-marching methods for determining LCO and flutter. Further, the nonlinear solutions of LCO using harmonic balance scheme in frequency domain could lead to a much better understanding of LCO physics. Its adopted Eigen-mode solution methodology on the other hand should render it readily acceptable by the industry practice. Finally, STTR Phase II plan is presented in detail. Commercialization strategy of the would-be production-ready software is also discussed.

20001205 049

14. SUBJECT TERMS		15. NUMBER OF PAGES
STTR Report, Limit Cycle Oscillation, Flutter, Proper Orthogonal Decomposition Technique, Reduced Order Modeling, Frequency Domain, Harmonic Balance, Eigen Mode Solution		16. PRICE CODE

17. SECURITY CLASSIFICATION OF REPORT UNCLASSIFIED	18. SECURITY CLASSIFICATION OF THIS PAGE UNCLASSIFIED	19. SECURITY CLASSIFICATION OF THIS ABSTRACT UNCLASSIFIED	20. LIMITATION OF ABSTRACT SAR

DTIC QUALITY INSPECTED 4

AF-TR-00-

NONLINEAR REDUCED ORDER MODELING OF LIMIT CYCLE OSCILLATIONS OF AIRCRAFT WINGS

P.C. CHEN
D.D. LIU
ZONA Technology, Inc.
7430 E. Stetson Drive, Ste. 205
Scottsdale, AZ 85251-3540

K.C. HALL
E.H. DOWELL
Duke University
Department of Mechanical Engineering and Materials Science
Durham, NC 27708

AUGUST 2000

STTR PHASE I FINAL REPORT FOR THE PERIOD AUGUST 1999 - JUNE 2000

FOREWORD

TABLE OF CONTENTS

LIST OF FIGURES

LIST OF FIGURES (cont.)

LIST OF FIGURES (cont.)

LIST OF TABLES

CHAPTER 1

INTRODUCTION

1.1   Limit Cycle Oscillations

Limit Cycle Oscillations (LCO) are known to occur on various operational vehicles. In particular, LCO has been a prevalent aeroelastic problem on several current fighter aircraft. It usually occurs for aircraft with external stores throughout the transonic flight regime (Refs 1-4). Complicated by the aircraft-store system, its mechanism still remains to be fully understood. Meanwhile, a business jet wing LCO was also reported recently (Refs 5,6). This has been a serious concern since there are few analytical techniques available for LCO prediction and an insufficient understanding of its physics.

LCO can be characterized as sustained periodic oscillations which neither increase or decrease in amplitude over time for a given flight condition. Using an s-domain unsteady aerodynamic model of the aircraft and stores, Chen, Sarhaddi and Liu (Ref 7) have shown that wing/store LCO can be a post-flutter phenomenon whenever the flutter mode contains low unstable damping. This type of flutter mode is called a *"hump mode"*. Since the aircraft structure usually contains structural nonlinearity, such as friction damping, this amplitude-dependent friction damping can suppress the growth of amplitude, thus resulting in a steady state oscillation. This is known as the nonlinear structural damping (NSD) model of the wing/store LCO. Although not thoroughly proven through tests or numerical simulations, results of the NSD show excellent correlation with flight test LCO data of F-16 throughout subsonic and transonic Mach numbers.

On the other hand, other researchers, notably Cunningham and Meijer (Ref 8) believe that the wing/store LCO is due largely to transonic shock oscillation and shock induced flow separation. This is called the Transonic Shock/Separation (TSS) model. Edwards has suggested the TSS model and viscous effects are two major factors that cause transonic LCO for wings. He also has studied the shock buffet phenomenon in addition to transonic LCO (Ref 9). It should be noted, however, that there is no conflict between the NSD model and the TSS model in that both physical effects may contribute to LCO.

Note that the method in Ref 7 used a damping correlation technique for LCO-onset prediction, whereas that of Ref 8 is a semi-empirical method that requires steady and unsteady data input from wind tunnel measurement.

1.2   LCO Prediction Methods

Recent renewed interest in LCO is motivated by the need to better predict and understand fighter LCO and also by the rapid advent of CFD methodology in aeroelasticity. Currently, there are two potential computational approaches for LCO prediction/investigation: *the time-marching approach* using a high-level CFD code such as CFL3D (Ref 10) developed and supported by NASA/Langley, and *the Frequency-Domain POD/ROM EigenMode approach* (Ref 11) originated by Dowell and Hall of Duke University. The former is a conventional time-domain

CFD method whereas the latter is a frequency-domain CFD method using aerodynamic eigenmodes.

For nearly twenty years, the aerospace industry has been lacking of a viable, efficient CFD method for transonic flutter applications. The time-marching CFD unfortunately remain inefficient as a practical tool.

Under an AFOSR/STTR Phase I contract, ZONA has recently conducted a feasibility study on the simulation of transonic LCO for a supercritical NLR7301 airfoil using the CFL3D/Navier-Stokes code. It was found that the time-marching LCO solution is turbulence-model dependent and time-step sensitive. One LCO solution case typically would take 96 hours on a 1GHz CPU computer.

Earlier work of Bendiksen (Ref 12) and recent work of Sheta et al (Ref 13) also used time-marching CFD approach for Euler transonic and N-S incompressible LCO simulations, respectively. Based on the cases studied by ZONA, the time-marching Euler simulation of a transonic LCO requires one half of the computing time required of a Navier-Stokes simulation, due to the reduction in grid points. The computing time required for incompressible Navier-Stokes LCO simulation is about two orders of magnitude less than a transonic Navier-Stokes LCO simulation, due to the absence of transonic nonlinearity, thus allowing much coarser time steps and a reduction in subiterations. For transonic Navier-Stokes simulation of LCO, the requirements in time steps, grid, subiterations, etc., become much more stringent, resulting in days of computing time for one LCO case. This leads to the conclusion that, if a *transonic Navier-Stokes simulation* were demanded, a time-marching approach would be computationally inefficient as a viable approach for realistic 3D transonic LCO prediction/investigations.

On the other hand, the Frequency-Domain POD/ROM (Proper Orthogonal Decomposition / Reduced Order Model) method of Duke University is considered a recent breakthrough in the transonic computational aeroelasticity. Within the last five years, the Frequency-Domain POD/ROM method of Dowell and Hall has been proven to be highly efficient and shown to be widely applicable to aeroelastic problems for turbomachinery cascades, control surface freeplay, airfoil/wing flutter and LCO (e.g., Refs 11, 14-16, Hall and Dowell, 3 Papers SDM2001 presented in Appendix A-C of this report). As evidenced by their recent studies, under AFOSR/STTR contract support, *the Frequency-Domain method with the Harmonic Balance scheme is about two-orders of magnitude faster than conventional time-marching methods.*

For example, the 3D Time Linearized code can generate the needed aerodynamic model in one day for a given Mach number and flutter points take less than 1 minute per Mach number on a workstation computer.

1.3   Frequency-Domain POD/ROM EigenMode Approach

Reduced-Order Models (ROM) EigenMode

The eigenmodes of a time-linearized system, which may be thought of as aerodynamic states, were computed and subsequently used to construct computationally efficient, reduced order

2

models of the unsteady flow field. An important advantage of the eigenmode based reduced order modeling technique is that once the eigenmode information has been computed, reduced order models can be constructed and used to calculate the response at different frequencies and mode shapes for almost no additional computational effort. Furthermore, only a very few eigenmodes or states (degrees of freedom) need to be retained in the model to accurately predict the unsteady aerodynamic response, making the method ideally suited for rapid flutter calculation and active control.

The POD Technique

The Proper Orthogonal Decomposition (POD) technique, also known as Karhunen-Loeve (Ref 12) expansions, was originally introduced to determine and model coherent structures in turbulent flow fields. Using the POD approach, one examines a series of "snapshots" of experimental or computational data, each at a different instant in time. These solution snapshots are used to form a small and more compact eigenvalue problem that is solved to determine a set of optimal basis functions for representing the flow field.

Frequency-Domain POD/ROM

Hall, Thomas, and Dowell (Ref 11) developed a frequency-domain form of the POD technique, and applied it to transonic flows about airfoils. In particular, they used a time-linearized CFD analysis to compute unsteady small-disturbance flow solutions for vibrating airfoils in the frequency domain over a range of frequencies. Basis vectors were then extracted from this frequency-domain data set using the POD technique. The resulting basis vectors were then used to construct low degree of freedom reduced-order models of the unsteady flow. Finally, the reduced-order aerodynamic model was combined with a structural dynamic model resulting in a compact, but accurate, flutter model.

Harmonic-Balance Method for Nonlinear LCO (Refs 14, 15)

In conjunction with the frequency-domain POD/ROM method, the harmonic balance (HB) technique can be used in the treatment of nonlinear LCO problems for oscillating wings (with stores). The harmonic balance technique is used to recast the proposed Euler equations into a set of "higher-order" equations of like harmonics. After introducing a pseudo-time term into the harmonic-balance equations so that they may be solved by time marching, these equations are solved by conventional CFD techniques. The method has a number of advantages over the more conventional time domain solutions. Because the solutions are computed in the frequency domain, the time-marching algorithm is only used to converge the solution to steady state. Thus, accelerating techniques, including pseudo time-marching with multi-grid acceleration can be used. Moreover, for problems where "engineering accuracy" is required, the harmonic balance series can be truncated into just a few harmonics. The result is that the proposed harmonic balance method is potentially two-orders of magnitude faster than conventional time-marching methods for determining LCO.

1.4   Merits of the Frequency-Domain Approach

There are several definite advantages of using the frequency-domain approach. First, the frequency-domain harmonic balance method, when applied to high-level equations, can be at least two-orders of magnitude faster than the nonlinear time-domain CFD simulations. Also, this method retains essential nonlinear features in an aeroelastic system, including nonlinear structural stiffness and damping as well as large transonic shock excursions including viscosity. Second, current transonic flutter methods using time-domain/time-marching CFD in conjunction with various versions of the indicial approach (Batina, Silva, Refs 17, 18) are very tedious and computationally expensive and their accuracy usually depends on the indicial motion imposed. By contrast, the frequency-domain formulation of POD/ROM directly solves for convenient aerodynamic mode shapes which can be stored and repeatedly applied for a large range of frequencies; hence, its a much more efficient and accurate method. Third, the frequency-domain approach with an eigenvalue solution method is a familiar practice to the structures/loads and flutter engineers. The proposed method after ZONA's further modification is expected to be well accepted within the industrial environment.

1.5   ZONA Technology's R&D in LCO

In recent years, ZONA has been extensively engaged in the R&D of LCO including its prediction methodology, control and F-16 and F-18 LCO data correlation. ZONA has collaborated closely with Lockheed-Martin/LMTAS and the Seek Eagle office of Eglin AFB on F-16 wing/store LCO investigations. The results including the definition of a NSD model were presented in two AIAA/SDM papers (Refs 7,19, Chen et al, Mignolet et al). Under a recent NAVAIR contract, ZONA also worked closely with team member Boeing/ St Louis on a successful R&D in the reconfigurable adaptive control of the F-18 LCO. (Ref 20, Nam et al). Supported by NASA/Langley, ongoing development of the CFD/CSD interfacing using BEM solver (Refs 21,22, Chen et al) will provide a new spline methodology for tightly coupled aerodynamic-structural interaction for 3D multiple mode LCO studies in Phase II.

1.6   STTR Phase I

In August 1999, the AFOSR awarded an STTR Phase I contract to the ZONA Technology (ZONA) team to *develop innovative computational aeroelasticity methodologies for understanding, predicting and controlling critical nonlinear aerostructural interaction (e.g., LCO/flutter) phenomena.* The ZONA team, consisting of ZONA Technology, Inc. and Duke University (Professors Earl Dowell and Kenneth Hall), has successfully accomplished the STTR Phase I contract. The recent work of Duke University deals with the further generalization of POD/ROM EigenMode method for 2-D/3-D flutter and LCO solutions (Refs 14,15,16).

Under this STTR contract, ZONA has generalized the structural compatible model, provided a 3D flutter solution methodology and conducted a 2D CFD simulation of transonic LCO (Ref 23).

4

1.7 Phase I Achievements

Significant milestones have been reached through the work of Phase I. These are in four related categories. Firstly, the modeling and prediction of flutter and LCO of an airfoil and control surface with structural freeplay in 2D transonic flow has been accomplished. Secondly, the modeling and prediction of flutter and LCO of an airfoil undergoing single degree of freedom pitch motions due to nonlinear aerodynamic effects associated with large (inviscid) shock motions in 2D flow has been achieved. Thirdly, the modeling and prediction of flutter of a 3D flow about an elastic wing has been accomplished. Note that in the latter category, we are modeling the nonlinear static or steady flow effects in the transonic regime even though the aerodynamic model is dynamically linear, i.e., the shock motions are assumed to be proportional to the airfoil motion in this model. And finally, a 2D numerical simulation of the NLR 7301 supercritical airfoil limit cycle oscillations was performed using the time-marching procedure of the CFL3D code. This fourth category of work is to establish benchmarks for the viscous POD/ROM methodology developed in Phase I and to be developed in Phase II.

In Chapters 2-5 we provide a summary of the approach and results obtained in each of these categories. These accomplishments provide a firm foundation on which to build for the Phase II work.

CHAPTER 2

TRANSONIC LIMIT CYCLE OSCILLATION ANALYSIS OF AN AIRFOIL WITH CONTROL SURFACE FREEPLAY

Summary

The transonic flutter and limit cycle oscillations of an airfoil with control surface freeplay have been determined using a new aerodynamic modeling technique that provides greater physical insight and understanding by tracing the true root locus of the corresponding linear aeroelastic system. This in turn enables a very computationally efficient harmonic balance technique to be used in determining the nonlinear limit cycle oscillations.

New physical insights gained include the rapid change in flutter mode that occurs in the transonic Mach number range. This phenomenon has been observed in experiments, but has not been previously predicted theoretically. With respect to LCO, these are the first results available in the transonic range for the configuration studied. The model also predicts significant changes in LCO behavior as a function of Mach number. However, these are as yet unconfirmed by experiments. Up to high subsonic Mach numbers, the flutter and LCO results are similar to those previously found at low Mach numbers.

Introduction

In this work, we will assume the shock motion is sufficiently small such that it is (linearly) proportional to the airfoil motion, e.g., airfoil motions are less than the equivalent of one degree in angle of attack. Using an Euler/CFD-based reduced order aerodynamic model, a thorough study of the flutter boundary with Mach number (M) is first presented in the absence of freeplay. Particularly noteworthy are the rapid changes of flutter modal content in the transonic range. This is attributed in part to the rapid changes of center of pressure location as the mean shock position changes with Mach number. These changes in the modal response content are also found in the limit cycle oscillations (LCO) which are encountered when control surface freeplay is present. Indeed for LCO, the modal content may change at a fixed Mach number when the dynamic pressure or flow density is varied.

Below M=0.80, the LCO and flutter oscillations are qualitatively similar to those previously found at low Mach number where earlier analyses and experiments have been carried out. However, the response behavior in the transonic flow regime is notably different. Of special interest is the occurrence of flutter in a narrow range of Mach number for pitch and flap (control surface) dominated motions. Moreover, beyond a certain high transonic Mach number (after the mean shock position reaches the trailing edge of the airfoil), neither flutter nor limit cycle oscillation occurs.

Significance of LCO

LCO is known to occur on various operational aerospace flight vehicles. This has been a source of serious concern since there are no analysis techniques available that have predicted LCO in an operational aircraft. There have been some semi-empirical techniques developed to correlate with LCO that have been observed in flight, and these are useful for understanding the LCO that has occurred (see Ref 24). However these techniques are not as satisfactory for the design of a new vehicle or the substantial modification of an existing one, e.g., new stores to be carried by an aircraft. In this regard, it should be noted that LCO may be beneficial as well as detrimental. Without the nonlinearities that lead to LCO, the onset of flutter may lead to catastrophic failure of the structure. Hence if we can understand and predict LCO, perhaps we can take advantage of these nonlinearities to shape more favorable responses of the aircraft leading to enhanced safety and performance.

Sources of Nonlinearities

The principal sources of the nonlinearities essential to the LCO are a subject of current debate among the experts in the field. The candidate sources are several:

Fluid
* Shock motions
* Separated flow

Structure
* Free-play
* Geometric, e.g., a nonlinear relationship between strain and displacement
* Material, e.g., dry friction

Also there is a further distinction between a static versus a dynamic nonlinearity. An important example of this is the role of a shock wave in the fluid. If a shock is present, then its creation is the result of a dynamic nonlinear process. However once a steady flow is established, and if the airfoil motion is sufficiently small, then the shock motion will also be small and proportional to the airfoil motion. Hence in this situation, the shock itself represents a nonlinear static (time independent) equilibrium and the motion may be treated as a dynamically linear perturbation about the mean shock position. In most of the following discussion, we assume a dynamically linear model of the shock motion, but also include a structural (dynamic) nonlinearity, i.e., freeplay in the connection of the control surface to the airfoil.

Airfoil with Control Surface Freeplay Model

A sketch of the configuration is shown in Fig 2.1. It is a conventional typical section model except that the spring that attaches the control surface to the airfoil has a nonlinear freeplay. The elastic restoring torque or moment provided by this spring is shown in Fig 2.2 as a function of control surface or flap rotation angle, β. The freeplay angle is δ. Note that when β is less than δ, there is zero restoring torque, while for β greater than δ, the spring stiffness is the nominal value in the absence of freeplay. The freeplay may be thought of as creating a stiffness or (uncoupled)

7

natural frequency of the spring that varies as a function of flap amplitude. This interpretation is shown in Fig 2.3. Here the flap uncoupled natural frequency normalized by the nominal value in the absence of freeplay is shown as a function of flap amplitude, β, normalized by the freeplay angle, δ. Note that given a certain flap amplitude, there is a corresponding "equivalent" flap frequency. Of course for a linear system the control surface or flap frequency would have a fixed value independent of flap amplitude.
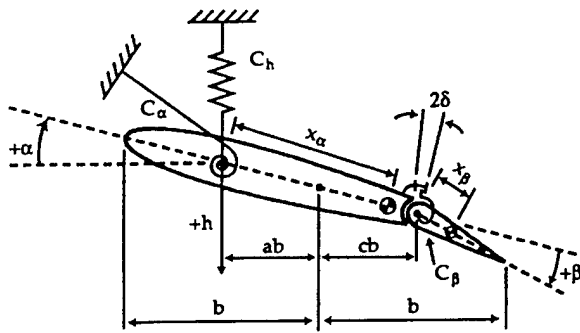
Figure 2.1 Airfoil with Control Surface
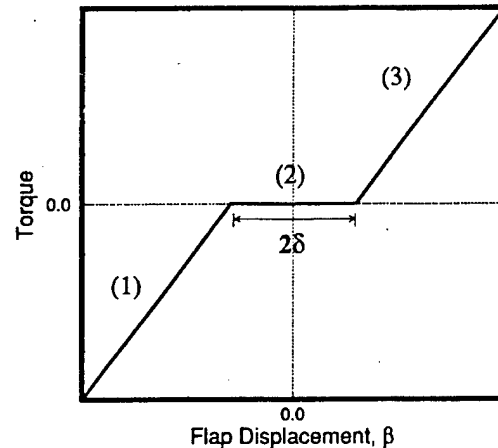
Figure 2.2 Restoring Moment As a Function of Control Surface or Flap Rotation Angle
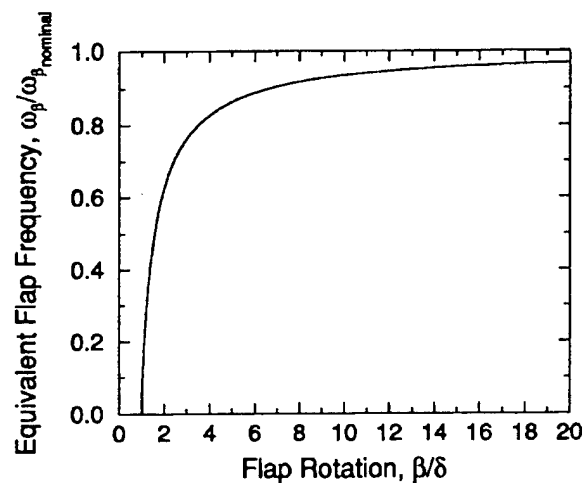
Figure 2.3 Equivalent Nonlinear Flap Frequency Versus Flap Rotation

Thus, conceptually and computationally, one may proceed as follows. First, one determines the neutrally stable motions of the system in the absence of freeplay for various flap frequencies from zero to the nominal value. Then one determines the corresponding neutrally stable nonlinear limit cycle motion, namely the flap amplitude, from Fig 2.3.

This approach has been used successfully at low Mach number and the theoretical results correlated with experiments (see Refs 25, 26).

Computational Fluid Dynamic (CFD) Modeling and its Modal Decomposition

A typical CFD model is very large in terms of the number of equations required to be solved. And this makes such models problematical for aeroelastic (and some other) analyses. For example, the CFD model used in the present work is based upon the Euler equations of fluid mechanics and has a spatial grid of 65 x 97 (6035) mesh points. At each grid point there are four fluid variables to be determined. Thus the CFD model per se has about 25,000 unknowns to be determined by solving 25,000 equations. This is a doable task if the structural motion is known. However if this CFD model is to be combined with a set of structural equations of motion, and solutions are to be found for many combination of structural and fluid parameters, then the calculation using the original CFD model quickly gets out of hand. Thus the search for an alternative approach.

Several semi-empirical methods have been derived to address the computational feasibility issue. These as well as the method to be described and used here are discussed in more depth in Ref 11. Among these methods are variations on the notion of a Padé approximant. The method used here is based upon the observation that virtually all CFD models can be thought of as having a modal composition. The simplest conceptual set of modes is perhaps the fluid or aerodynamic eigenmodes of the CFD model, and these modes have been used successfully in creating reduced order models (ROM) that are computationally and conceptually attractive. See the discussion in Ref 11 and the forthcoming Ref 27.

However it turns out that determining the aerodynamic eigenmodes of a large CFD model is itself a challenging task. Hence a method called Proper Orthogonal Decomposition (POD) is employed here and in (Ref 11).

For the present analysis, 63 POD modes are found from the frequency responses (aerodynamic transfer functions) in flap, pitch and plunge respectively at 21 frequencies at each Mach studied using the original CFD model. Based upon previous experience, one might use an even smaller number of aerodynamic modes than this. However, even with this generous number of modes, the computations described below were all done in a few days. The computational grid used for the CFD model is shown in Fig 2.4.
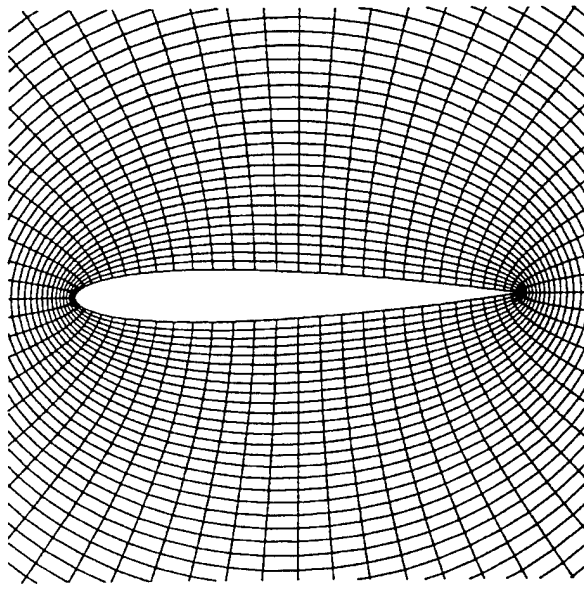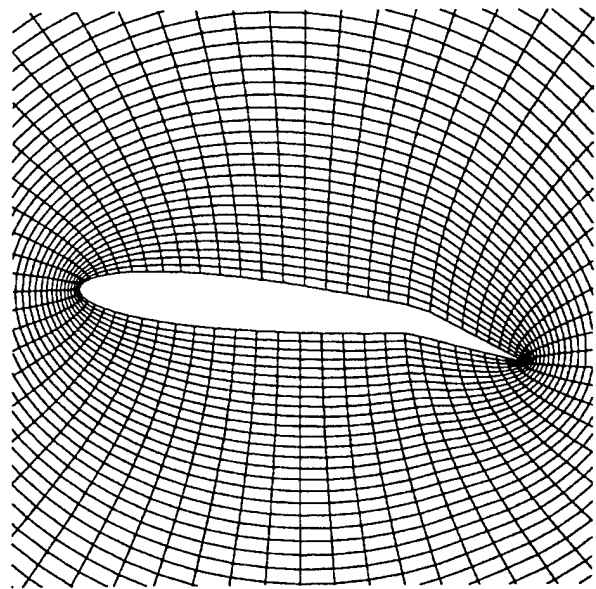
(a) Baseline   **(b) Grid Motion**

Figure 2.4   NACA 0012 Grid: 65 x 97 Computational Nodes, Outer Boundary Radius=15c

Linear Instability (Flutter)

First, consider the flutter behavior for this system in the absence of freeplay. The stability of this system was assessed by constructing a root locus (migration of the true aeroelastic eigenvalues) as a function of the nondimensional airspeed or dynamic pressure for each Mach number. The usual structural and flow parameters are defined in (Refs 24, 25).

A representative root locus result is shown in Fig 2.5 for M=0.80. Root locus results are available for all Mach numbers used to construct the flutter boundary which is shown in Fig 2.6.

Figure 2.5   Aeroelastic System Eigenvalue Root-Loci: M = 0.80, α = 0.0 deg.

Note especially that the "plunge" aeroelastic mode has a root that for low "gain" (or flow velocity or dynamic pressure) moves to the left and becomes more stable. But then as the flow velocity increases, it reverses direction and moves into the right half plane becoming unstable. And then at even higher velocities, it moves back into the left hand plane and becomes stable again. However by then, the pitch mode has moved into the right half plane and become

10

unstable. Hence the aeroelastic system remains unstable once the plunge mode becomes again stable at this velocity and Mach number.

(a) Flutter Speed   (b) Flutter Frequency
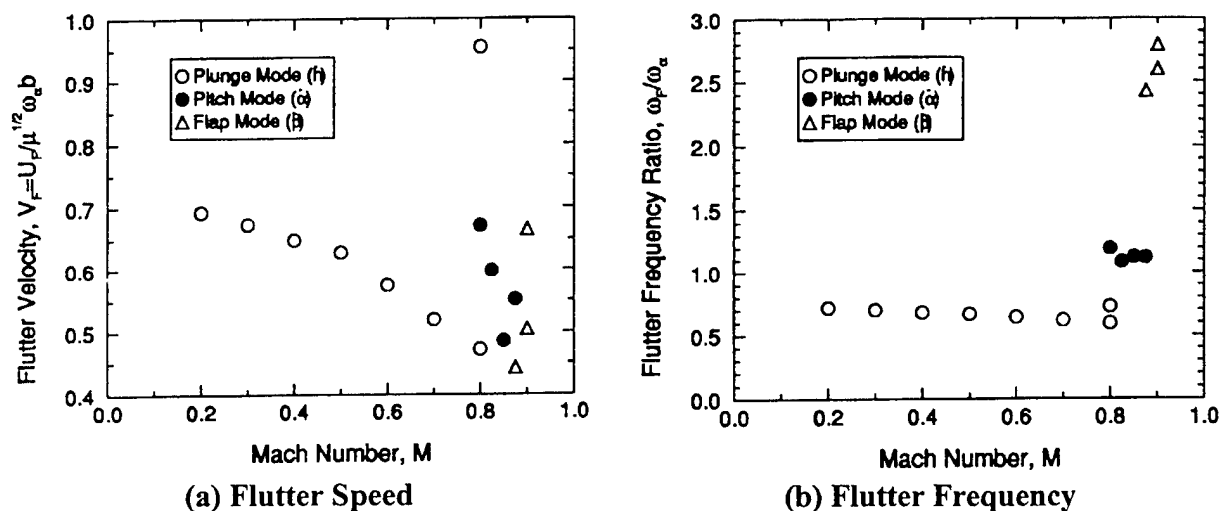
Figure 2.6   Mach Number Flutter Trend: $\alpha = 0.0$ deg.

All the other roots in this figure which appear to originate from near the origin are essentially aerodynamic roots, and these roots all move off into the left half plane indicating they are always stable and increasingly so as the dynamic pressure increases. As the Mach number becomes higher, the most critical root may change. For example, at M=0.85 the pitch root becomes unstable first, and for M=0.90, it is the flap root. At yet higher Mach numbers, no roots become unstable. For brevity these other root loci are omitted here. Taking all of this information from the root loci at various Mach numbers, the flutter boundary trend with Mach number can be determined, and is presented in Fig 2.6.a.

There are several interesting features to this flutter boundary. Up to M=0.80, the root-loci are rather similar, and it is always the plunge root that is critical for flutter. Starting at M=0.80, the pitch root also shows instability, and at M=0.825 and 0.85, it is most critical for flutter. At M=0.875 and 0.90, the flap mode is most critical for flutter, and for M=0.925 to at least M=1.1, no flutter is observed for a non-dimensional flow velocity up to at least one. The corresponding frequencies of the flutter oscillations are shown in Fig 2.6.b. Note that in Fig 2.6.a when two data points are shown for say the plunge root at a fixed Mach number, the lower velocity point is when flutter begins, and the higher velocity point is when the root returns to the stable left half plane and flutter ceases in that root. Note also the narrow range of Mach number where the change in flutter mode occurs. Results of this type have been observed in experiments where they are called "chimneys" (see Ref 28).

Limit Cycle Oscillations

Now the freeplay is added to the model and thus LCO may occur. As is perhaps obvious from physical intuition, when freeplay is added, the stiffness of the control surface freeplay is reduced

11

for small motions. Hence one expects limit cycle oscillations to occur below the flutter boundary, i.e., at flow velocities less than those shown in Fig 2.6.a. Indeed a few moments of reflection may lead one to expect that once the linear flutter boundary shown in Fig 2.6.a is exceeded, then exponentially explosive flutter will occur when the nonlinearity is due to freeplay. That is found to be the case as shown by the present analysis and also by the analysis and experiments of Refs 25 and 26.

The LCO results shown in Fig 2.7 have several interesting features. First of all, the limit cycle amplitude is normalized by the freeplay angle, δ. The theory predicts and experiments agree, (see Ref 26), that when the results are normalized in this manner, they are universal. That is, the limit cycle amplitude is proportional to the freeplay angle. Secondly, for the lowest velocity at which LCO may, a finite disturbance is required to generate LCO at this lowest velocity and for a small velocity range thereafter. LCO's for any disturbance, no matter how small, will only occur when the flutter velocity for a flap natural frequency of zero is exceeded, at a somewhat higher velocity, about 0.22 in Fig 2.7.a. The unstable LCO's, which are shown along with the stable LCO's (those that are observed in an experiment), provide a measure of the level of disturbance required to initiate the LCO at the lower flow velocities.

The results Fig 2.7 are typical until one reaches the higher transonic Mach numbers where linear theory predicts flutter will cease. At the highest Mach number considered here where flutter and LCO may occur, M=0.90, the LCO has a somewhat different character. Again the LCO is first encountered at the minimum velocity at which flutter will occur over the range of flap frequencies. But now the corresponding flap frequency is zero. Moreover, when the flow velocity increases to higher values, there are two stable limit cycles. The nature of the disturbances to the system would determine which of these two LCO would be observed in a wind tunnel experiment or in flight. For brevity, the M=0.9 results are not shown.

(a) LCO Flap Rotation   (b) LCO Frequency Ratio
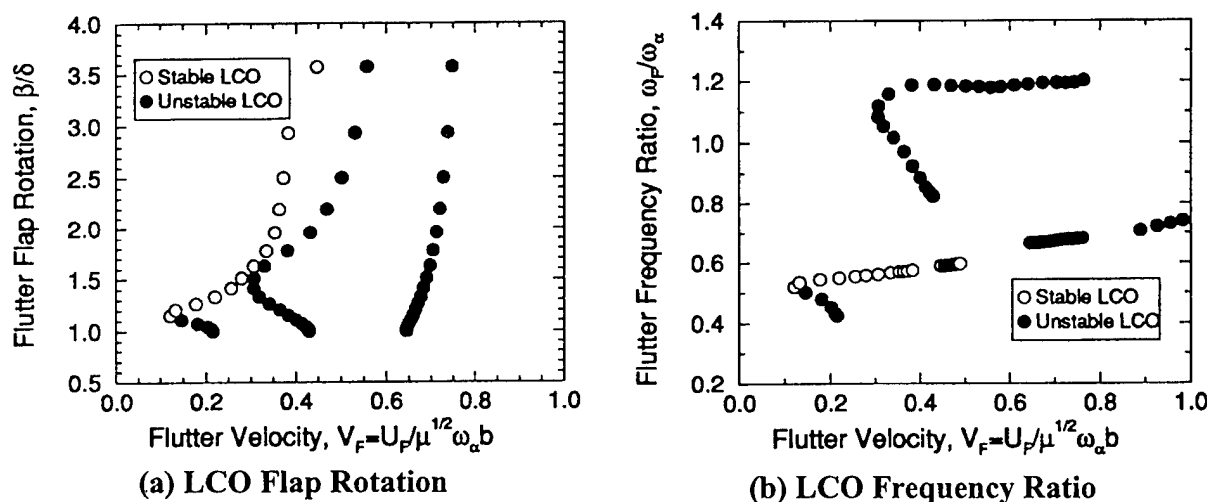
Figure 2.7   Limit Cycle Behavior: M = 0.80, α = 0.0 deg.

For additional details of the work presented in this Chapter, please see the paper (Ref 14) included in Appendix A.

CHAPTER 3

NONLINEAR INVISCID AERODYNAMIC EFFECTS ON TRANSONIC DIVERGENCE, FLUTTER AND LIMIT CYCLE OSCILLATIONS

Summary

Aerodynamic nonlinearities may be give rise to LCO, and these may be either stable (favorable) or unstable(unfavorable). An example of the former is shown here as the nonlinear counterpart of classical linear aeroelastic divergence. An example of the latter is also shown here as the nonlinear counterpart of single-degree-of-freedom pitch flutter. Future work will be directed toward the study of the nonlinear counterpart of classical bending/torsion flutter where similar methods may be used.

Introduction

Limit cycle oscillations (LCO) in aeroelastic systems appear to be more prevalent in transonic flow than in subsonic flow. Hence it has been thought that at least for some configurations the source of the nonlinearity that leads to LCO is in the aerodynamic flow. See Ref 29 and 26 for a discussion of structural nonlinearities relevant to LCO. Thus, we consider the effects of nonlinearities arising from inviscid transonic aerodynamics. The principal physical effect of interest is the relatively large motion of the shock wave as the amplitude of say the pitch motion of the airfoil becomes sufficiently large. This in turn leads to a movement of the center of pressure with amplitude. Hence one expects to see an effect of amplitude on the neutrally stable motions that may occur. Moreover this may lead to limit cycle motions rather than the catastrophic exponentially growing oscillations predicted by time linearized models. The latter models capture the effect of the mean position of the shock and small shock motions about this mean position by assuming the shock motion is dynamically linear, i.e., the shock motion is proportional to the airfoil motion. This is not true for dynamically nonlinear aerodynamic models that allow for larger and more general shock motions including the possible appearance and disappearance of a shock during a cycle of airfoil motion. The latter is our concern here.

We will consider two distinct aeroelastic phenomena, divergence and flutter, and their associated limit cycle oscillations. To keep the discussion focussed on the fundamental physical phenomena, and to ease the interpretation of the inherently complex phenomena, only a single structural degree of freedom will be studied. However the aerodynamic model will be a state-of-the-art computational fluid dynamics (CFD) based upon the Euler equations of nonlinear, rotational inviscid aerodynamic theory.

Here we emphasize that the solution technique is for a large system of ordinary differential equations in time, which represents the time variation of the fluid unknowns at each spatial grid point in the CFD model. The unknowns are four in number at each grid point for a two-dimensional Euler flow and, for example, could be density, the two scalar components of momentum, and the total energy at each grid point. The present CFD model has about 17,000

total flow variable unknowns, and therefore an efficient solution method is imperative to carry out the studies reported here.

Harmonic Balance Solution in the Frequency Domain

The pioneering work of Ueda and Dowell, (Ref 30) and Lan and his colleagues, (Ref 31) should be recalled. Ueda and Dowell used a describing function technique whereby the dominant harmonic was extracted from a time marching CFD model, LTRAN2, using both indicial and harmonic motions of the airfoil. They considered a two degree of freedom typical airfoil section. Lan et al used the method of harmonic balance to study the unsteady transonic aerodynamics for flutter and limit cycle oscillation prediction. In their work, they used the transonic small disturbance potential flow model, as did Ueda and Dowell, and only considered a single harmonic. In the present work, we employ the Euler equations of fluid dynamics and also retain multiple harmonics in the aerodynamic model. It is found that using several harmonics improves the theoretical prediction of the aerodynamic forces. However in the aeroelastic analysis, when the fluid and structural models are coupled, only a single harmonic is used. The effects of higher harmonics on this single harmonic are retained as they are found to be significant in the fluid model.

The Aeroelastic System and Its Solution

The structural equation of motion is a simple single degree of freedom model in pitch. See Fig 3.1 for a depiction of the airfoil and the CFD grid used in the numerical calculations. By carefully selecting the pitch axis and mass ratio, we can insure that the system will either undergo classical linear aeroelastic divergence or flutter. Divergence can occur when the aerodynamic "negative" stiffness overcomes the structural stiffness, while flutter may occur when the aerodynamic negative damping overcomes the structural damping. As will be shown, each of these classical linear aeroelastic phenomena has a distinctively different limit cycle or nonlinear behavior.

(a) Close Up   (b) Entire Grid
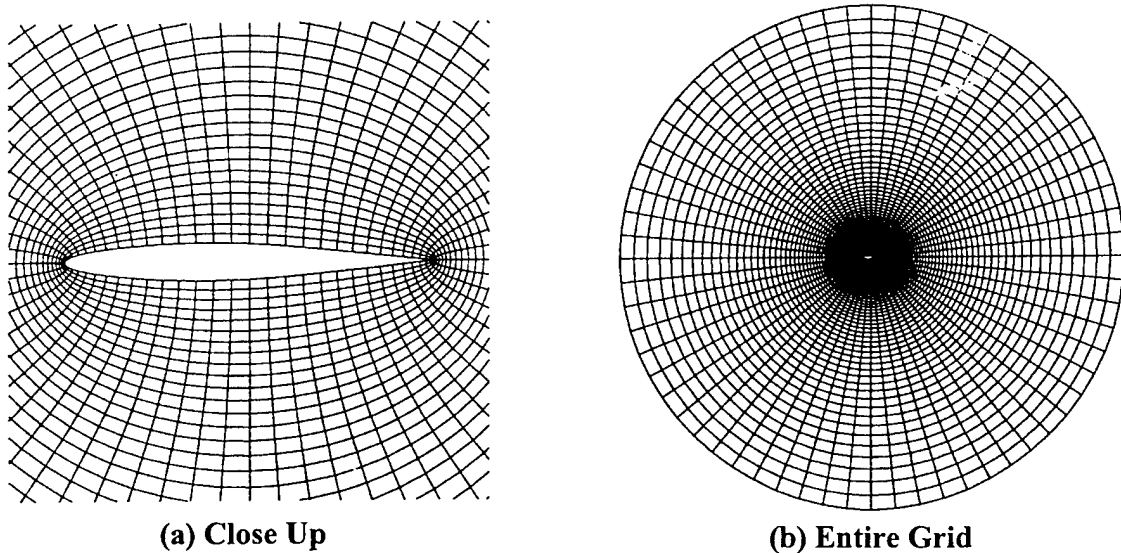
Figure 3.1   NACA 64A010A Computational Grid

14

The Mach number for these studies is M=0.80 and a NACA 64A010A airfoil is considered. The NACA 64A010A is a symmetric (10.6% thickness ratio) variant of the "Ames" AGARD 156 benchmark section. The elastic axis is considered at the mid-chord. Employed for the CFD calculations is an ``O''-type computational mesh with 65 x 65 radial and circumferential nodes that has an outer boundary radius of 10 chord lengths. The center of pressure (x_{cp}) as a function of static angle of attack is shown Fig 3.2 where it is seen the center of pressure moves from 32% chord to 40% chord as the angle of attack varies from 0.0 to 5.0 degrees. This is a key characteristic of the flow field for LCO.
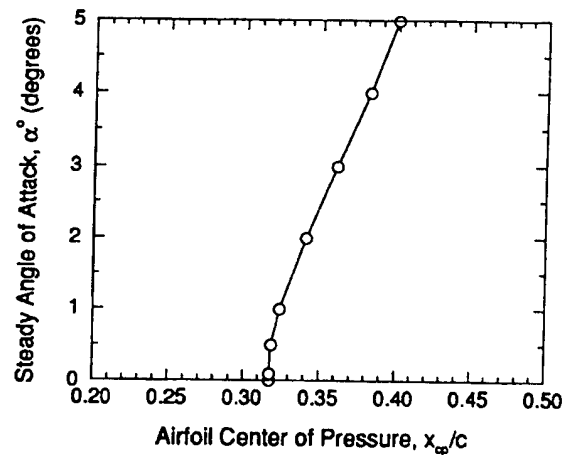
Figure 3.2 Center of Pressure Variation with Angle of Attack: NACA 64A010A Airfoil Section, M = 0.80

Linear and Nonlinear Divergence

Divergence is perhaps the simpler of the two phenomena since by definition it is time independent, i.e., we are dealing with a static linear instability and its nonlinear counterpart. In this case, the structural equation of motion becomes an equation of static equilibrium. And for the aerodynamic model, we only need to determine the lift and moment about some appropriate axis as a function of angle of attack. For small angle of attack, we will recover the classical linear aeroelastic divergence phenomena. But the question is, what are the effects of the nonlinearity?

Qualitatively one can anticipate the effect of the aerodynamic nonlinearity by examining the aerodynamic moment variation with angle of attack. A necessary condition for divergence to occur is that the aerodynamic moment be positive in the same direction as the twist angle. Moreover, if the nonlinear aerodynamic model predicts a moment less in magnitude than that predicted by linear aerodynamic theory, the effect of the nonlinearity will be to stabilize the divergence. And vice versa if the nonlinear theory predicts an increase in aerodynamic moment over that given by linear theory. Hence by examining the slope of the moment vs. angle of attack curve with increasing angle of attack, we will know whether the effect of the nonlinearity is favorable or unfavorable.

In the example below, the effect is favorable. That is, once the divergence dynamic pressure for a small angle of attack is exceeded (this is the classical linear aeroelastic divergence dynamic pressure), then the angle of twist of the pitch spring remains finite and smoothly increases from zero beyond the divergence dynamic pressure.

15

See Fig 3.3 where the angle of twist is plotted vs. the non-dimensional dynamic pressure. Also shown are results with an initial angle of attack. In this latter case, there is some twist over the full range of dynamic pressure. Indeed even if the initial angle of attack is only a few degrees, it would be difficult to detect the classical divergence dynamic pressure experimentally for this example. For readers who have studied buckling of systems in the presence of imperfections (e.g. beams, plates or shells with initial curvature), this behavior will be familiar.
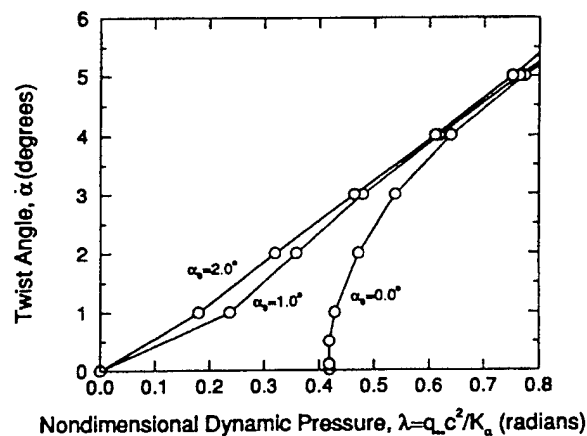
Figure 3.3 Divergence and Post-Divergence of an Airfoil Including Transonic Nonlinear Inviscid Aerodynamics: NACA 64A010A Airfoil Section, M = 0.80, Elastic Axis Location, a = e/b = 0.0

In this example, recall the center of pressure moves from 32% chord at low angles of attack to 40% chord at 5.0 degrees angle of attack. This is the principal reason for the stabilizing effect of nonlinear aerodynamics on the post-divergence condition. Had the change of the slope of the aerodynamic moment curve been in the opposite direction, then the angle of twist vs. dynamic pressure curve would have bent the other way. That is, for dynamic pressures below the classical divergence dynamic pressure, there would be non-trivial (non-zero) twist angles that represent possible static nonlinear equilibrium solutions. Intuitively one recognizes that these latter solutions would themselves be unstable, i.e., such results would be interpreted physically as the magnitude of the disturbance required to generate non-trivial twist at dynamic pressures below the classical divergence dynamic pressure. In our studies to date, only the stable nonlinear effect has been observed for statically divergent systems. However, this is not to say that unstable nonlinear divergence systems may not be encountered for some other parameter combinations.

Of course, divergence is a very special case of nonlinear aeroelasticity as it is for linear aeroelasticity, because the frequency of oscillation is zero when divergence and post-divergence occurs. Thus we now turn to an oscillatory case.

Flutter and Associated LCO

Now consider single-degree-of-freedom flutter in pitch. Here the classical flutter arises from a negative damping in the aerodynamic moment beyond a certain reduced frequency. However the reduced frequency at which the aerodynamic damping moment becomes negative increases as the angle of pitch oscillation increases. Hence the reduced velocity decreases as the angle of pitch increases, which suggests that this will lead to an unstable LCO as indeed it does.

In the example considered, we have moved the elastic axis to 20% chord to preclude divergence and to induce flutter.

16

It should be emphasized that in the present analysis, we are using a single harmonic to represent the pitch oscillation. However in the calculation of the aerodynamic moment, we include up to three harmonics to determine the effect of higher harmonics on the first harmonic of the aerodynamic moment. It turns out that the effect of the third harmonic is negligible. Indeed, if one only retains a single harmonic in the aerodynamic analysis, the results are qualitatively correct and have fair quantitative accuracy.

Results for the first harmonic for the moment about the pitch or elastic axis are shown in Fig 3.4. These results are for two harmonics retained in the aerodynamic analysis. Note that the results at a reduced frequency of zero were those used in the divergence analysis discussed previously. Of course, a transformation of the pitch axis is used for the divergence analysis.

(a) Real Unsteady Moment

(b) Imaginary Unsteady Moment
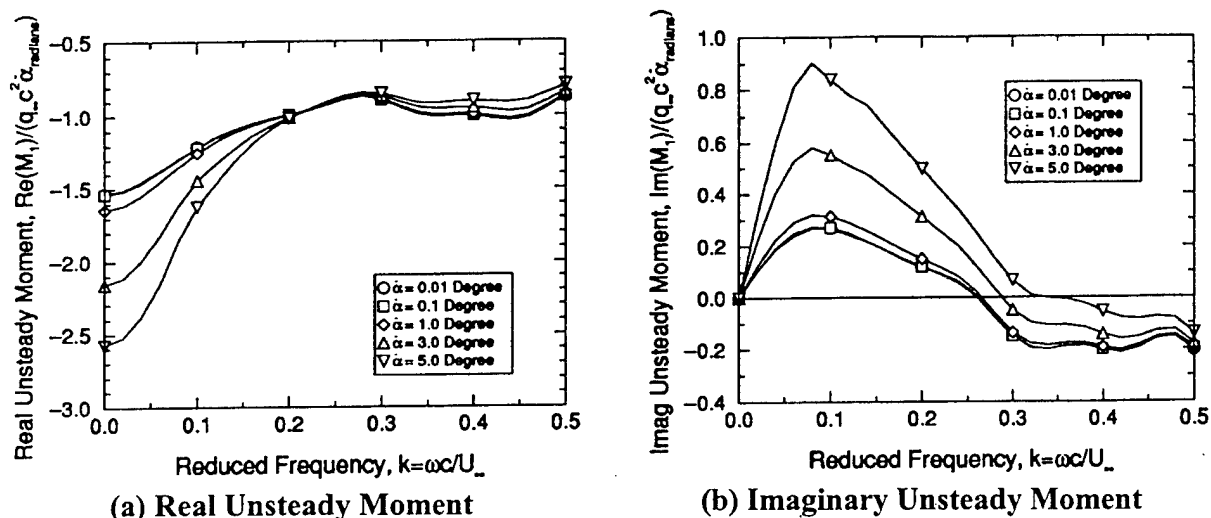
Figure 3.4 **Unsteady Lift and Moment for Various Pitch Amplitudes: NACA 64A010A Airfoil Section, M = 0.8, α_0 = 0.0 deg., Elastic Axis Location, a = e/b = -0.6, Two Harmonics Employed in Harmonic Balance Expansion**

While structural damping is readily included in the analysis, it will be helpful to understand the essence of the results by first considering the solution for zero structural damping.

Zero Structural Damping

In this case, a neutrally stable oscillation will occur when the imaginary part of the aerodynamic moment becomes zero. This will occur at some reduced frequency for a particular angle of pitch oscillation (and other parameters fixed such as Mach number). Then one can solve for the frequency of this neutrally stable oscillation. For sufficiently small motions, this is the flutter solution; for larger motions, we determine a limit cycle oscillation. The solution procedure then is to select an amplitude of oscillation, determine the reduced frequency at which the imaginary part of the aerodynamic moment is zero from Fig 3.4, and then determine the frequency of the oscillation. Note this is essentially the same computational procedure as for a classical flutter solution, except now the reduced frequency, the frequency of oscillation, and the reduced velocity are all functions of the pitch amplitude. It should be noted however that just because the

17

imaginary part of the aerodynamic moment vanishes (i.e., the aerodynamic damping becomes zero), that alone does not insure that a neutrally stable oscillation will occur. This is because the frequency determined must be physically possible.

Large Pitch Moment of Inertia Now if the mass ratio or moment of inertia is larger, a not uncommon circumstance, then the flutter or LCO frequency is simply equal to the structural pitch natural frequency. With this approximation, the results of Fig 3.5 are obtained for both zero and non-zero structural damping. Note that the curves bend to the left which is indicative of an unstable LCO. That is, these results are to be interpreted as the amplitude of a disturbance required to initiate explosive flutter below the classical flutter velocity for this single-degree-of-freedom pitch oscillation.
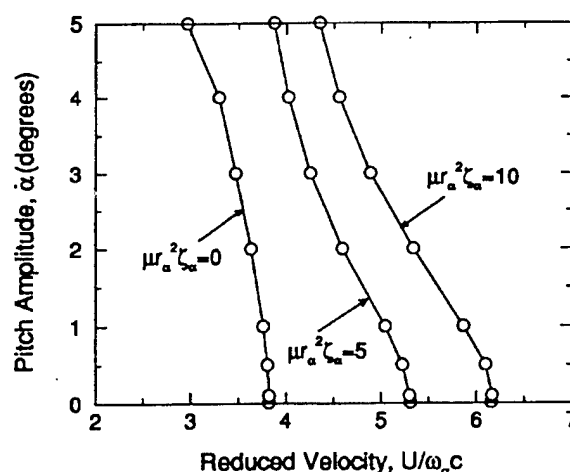
Figure 3.5 LCO Amplitude Versus Reduced Velocity: NACA 64A010A Airfoil Section, M = 0.80, α = 0.0 deg., Elastic Axis Location, a = e/b = -0.6.

Effects of Finite Pitch Moment of Inertia

For general values of moment of inertia and structural damping, the solution algorithm proceeds as follows. First select a Mach number and pitch axis, and for a range of pitch amplitudes, determine the first harmonic of the aerodynamic moment (including higher harmonics of the aerodynamic model and their effect on the fundamental harmonic). Then for a given pitch amplitude, choose a reduced frequency and determine the flutter or LCO oscillation frequency. This frequency will be proportional to the pitch structural frequency, of course. With the flutter or LCO frequency determined, and the reduced frequency selected, one then knows the flow velocity corresponding to the chosen pitch amplitude. Finally, determine the structural damping value necessary to give a neutrally stable flutter or limit cycle oscillation. From this perspective, the flutter condition is simply the neutrally stable motion that may exist at small angles of twist, and the LCO are the neutrally stable oscillations that may exist when the pitch amplitude is finite. Of course the flutter or LCO may become unstable when it is perturbed (e.g., by perturbations in the amplitude of oscillation), and this is indeed the case in the example treated here.

Up to this point, we have assumed that the pitch moment of inertia is well above its asymptotic value. Hence the flutter frequency is the same as the structural natural pitch frequency.

18

Now we consider the more general case and a range of pitch inertias such that the flutter frequency is no longer precisely equal to the structural natural frequency in pitch. Results are shown for non-dimensional pitch inertias of 200,100,50,37.5 and 25 in Fig 3.6. These are for LCO amplitude versus reduced velocity. The asymptotic or large pitch inertia results are also shown for reference.

As expected, for sufficiently large pitch inertia, say greater than 200, the asymptotic results are good approximations. However for pitch inertias less than 100, the results show a more sensitive dependence on pitch moment of inertia. For sufficiently small pitch moment of inertia, of course, no flutter or LCO is possible.
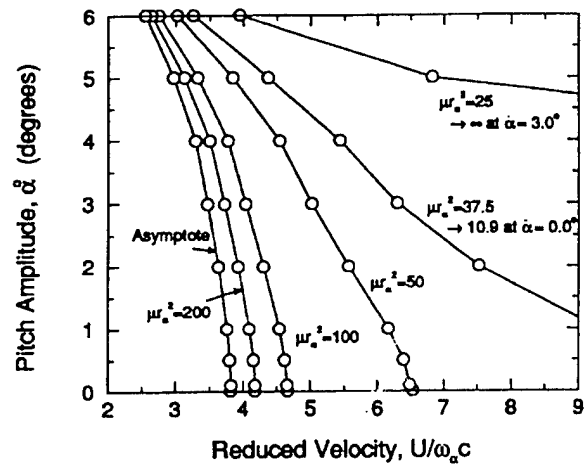
Figure 3.6   LCO Amplitude Versus Reduced Velocity for Various Pitch Inertias: NACA 64A010A Airfoil Section, M = 0.80, α = 0.0 deg., Elastic Axis Location, a = e/b = -0.6.

For additional details of the work presented in this Chapter, please see the paper (Ref 15) included in Appendix B.

19

CHAPTER 4

THREE DIMENSIONAL TRANSONIC AEROELASTICITY USING PROPER ORTHOGONAL DECOMPOSITION BASED REDUCED ORDER MODELS

Summary

The POD/ROM method has been demonstrated for the flutter analysis of a three-dimensional transonic wing configuration. We have shown that the number of ROM DOF's necessary to create accurate models is on the order of a few dozen as is the case in two-dimensions. We have also shown that it is unnecessary to compute a completely new ensemble of solution snapshots based on the vibratory mode shapes for each new structural configuration that might be under consideration. One can simply compute a set of snapshots based on some basic wing motions at a number of frequencies. Then snapshots only at the end points of the frequency range of interest need to be computed for the specific mode shapes of the configuration of interest. These end point snapshots "lock in" the unsteady fluid dynamic characteristics for the particular mode shapes, and the simple motion snapshots then act to resolve the dominant dynamics of the flow throughout the full frequency range of interest.

Introduction

Here, we demonstrate how the recently devised proper orthogonal decomposition (POD) based reduced order modeling (ROM) technique (Refs 11, 32) can be used to model unsteady aerodynamic and aeroelastic characteristics of three-dimensional transonic wing configurations. Although transonic Euler flows are considered in Refs 11 and 32, the initial demonstrations of the POD/ROM method as presented in these references are for two-dimensional flow and two structural degree-of-freedom airfoil configurations. Also in Ref 33, an application of the POD/ROM technique to the well known vortex lattice method has been presented.

In extending the POD/ROM technique to three-dimensions, two primary issues have been of concern. First, the size of the computational fluid dynamic (CFD) model will in general be at least an order of magnitude greater than for two-dimensions. Whereas a typical CFD model for a realistic two-dimensional configuration might have on the order of 10's or even 100's of thousands of degrees of freedom (DOF), a CFD model for a three-dimensional configuration might easily have on the order of at least hundreds of thousands if not millions or more DOF's. In two-dimensions, we have found that very accurate ROM's with on the order of only a few dozen DOF's can be devised using the POD/ROM methodology. A first issue to address has thus been whether or not in three-dimensions one can also generate accurate ROM's, which require at most a few dozen DOF's.

The second concern is, for any variation of the structural properties of a given wing under consideration, will a completely new ensemble of solution vector "snapshots" have to be computed in order to devise an accurate POD/ROM. A basic aspect of the POD/ROM method is

that an ensemble of solution vectors is first assembled by computing unsteady CFD solutions at a number of discrete frequencies within a frequency range of interest for the unsteady structural motions that are also of interest. In two dimensions, this step is relatively straight forward since one only has to consider a few possible motions, e.g., pitch and plunge.

In three-dimensions however, the wing vibratory mode shapes will be different for each different structural configuration of a given wing. There can in fact be an infinite number of unsteady motions (or at least a substantial number of motions equivalent to the number of DOF's of the discrete structural model). Thus the second concern about extending the POD/ROM to three-dimensions has been whether or not it is necessary to compute a completely different ensemble of solution snapshots for every possible structural configuration. For example, say one computes solution snapshots for a given wing configuration based on the wing's particular vibratory modes shapes in order to develop a POD/ROM to model the configuration's aeroelastic characteristics. Then the question is, if the structural make-up of the wing changes, does one have to compute a whole new ensemble of solution snapshots for the same wing, but for the different set of vibratory modes shapes.

Fortunately in addressing these two issues, we have found that accurate POD/ROM's with just a few dozen degrees of freedom can in fact be created for a realistic transonic three-dimensional configurations. This is true even though in the model problem to be shown subsequently, the CFD model is easily an order of magnitude larger than anything we have previously studied in two-dimensions. Furthermore, we have discovered that a "fundamental" ensemble of solution snapshots, based on wing motions that need not be related to the structural modes under consideration, can be assembled as a first step. Accurate POD/ROM's for a given wing configuration can then be created by simply adding to this "fundamental" ensemble, the snapshots corresponding to actual wing structural modal motions solely at the frequencies corresponding to the end points of the frequency range of interest. In general, these two snapshots prove to be sufficient to "lock in" the conditions corresponding to the particular structural motion, and indeed the fundamental ensemble of solution snapshots is sufficient to reveal the unsteady dynamics of the fluid dynamic model. The fundamental ensemble of snapshots can be used again and again even as the structural mode change, and thus the computational cost of having to compute an entirely new snapshot ensemble for every new structural configuration is greatly reduced.

POD/ROM Methodology

In the following, we will be considering inviscid three-dimensional Euler flows. More specifically, linearized (about some nonlinear background steady flow) unsteady frequency-domain CFD solutions to the Euler equations are computed. The POD/ROM procedure can be considered as a "wrapper" around any typical CFD method, and the CFD method we have employed for the present analysis is a variant of Ni's (Ref 34), approach to the standard Lax-Wendroff method. The frequency domain CFD method in effect represents a linear system formulation of the unsteady fluid dynamic model, i.e.

$$\mathbf{A}q = -\mathbf{B}\zeta \qquad (4.1)$$

21

where **q** is an N dimensional vector (N is the number of mesh points time the number of dependent flow variables) of the unknown flow variables a each mesh point in the CFD domain, and ζ is the L dimensional vector (L is the number structural mode shapes) of modal coordinates for the structural model. **A** is the $N \times N$ fluid dynamic influence matrix, and **B** is the $N \times L$ matrix which relates the flow solver boundary conditions to each particular mode shape. Both **A** and **B** are functions of the background flow and unsteady frequency ω. The structural equations for the wing configuration being modeled within the flow can be written as

$$\mathbf{D}\zeta = -\mathbf{C}\mathbf{q} \tag{4.2}$$

where **D** represents the $L \times L$ structural influence matrix (i.e., $\mathbf{D} = -\omega^2 \mathbf{M} + \mathbf{K}$ where **M** and **K** are the generalized mass and stiffness matrices, and **C** is the $L \times M$ matrix which represents the discrete integration used to obtain the generalized forces associated with each modes shape based on the unsteady flow **q**. When Eqs (4.1) and (4.2) are put together,

$$\begin{bmatrix} \mathbf{A} & \mathbf{B} \\ \mathbf{C} & \mathbf{D} \end{bmatrix} \begin{Bmatrix} \mathbf{q} \\ \zeta \end{Bmatrix} = \begin{Bmatrix} 0 \\ 0 \end{Bmatrix} \tag{4.3}$$

The resulting Eq (4.3) is a fully coupled aeroelastic system of equations, which for nontrivial **q** and ζ, represents an eigenvalue problem with ω being the eigenvalue. Any eigenvalues with a positive real part imply the aeroelastic system is unstable.

The problem with constructing and solving this eigenvalue problem is that **A** is simply too large for realistic configurations. As mentioned in the introduction, N can easily be on the order of 10,000 or 100,000 for two-dimensional configurations, and on order of 100,000 to 1,000,000 or even more for three dimensional configurations. For such large cases, even attempting to set up **A** is well beyond the memory limits of todays largest computers.

The basic premise of the POD/ROM methodology is that we assume the unknown flowfield solution vector **q** can be expressed as a Ritz type expansion of the form

$$\mathbf{q} \approx \sum_{k=1}^{K} \xi_k \phi_k \qquad K \ll N \tag{4.4}$$

where ξ_k is a generalized coordinate sometimes referred to as an augmented aerodynamic state variable, and ϕ_k is the corresponding Ritz vector. Eq (4.4) can also be written in matrix form as

$$\mathbf{q} = \Phi\xi, \text{ where } \Phi = \begin{bmatrix} | & | & & | \\ \phi_1 & \phi_2 & \cdots & \phi_K \\ | & | & & | \end{bmatrix} \text{ and } \xi = \begin{Bmatrix} \xi_1 \\ \xi_2 \\ \vdots \\ \xi_K \end{Bmatrix} \tag{4.5}$$

22

Here, Φ is an $N \times K$ matrix whose k'th column is the shape vector ϕ_k, and ξ is the K dimensional vector of augmented aerodynamic state variables ξ_k.

A reduced-order representation of the fluid dynamic and aeroelastic systems can be formulated by substituting Eq (4.5) into Eq (4.1) and/or (4.2) and pre-multiplying by the Hermitian transpose $\left(\Phi^H\right)$ of Φ, i.e.

$$\Phi^H \mathbf{A} \Phi \xi = \Phi^H \mathbf{B} \zeta \quad \text{or} \quad A\xi = -B\zeta \tag{4.6}$$

and

$$\left\{\Phi^H \quad \mathbf{I}\right\} \begin{bmatrix} \mathbf{A} & \mathbf{B} \\ \mathbf{C} & \mathbf{D} \end{bmatrix} \begin{Bmatrix} \Phi\xi \\ \zeta \end{Bmatrix} = \begin{bmatrix} A & B \\ C & D \end{bmatrix} \begin{Bmatrix} \xi \\ \zeta \end{Bmatrix} = \begin{Bmatrix} 0 \\ 0 \end{Bmatrix} \tag{4.7}$$

If the Ritz approximation is a good one, $(K << N)$, and Eqs (4.6) and (4.7) will represent much smaller systems that can readily be solved using conventional eigenvalue techniques.

The next question becomes what are good choices for the Ritz vectors ϕ_k that will in fact result in good Ritz approximations. Previous studies as detailed in Refs 11 and 32 have demonstrated that shape vectors derived via the proper orthogonal decomposition technique (see for instance Refs 35, 36, and 37) are an excellent source. For the sake of brevity, the of details are omitted here, but a discussion of how the shapes are derived can be found in Refs 11 and 32. The basic premise behind their formulation is that a number solution ``snapshots'' are directly computed for a number of discrete frequencies and unsteady structural motions of interest. From this ensemble of solution vectors, the POD shapes are easily derived by solving a small (the size of the number of snapshots) eigenvalue problem. The first few POD modes describe the most dominant dynamic characteristics of the fluid dynamic system, and as such, the POD shapes have proven to be an excellent set of Ritz vectors for fluid dynamic and/or aeroelastic models.

Model Problem

The configuration under consideration is the AGARD model 445.6 wing (Refs 38, 39). This is a 45 degree quarter chord swept wing using the NACA 64A004 airfoil section that has an aspect ratio of 3.3 (for the full span) and a taper ratio of 2/3. Fig 4.1 illustrates the computational mesh employed for this configuration. The grid is an "O-O" topology that employs 49 computational nodes about each airfoil section, 33 nodes normal to the wing, and 33 nodes along the semispan. The outer boundary of the grid extends five semispans from the midchord of the wing root section. The particular structural configuration of the wing is referred to as the 2.5 ft. weakened model 3 (again see Refs 38 and 39).
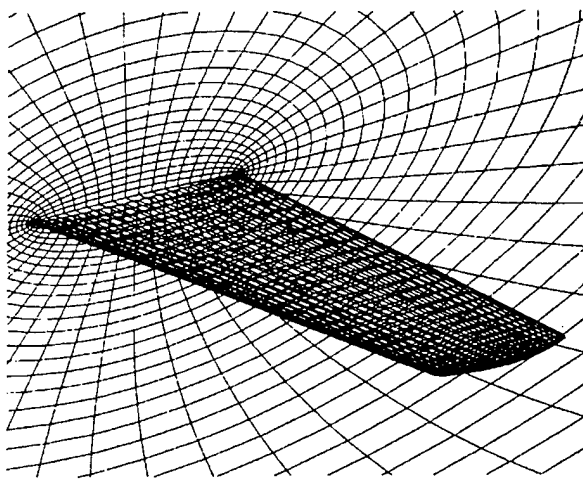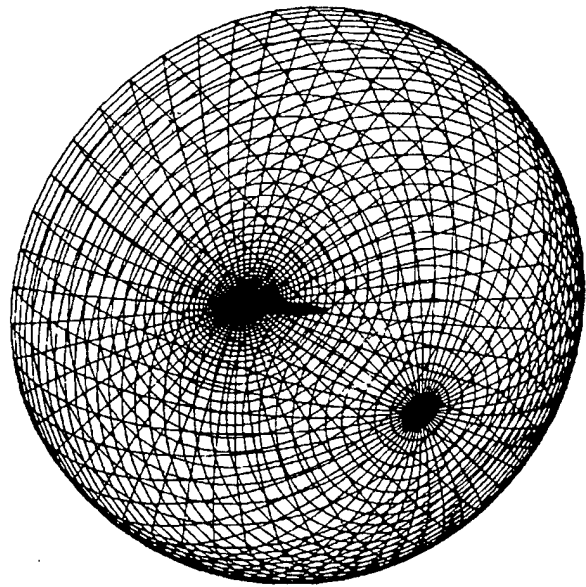
(a) Wing surface and symmetry plane grids   **(b) Outer boundary grid**

Figure 4.1   AGARD 445.6 Wing Grid Topology

We have examined the computed wing surface and symmetry plane steady flow pressure contours for freestream Mach numbers of 0.960 and 1.141. A relatively weak shock can be seen at the trailing edge for M=0.960. This shock appears to get stronger at M=1.141. The wing section is quite thin 4%, so a strong shock is not really expected. Comparing contours, our flowfields look very comparable to those of Lee-Rausch and Batina (Ref 40), although they employed a much larger mesh. We have examined the computed wing surface and symmetry plane steady flow pressure contours for the Mach numbers of 0.960 and 1.141. A relatively weak shock can be seen at the trailing edge for M=0.960. This shock appears to get stronger at M=1.141. The wing section is quite thin (4%), so a strong shock is not really expected. Comparing contours, our flowfields look very comparable to those of Lee-Rausch and Batina (Ref 40), although they employed a much larger mesh.

Computational Steps for Flutter Analysis

The first step is to compute the "snapshots" for one Mach number and several structural modes, say five. These are overnight runs, so the wall clock time is about 24 hours to do this. Moreover we have shown that if the structural modes change, then the computation of all of the "snapshots" does not need to be repeated. This reduces the number of new "snapshots" needed and the corresponding computer time by about a factor of five.

The second step involves taking the above data and constructing the reduced order model which requires about 15 minutes of computer time.

With the information from steps one and two above, in the third step each aeroelastic solution for a given Mach number and set of structural modes and one combination of all parameters takes a fraction of a second. This provides the true frequency and damping (i.e., this is a p method) for

each aeroelastic mode. To construct a root locus using say 100 dynamic pressure values takes less than one minute.

Flutter Results

Fig 4.2 shows the eigenvalue root-loci when sweeping through various mass ratios (to which there is a corresponding flutter speed index) when solving the aeroelastic eigenvalue problem posed by the reduced-order aeroelastic model (Eq (4.7)) for various Mach numbers. Solution snapshots are computed for the first five given wing mode shapes for reduced frequencies ($k = \omega b / U_\infty$) from $k = 0.0$ to $k = 0.5$ in $\Delta k = 0.1$ increments. This configuration flutters for frequencies less than 0.5, and as such, solution snapshots for $k > 0.5$ are unnecessary. This results in a total of 55 available POD shape vectors. In Fig 4.2, the curves represent the eigenvalues corresponding to the primarily structural natural modes as mass ratio is varied. Our method also determines the aeroelastic modes originating from the fluid dynamic modes of the POD/ROM. For the range of mass ratios ($0 < \mu \leq 500$) swept through in these parametric analyses, the fluid dynamic modes are very damped, and as such lie to the left and outside of the eigenspectrum range we show. As can been, for each of the Mach numbers, the first structural mode tends to be the critical flutter mode. For the highest Mach number however, the third structural mode can go unstable if the mass ratio is large enough. Also from this figure, it is evident that it is unnecessary to use all 55 of the available POD shapes. If fact, with less than one half of the POD modes (25 for instance), relatively converged results (in the sense of POD mode refinement) can be achieved.

Fig 4.3 shows the computed POD/ROM flutter speed and flutter frequency ratios, along with experimental data (Ref 38), and data from two other computational methods (Refs 40, 41), as a function of Mach number.

As can be seen, using our methodology, we produce the well known transonic flutter speed dip, and our results are all within the same tolerance to the experimental results as the other computational methods. Gupta (Ref 41), does show better agreement with experiment at the two supersonic Mach numbers, and Gupta attributes this better agreement to better CFD grid refinement. In future work, we will also address this issue.

Figure 4.2 Aeroelastic Root-Loci at Various Mach Numbers for the AGARD 445.6 Wing "Weakened" Configuration, $\alpha = 0.0$ deg

(a) Flutter Speed
(b) Flutter Frequency Ratio

Figure 4.3 Mach Number Flutter Trend for the AGARD 445.6 Wing "Weakened" Configuration, $\alpha_0 = 0.0$ deg.

26

One of the key concerns towards in the POD/ROM method to three-dimensional flows has been whether or not an entire set of solution snapshots must be computed for each possible structural configuration of interest. That is, say we wish to consider a similarly shaped wing that has a slightly different structural configuration, which in turn means the wing vibratory mode shapes are different. Does this mean that one has to go through and compute a whole new ensemble of solution snapshots based on these new structural motions in order to do a flutter analysis for the new wing configuration. Fortunately, although a few snapshots based on the new modal motion will need to be computed, the larger number of snapshots computed at numerous frequencies will be unnecessary. The snapshots computed from a previous wing structural configuration will still serve the purpose. That is, a couple of solution snapshots will be needed for the new structural motions, however, these will only need to be computed at the end points of the frequency range of interest. Fig 4.4 demonstrates how this works.

Fig 4.4 shows the real and imaginary parts of the coefficient of the generalized aerodynamic force corresponding to the first mode pressure acting through the first mode shape as a function of reduced frequency at a Mach number of 0.960. The coefficient of the generalized aerodynamic force is defined as

$$C_{Q_{i,j}}(k) = \frac{1}{q_\infty c_r^2} \iint \phi_i p_j(k) n_x dA \tag{4.8}$$

where $q_\infty = \rho_\infty U_\infty^2 / 2$ is the freestream dynamic pressure and c_r is the root chord length. In this definition, $p_j(k)$ represents the frequency dependent unsteady pressure resulting from a wing deformation motion of

$$\frac{x}{c_r} = \phi_j \tag{4.9}$$

The curves presented in Fig 4.4 are based on the actual solution snapshots and thus are what we desire the POD/ROM to model. In Fig 4.4.b, the POD/ROM of $C_{Q_{1,1}}$ based on snapshots for each of the five structural mode shapes at frequencies of $k=0.0$ and $k=1.0$ (for a total of 10 snapshots) is compared against $C_{Q_{1,1}}$ for the actual snapshots for all frequencies between $k=0.0$ and $k=1.0$. As can be seen, the POD/ROM matches at the end points of the frequency range as is expected, however this crude POD/ROM performs rather poorly for the intermediate frequencies. Of course, if we use snapshots at all the frequencies between $k=0.0$ and $k=1.0$, the POD/ROM would exactly reproduce the data.

(a) Snapshots
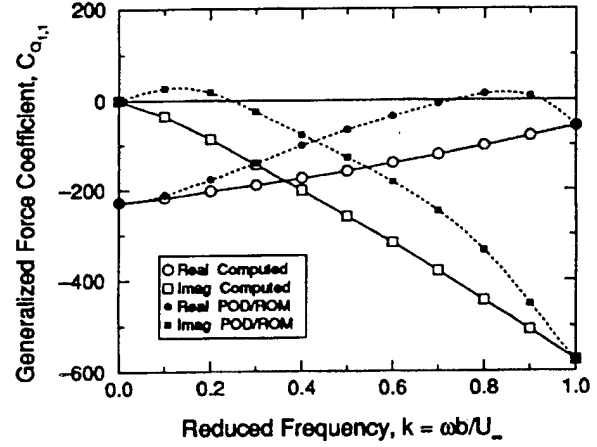
(b) POD/ROM based on k=0.0 and k=1.0
modal snapshots
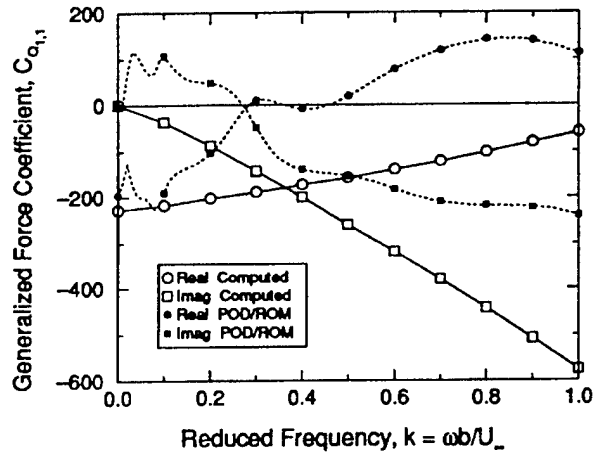
(c) POD/ROM based on basic motions
snapshots
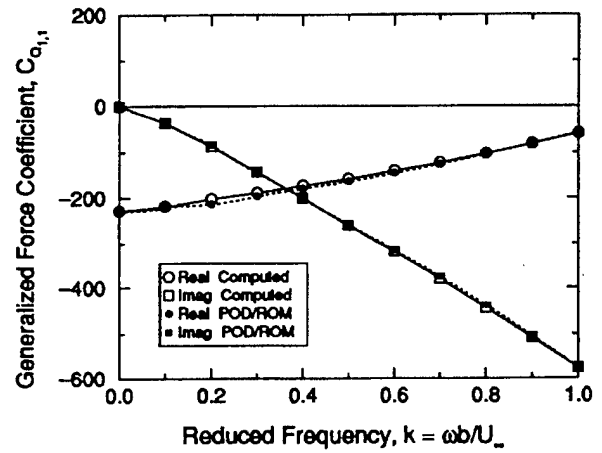
(d) POD/ROM based on k=0.0 and k=1.0
modal snapshots and basic motions
snapshots

Figure 4.4   Generalized Force Modeling with Unrelated Mode Shape Snapshots

Next, in Fig 4.4.c, a new POD/ROM for $C_{Q_{1,1}}$ now based on solution snapshots unrelated to the actual mode shapes is shown. The simple wing motion snapshots are for a full wing plunge motion (up/down), full wing pitch about the quarter chord, a first bending type of motion (wing is fixed at the root, and the z coordinate component of deflection varies linearly with span), and a first twist type of motion (wing is fixed at the root, and the pitch varies linearly with span) for frequencies from $k=0.0$ to $k=1.0$ at $\Delta k = 0.1$ increments for a total of 44 solution snapshots. As can be seen, the POD/ROM in this case also perform very poorly. Unbeknownst however, these solutions are in fact helping to reveal the dynamics of the system. In fact, when one uses these snapshots in combination with the actual structural mode snapshots solely at the end points of the

28

frequency range of interest, one gets a POD/ROM which produces very accurate results to $C_{Q_{1,1}}$ as is evident from Fig 4.4.d.

A comparison of the POD/ROM Mach number flutter trends in the case where first, the POD/ROM is based on solution snapshots corresponding to the actual modal shapes of the wing to the case where second, the POD/ROM is based on snapshots using the simple wing motion mode shapes as discussed in the previous paragraph has been made. The results are virtually identical at all but the highest Mach number. There is some difference at the highest Mach number, again suggesting supersonic flow is more sensitive for this wing.

For additional details of the work presented in this Chapter, please see the paper (Ref 16) included in Appendix C.

CHAPTER 5

SIMULATION OF TRANSONIC LIMIT CYCLE OSCILLATIONS USING A CFD TIME-MARCHING METHOD

Summary

We have conducted a transonic LCO investigation for an NLR 7301 airfoil using NASA/Langley CFL3D/N-S time-marching approach to validate with measured LCO/flutter data of DLR. The present LCO study is a parallel effort to that of Duke University whose CFD method is based on a frequency-domain POD/ROM EigenMode approach.

The primary objective of the CFL3D/N-S effort was aimed at to investigate the impact of turbulent models and computing time on a viable CFD tool for transonic LCO. We found that the LCO solution is turbulent-model dependent and time-step size sensitive. These issues along with the possible influence on LCO due to initial conditions and transition points remain to be subjects for further research.

In using the Spalart-Allmaras turbulent model, the present study for NLR7301 shows that the time-marching CFL3D computation can predict LCO and with good frequency agreement, which to a large extent validates the transonic test result of Schewe et al at DLR. However, in order to obtain a fully developed LCO, this time-marching computation typically requires about 96 hours of computer time on a 1 GHz computer. In view of its long computing time, a CFD time-marching scheme such as CFL3D/N-S would be computationally inefficient as a tool for 3D transonic LCO investigation. The above observation suggests Duke's frequency-domain POD/ROM EigenMode. approach, for given computer limitation, may very well be the only viable tool for 3-D transonic LCO investigation at present.

Introduction

Limit Cycle Oscillation (LCO) has been a persistent problem on several current fighter aircraft and is generally encountered with external store configurations. Denegri (Ref 1) provided a detailed description of the aircraft/store LCO phenomenon. Norton (Ref 2) gave an excellent overview of LCO of fighter aircraft carrying external stores and its sensitivity to store carriage configuration and mass properties.

LCO can be characterized as sustained periodic oscillations which neither increase or decrease in amplitude over time for a given flight condition. Using an s-domain unsteady aerodynamic model of the aircraft and stores, Chen, Sarhaddi and Liu (Ref 7) has shown that wing/store LCO is a post-flutter phenomenon whenever the flutter mode contains low unstable damping. This type of flutter mode is called the *"hump mode"*. Since the aircraft structure usually contains structural nonlinearity such as friction damping, this amplitude-dependent friction damping can suppress the growth of amplitude, thus resulting in a steady state oscillation. This is known as the nonlinear structural damping (NSD) model of the wing/store LCO. Although not thoroughly

proven through tests or numerical simulations, results of the NSD show excellent correlation with flight test LCO data of F-16 throughout subsonic and transonic Mach numbers.

On the other hand, other long-standing researchers, notably Meijer and Cunningham (Ref 8), believe that the wing/store LCO is due largely to the transonic shock oscillation and shock induced flow separation, called Transonic Shock/Separation (TSS) model. Edwards considers the TSS model and viscous effects are two major factors that cause transonic LCO for wings. He also delineates the shock buffet phenomenon as opposed to that of transonic LCO (Ref 9). It should be noted that, however, there is no conflict in the NSD model and the TSS model in that TSS is only a transonic subset of NSD. That is to say that NSD model could consistently interpret the LCOs occurrence at subsonic and supersonic speeds as well, whereas TSS can not.

Recent renewed interest in LCO is perhaps motivated by the need of further resolving fighter LCO and the current advent of CFD methodology in aeroelasticity. There are two potential computational methods for LCO prediction/investigation: the *CFL3D.AE code* (Ref 10) developed and supported by NASA/Langley and the *POD/ROM EigenMode approach* (Ref 11) originated by Dowell and Hall of Duke University. The former is a conventional time-domain CFD method whereas the latter a frequency-domain CFD method, using aerodynamic eigen modes.

Objectives of CFD Simulation

Using the Navier-Stokes option of CFL3D.AE for LCO investigation, ZONA selects an NLR7301 airfoil (shock-free design condition at M = 0.747, C_l = 0.455) as the case studied. Primarily, a thorough wind-tunnel transonic LCO/flutter study was performed for a 2D supecritical wing with NLR7301 airfoil section by Schewe and his associates at DLR (Refs 42-44). To our best knowledge, Schewe's work is perhaps the only experimental work available for measuring 2-D transonic LCO. With Schewe's data, we began to validate our CFD simulated results with the following objectives:

- Attempt to understand the LCO physics
- Investigate the impact on LCO solutions due to different various flow parameters
- Evaluate necessary computer resource including computing time required
- Establish benchmarks and identify an efficient 3-D CFD method for LCO/flutter prediction.

LCO Study of NLR 7301 Airfoil Using CFL3D

Schewe and Deyhle (Ref 42) conducted an experiment on transonic flutter of a 2-D supercritical wing with an NLR 7301 airfoil section. The emphasis of this experiment was to investigate the effect of the flow nonlinearity on the aeroelastic response including transonic dip and transonic LCO. From the aeroelastic point of view, an aeroelastic experiment of a 2-D wing is more difficult and complicated than that of a 3-D wing. To validate a CFD methodology with such valuable data will help accomplishing the present objectives. The following is an account of our theoretical modeling of the experimental set up.

31
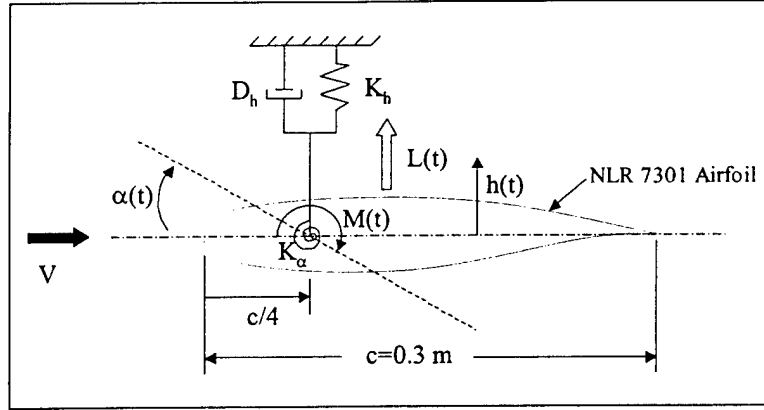
Figure 5.1 Two-Degree-of-Freedom Dynamic Model

Fig 5.1 depicts a simplified model of the 2-degree-of-freedom test set-up. The 2-D wing has a chord length of 0.3 m (c = 0.3 m) and a span of 1 m (b = 1 m). The pitching spring and heaving spring are attached to the same c/4 position. The corresponding 2-degree-of-freedom equation of motion of the set-up reads,

$$
\begin{bmatrix} m_h & -s_\alpha \\ -s_\alpha & I_{c/4} \end{bmatrix} \begin{Bmatrix} \ddot{h} \\ \ddot{\alpha} \end{Bmatrix} + \begin{bmatrix} D_h & 0 \\ 0 & D_\alpha \end{bmatrix} \begin{Bmatrix} \dot{h} \\ \dot{\alpha} \end{Bmatrix} + \begin{bmatrix} K_h & 0 \\ 0 & K_\alpha \end{bmatrix} \begin{Bmatrix} h \\ \alpha \end{Bmatrix} = \begin{Bmatrix} L(t) \\ M(t) \end{Bmatrix} \tag{5.1}
$$

where

m_h	is the total mass (m_h = 26.64 kg)
$I_{c/4}$	is the mass moment of inertia about c/4 ($I_{c/4}$ = 0.086 kg.m^2)
s_α	is the static unbalance (s_α = 0.378 kg.m)
D_h and D_α	are the damping factors of the heave motion (h) and the pitch motion (α), respectively (D_h = 82.9 kg/s and D_α = 0.197 kg.m^2/(rad-s))
K_h and K_α	are the stiffness of the heaving spring and pitching spring, respectively (K_h = 1.21 x 10^6 N/m and K_α = 6.68 x 10^3 N-m/rad), and

$L(t)$ and $M(t)$ are the aerodynamic lift and moment, respectively.

The numerical values of the structural terms in Eq (5.1) can also be found in Ref 43. To perform the time-marching CFD computation, it is convenient to convert Eq (5.1) from the physical degrees of freedom to the modal coordinates, i.e.:

$$
\begin{Bmatrix} h \\ \alpha \end{Bmatrix} = [\phi] \{q\} \tag{2}
$$

32

where q is modal coordinate and ϕ is the modal matrix of the undamped structure

$$\phi = \begin{bmatrix} -0.1735 & 0.1004 \\ 0.9277 & 3.403 \end{bmatrix}.$$

Substituting Eq (5.2) into Eq (5.1) and pre-multiplying the resulting equation by ϕ^T yield:

$$[I]\{\ddot{q}\} + \begin{bmatrix} 2\omega_h \zeta_h & 0 \\ 0 & 2\omega_\alpha \zeta_\alpha \end{bmatrix} \{\dot{q}\} + \begin{bmatrix} \omega_h^2 & 0 \\ 0 & \omega_\alpha^2 \end{bmatrix} \{q\} = q_\infty\, b\, \phi^T \begin{Bmatrix} c\, C_L(t) \\ c^2\, C_m(t) \end{Bmatrix} \quad (5.3)$$

where

ω_h and ω_α are the undamped natural frequencies of the heaving and pitching motions, respectively (ω_h = 205.4 rad/s and ω_α = 299.5 rad/s)

ζ_h and ζ_α are the heaving and pitching damping ratios, respectively (ζ_h = 0.00648 and ζ_α = 0.00474). Note that the off-diagonal terms in the damping matrix are assumed to be zero for simplicity.

q_∞ is the dynamic pressure, and

$C_L(t)$ and $C_m(t)$ are the non-dimensional aerodynamic lift and moment coefficients of the 2-D section of the wing, i.e.:

$$C_L(t) = \frac{L(t)}{q_\infty\, b\, c} \quad \text{and} \quad C_m(t) = \frac{M(t)}{q_\infty\, b\, c^2} \quad (5.4)$$

$C_L(t)$ and $C_m(t)$ are computed by the CFL3D code based on the NLR 7301 full chord length.

- *Steady State Results*

Fig 5.2 shows a C-type grid with 273x93 mesh points around the NLR 7301 airfoil. For validation, we first performed a 2-D steady computation with the Baldwin-Lomax and Spalart-Allmaras turbulence models assuming fully turbulent flow
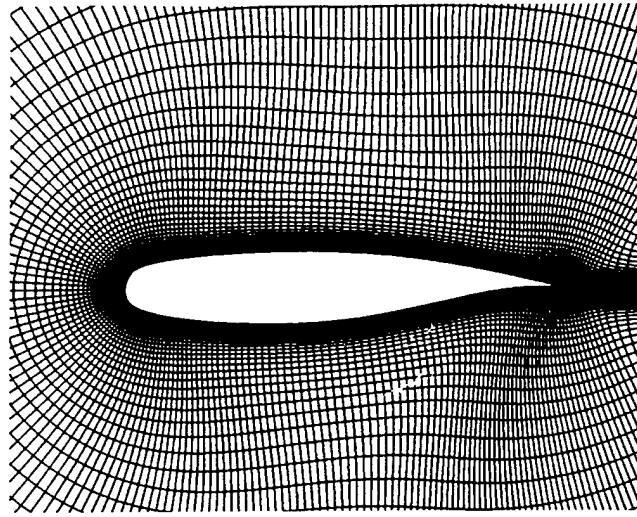
Figure 5.2 C-Type Grid Around NLR 7301 Airfoil (273 x 93)

The comparison of the computed pressure coefficient (C_P) with the experimental data is shown in Fig 5.3. Good agreement between these two sets of C_P distribution can be seen except at the 20% chord on the suction side. Weber et al (Ref 45) presented a similar result and suggested that this fully turbulent result can be improved by taking a fixed transition into account. However, due to the lack of test data in the transition onset location, no fixed transition model is considered in the present steady and unsteady aerodynamic computations.
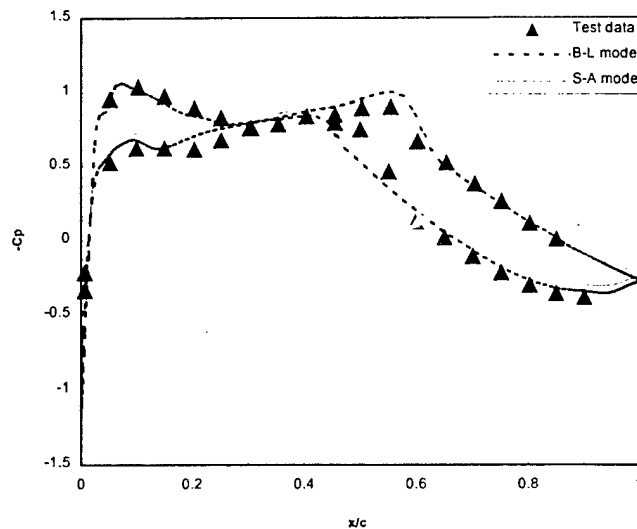
Figure 5.3 Steady Pressure Distribution
CFL3D: Mach No.= 0.753, AOA=-0.08°, Re=1.727x10^6
Experiment: Mach No.= 0.768, AOA=1.28°, Re=1.727x10^6

34

- *Time Step Size for Convergence*

It is well known that the transonic flow characteristics of the supercritical airfoil is very sensitive to off-design conditions. The position and strength of the transonic shock can change rapidly due to a small angle-of-attack and/or Mach number perturbation (Ref 46). This indicates that for transonic unsteady flow computation of supercritical airfoils, the time step must be kept sufficiently small and the number of Newton sub-iterations within each time step must be adequate to ensure the solution convergence. On the other hand, this stringent condition for low speed unsteady flow computation can be largely relaxed.

To show this, we conducted a time-step size study for solution convergence on the NLR 7301 airfoil at $M=0.05$ and $M=0.753$ by imposing a sinusoidal motion with oscillatory frequency at 50 Hz and pitching amplitude of 1 degree.

For the transonic case ($M=0.753$), the time histories of the lift coefficient with N=200/subit=3, N=800/subit=6, and N=800/subit=9 is shown in Fig 5.4.a, where N is the number of time steps within each cycle and "subit" is the number of Newton subiterations within each time step. It can be seen that the solution varies largely from N=200/subit=3 to N=800/subit=6 and thereupon it varies little up to N=800/subit=9, suggesting that a time step size corresponding to N=800/subit=9 must be adopted for transonic unsteady aerodynamic computation.

The same type of time histories for the low speed unsteady flow ($M=0.05$) is shown in Fig 5.4.b, but with N=800/subit=9, N=200/subit=3, and N=25/subit=3. Little variations of the solutions from N=800/subit=9 to N=25/subit=3 can be seen, suggesting that a time-step corresponding to N=25/subit=3 is sufficient for low speed unsteady flow computation. this also indicates that the transonic LCO analysis requires at least two orders of magnitude more computing time than that of a low speed analysis. In fact, in the following sections we will show that to obtain a fully developed transonic LCO time history takes several days of computer time on a 1 GHZ computer.
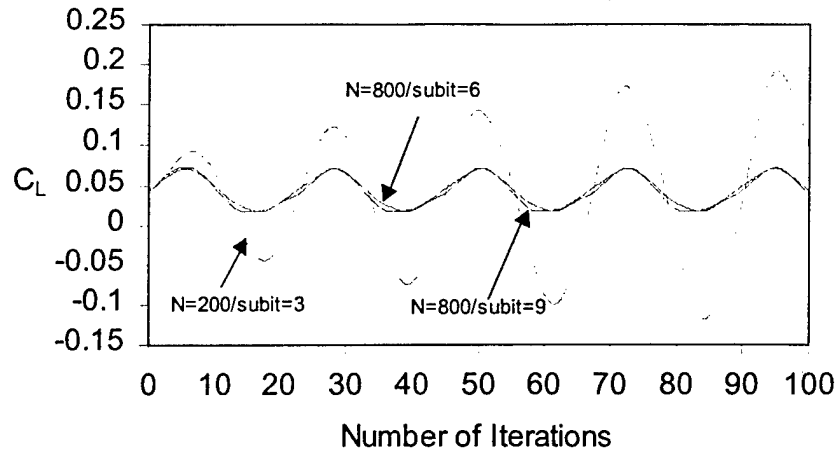
(a) M=0.753
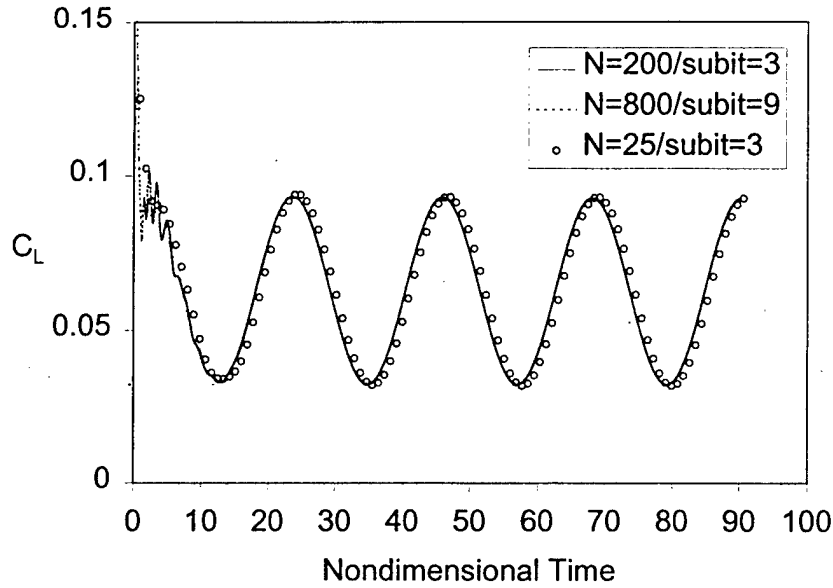
(b) M=0.05

Figure 5.4   Time Step Size for Solution Convergence

- *Steady AoA   Condition and Static Aeroelastic Equilibrium (SAE)   Condition*

Based on the complete Eq (5.3), the time-marching computation can then follow with the resulting SAE condition being the initial condition. Here, the initial conditions in terms of generalized coordinates are imposed at the values of $q_1 = 0$ and $q_2 = q_2(0)/2$, see Table 5.2. In passing, we note that different initial conditions could affect the resulting LCO solution in the presence of flow   nonlinearity.   Nonetheless, we merely leave the question of the initial-condition influence on LCO as a future research topic.

In Schewe's experiment, there exist two starting flow conditions: namely, a steady AoA condition and a static aeroelastic equilibrium (SAE) condition. A steady AOA condition is defined by the initially selected flow condition, whereas the SAE condition is the subsequent measured mean AoA position during the steady state oscillation. In terms of our numerical simulation, the SAE condition is one which obtained from solving the static aeroelastic version of Eq (5.3), i.e., by imposing a very large structural damping in order to nullify the velocity and acceleration terms.

Presented in Table 5.1 are the starting flow conditions of Schewe and those of two simulated methods. The difference in the test and simulated values of the steady AoA condition results from correlation of the corresponding Cp's and lift coefficients. The slight discrepancy in the SAE AoA between two simulated approaches remained to be clarified. Table 5.2 presents the SAE generalized coordinates as converted from the resulting SAE flow conditions.

Table 5.1 Two Starting Flow Conditions

	Steady AOA Condition	Static Aeroelastic Equilibrium (SAE) Condition
Knipfer et al (Ref 44)	M = 0.768, α = 1.91°	M = 0.768, α = 1.28°
Weber et al (Ref 45)	M = 0.753, α = 0.6°	M = 0.753, α = - 0.08°
Present	M = 0.753, α = 0.6°	M = 0.753, α = 0.078°

Table 5.2 SAE Generalized Coordinates

Dynamic Pressure	Generalized Coordinates	
	$q_1(0)$	$q_2(0)$
$P_{dynamic} = 15$ kPa	- 0.0059	- 0.0031
$P_{dynamic} = 12.6$ kPa	- 0.0051	- 0.0023
$P_{dynamic} = 9.5$ kPa	- 0.0045	- 0.0017

- *Verification of Flutter Boundary at M = 0.753*

Fig 5.5 presents Schewe and Deyhle's experimental flutter boundary for a 2-D supercritical wing with NLR 7301 airfoil section (Ref 42). In the subsonic range up to M = 0.74, the critical value of dynamic pressure is nearly constant. Transonic dip occurs when M > 0.74 where a dramatic drop of the critical dynamic pressure can be seen. In this transonic dip region, Schewe and Deyhle reported that various types of LCOs were observed. Using a Fourier transformation of the Navier-Stokes solver generated unsteady aerodynamics, Knipfer and Schewe (Ref 43) performed a frequency-domain flutter analysis and concluded that these LCO were genuine flutter cases. This conclusion can be further supported by the fact that the LCO appears already at Mach number below the buffet limit. To verify this, we performed two CFL3D aeroelastic computations at M = 0.753, one at q_∞ = 9.5 kPa and the second one at q_∞ = 15 kPa. In both computations, the speed of sound is fixed at 254.7 m/s and invariant to the air density.

The time histories of the heaving motion (h) and the pitching motion (α) of these two cases are presented in Figs 5.6 and 5.7, respectively. As expected, divergent motions at q_∞ = 15 kPa and convergent motions at q_∞ = 9.5 kPa are obtained. This confirms that the LCO of the 2-D supercritical wing with NLR 7301 airfoil section is indeed a post-flutter phenomenon, which initiates from a classical flutter instability.
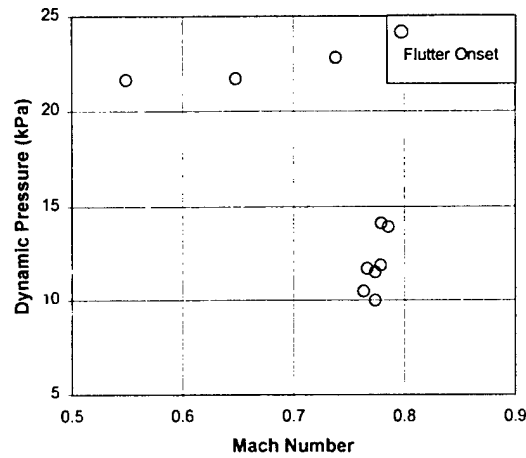
Figure 5.5   Flutter Boundary: Dynamic Pressure vs. Mach Number
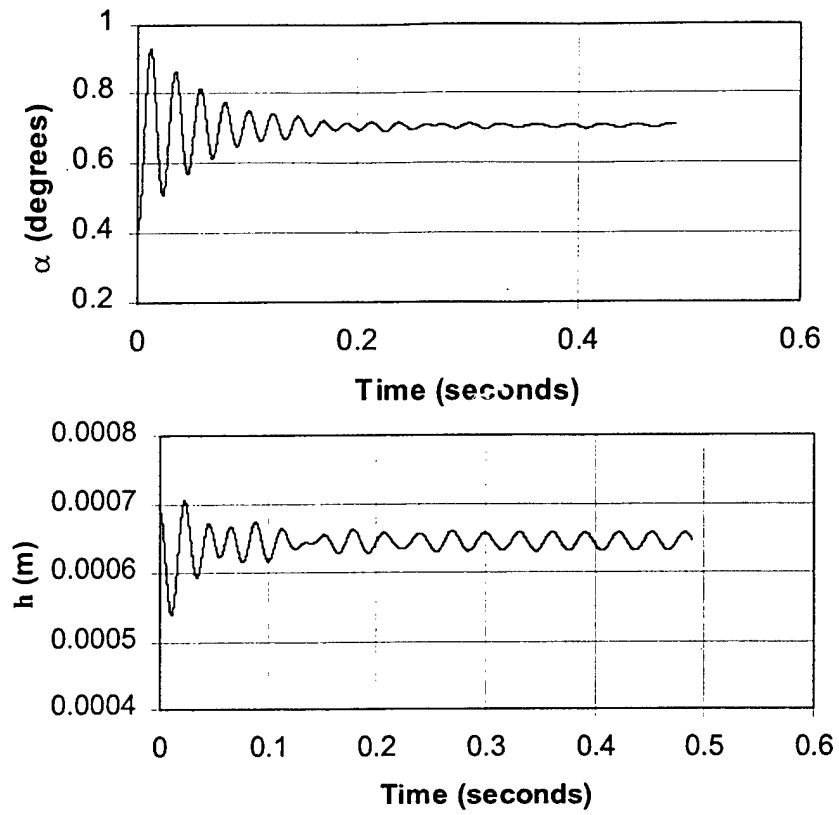
Figure 5.6   Time History at Mach 0.753, AOA=0.6°, q=9.5 kPa, Re=1.727x10^6
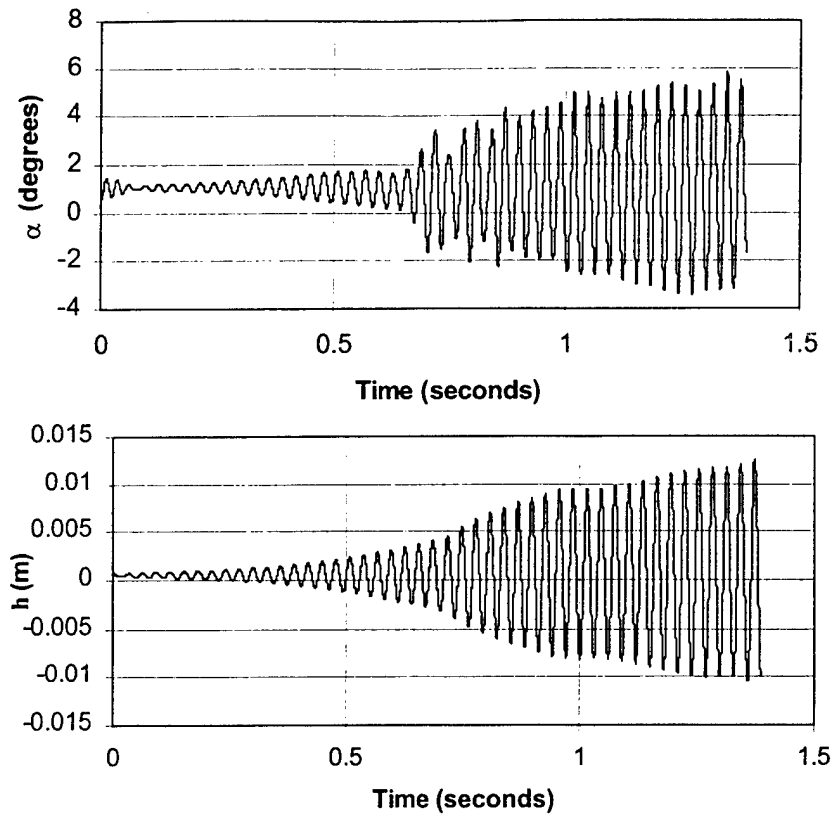
Figure 5.7 Time History at Mach 0.753, AOA=0.6°, q=15 kPa, Re=1.727x10^6

• *LCO Study at M = 0.753 with Various Turbulence Models*

LCO is generally caused by the nonlinearity of a dynamic system. The structural set up of the 2-D supercritical wing section is basically linear, whereas the LCO observed in the experiment results from unsteady nonlinear transonic flow including effects of transonic shock movement and possibly shock-induced separation. This suggests that, in order to correlate with the experimental LCO results, the impact of different turbulence models on the predicted LCO must be studied first. To do this, we first performed a CFL3D computation with the Baldwin-Lomax model at M = 0.753, q_∞ = 12.6 kPa and Re = 1.727 x 10^6. Since the q_∞ = 12.6 kPa condition is already beyond the flutter boundary, an initially divergent motion at small amplitude is expected from the CFL3D result. This is verified by the resulting time histories of the h and α motions presented in Fig 5.8 where the divergent motions up to t = 1.0 sec can be clearly seen. At t = 1.2 sec, a sudden increase of amplitude occurs but the divergent rate of the motion decreases. However, when further extending the time-marching computation from t = 1.5 to 2.8 sec, the divergent motion slows down yet still sustaining and does not reach a steady state oscillation, after 96 hours computation on a 1 GHz computer. In many instances of such LCO computing tasks, the difficulty we faced is that a once started the computation must be carried on typically for several days until a LCO reveals itself. Otherwise, the computation shall be terminated by computing time limitation, if a LCO has not yet been reached by then; this undetermined LCO is marked as a divergent case.

40

Next, the CFL3D computation was repeated at the same flow condition but using the Spalart-Allmaras turbulence model and the result is shown in Fig 5.9. Similar type of divergent motion up to t = 1.0 sec to that of the Baldwin-Lomax model is obtained. But this time, a steady state oscillation is finally reached by extending the time-marching computation up to t = 2.4 sec. The predicted LCO frequency is approximately 34 Hz which correlates well with that of the experiment. But the predicted LCO pitch amplitude is approximately 4° which is off by an order of magnitude comparing to the experimental LCO amplitude (what Schewe measured is 0.6°). Similar disagreement in terms of the LCO amplitude was found by Weber et al (Ref 45). Closer agreement of the LCO amplitude was obtained by Castro et al (Ref 47) where the wind tunnel interference effects was included in their CFD simulation. Note that the interference effect is not considered in the present LCO study and that of Weber et al.
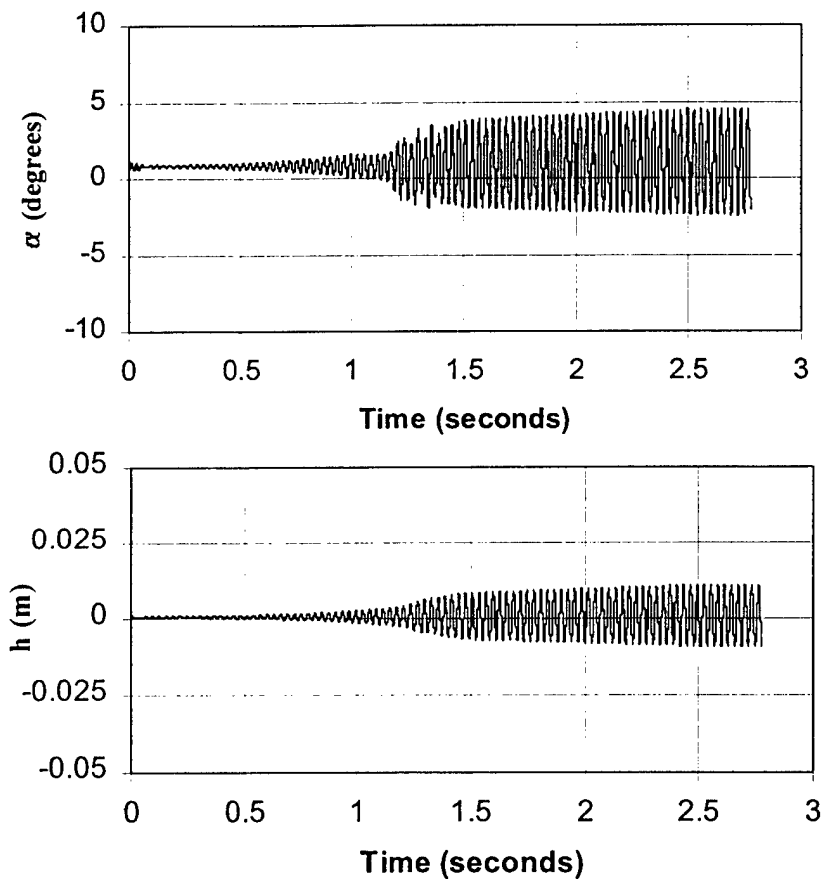
Figure 5.8 LCO Study Using Baldwin-Lomax Model
at Mach 0.753, q=12.6 kPa, Re=1.727x10⁶.
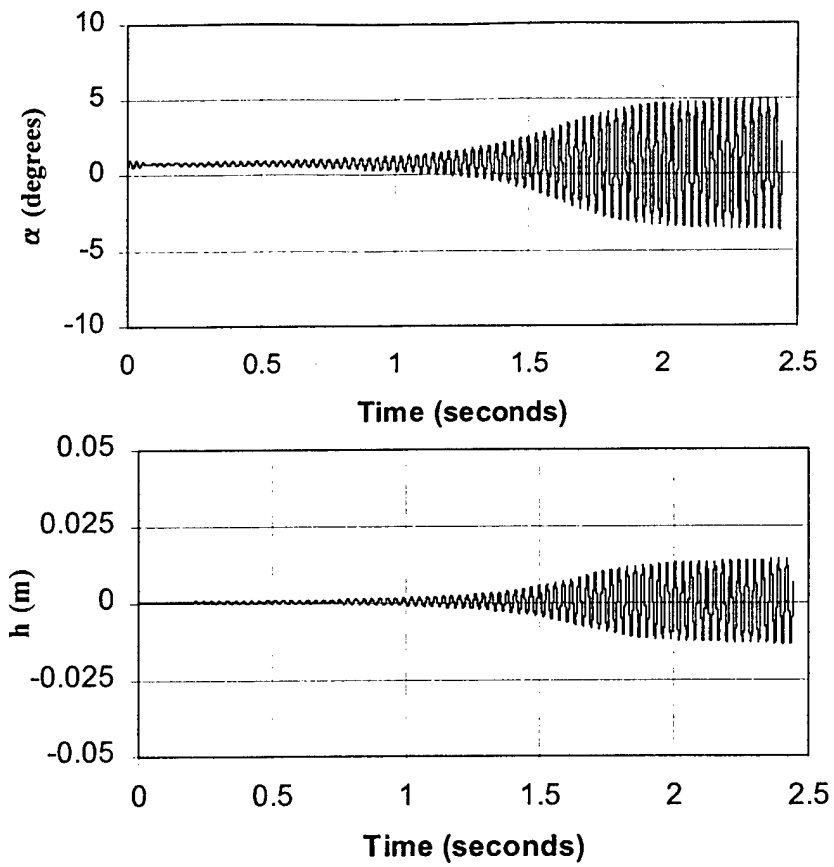
Figure 5.9 LCO Study Using Spalart-Allmaras Model
at Mach 0.753, q=12.6 kPa, Re=1.727x10^6.

CHAPTER 6

PHASES II / III PLAN

Summary

The ZONA Technology/Duke University team proposes a challenging set of tasks to be accomplished in two years time that builds upon the very substantial progress already made in Phase I. Specifically, the 2D, Euler Equations CFD model (developed in Phase I) that uses a harmonic balance solution technique will be extended to include the effects of viscosity (Navier-Stokes equations) and multiple structural modes. In parallel the 3D, Euler Equations CFD time linearized model (also developed in Phase I) which already includes multiple structural modes and uses a POD/ROM solution method will be extended to now include full dynamic nonlinear effects using a harmonic balance solution; and then further extended to include the effects of multi-bodies (e.g. wings plus tip missiles and stores). With each new advance in modeling and solution technique, flutter and LCO analysis and prediction will be made and the results compared to existing data for 2D flow over airfoils and 3D flow over wings and wing/stores. The culminating prediction and analysis will be for the F-16 and F/A-18 aircraft. Based upon the very encouraging results of Phase I using the POD/ROM and Harmonic Balance solution techniques and in comparison with benchmarking calculations using a state-of-the-art time marching 3D flow solver (CFL3D), we anticipate that the computer models to be developed in Phase II (like their Phase I predecessors) will enjoy a very substantial computational efficiency advantage over other existing unsteady CFD models. Typical computer time reductions are expected to be a least two orders of magnitude for LCO calculations and even more for flutter boundary analysis per se.

ZONA Technology, Inc. and Duke University, the ZONA team, jointly hereby propose a three-phase global program entitled *"Nonlinear Reduced-Order Modeling of Limit Cycle Oscillations of Aircraft Wings and Wing/Stores"*. The overall objective of the proposed program is to develop the frequency-domain POD/ROM/HB EigenMode method in order to further the understanding, accurate and efficient prediction, and control of LCO/flutter for aircraft wings and wing/stores.

6.1 Program Goals

The overarching goal for the Phase II work is to build on the very substantial progress made in Phase I and to develop a capability for a highly computationally efficient and physically accurate mathematical modeling of limit cycle oscillations (LCO) and other nonlinear aeroelastic phenomena. The approach uses the concepts of aerodynamic modes as well as structural modes. Such models provide substantially improved physical understanding and also more accurate prediction of LCO in particular and nonlinear aeroelastic responses in general. This capability may also lead to a rational prediction of buffet onset due to aerodynamically nonlinear oscillations. Such models will include the following physical effects:
- Three dimensional (3D) as well as 2D flows
- Nonlinear as well as time linearized aerodynamic pressures and forces
- Multi-body, e.g., wings plus stores, as well as single body (e.g., wing only) configurations
- Many as well as few structural modes
- LCO (nonlinear) as well as flutter (linear) aeroelastic predictions

6.1.1 The Roadmap: Overall Program Approach

In Fig 6.1, a roadmap to achieve this ambitious set of goals is shown. Concluding with Phase III, all of the above capability will be achieved.

CFL3D Time-marching LCO Study

- LCO correlation with experiment for NLR 7301 airfoil
- Assess computer resources needed
- Impact of turbulence models

Determine frequency domain approach to be computationally advantageous

Time-linearized Inviscid Flow

- Single body, i.e. wing
- Multi-structural modes
- POD/ROM technique
- Flutter Analysis
  - transonic dip of AGARD 445.6 wing
  - Assess computer resources needed

Nonlinear Inviscid Flow

- Euler equations by harmonic balance technique
- Single body, i.e. airfoil
- One or two structural modes
- LCO analysis
  -conventional airfoil in transonic flow
  -bending/torsion DOF

Adding harmonic balance

Adding viscosity

Nonlinear Viscous Flow

- N-S equations by harmonic balance
- Single body, i.e. airfoil
- One or two structural modes
- LCO analysis
  - supercritical airfoil in transonic flow
  - flap motion with free-play

Nonlinear Inviscid Flow

- Euler equations by harmonic balance technique
- Single body, i.e. wing
- Multiple structural modes
- LCO analysis
  - business jet wing
  - another wing to be chosen

Adding multi-structural modes

Adding multi-body geometries e.g., stores

Nonlinear Viscous Flow

- N-S equations by harmonic balance
- Single body, i.e. airfoil
- multi-structural modes
- LCO analysis
  - supercritical airfoil in transonic flow
  - 3 DOF motion including control surface with free-play

Nonlinear Inviscid Flow

- Euler equations by harmonic balance
- Multi-body, i.e. wing + store
- Multiple structural modes
- LCO analysis
  - F-16 with store
  - F-18 with store

Adding viscosity

3D Nonlinear Viscous Flow

- N-S equations by harmonic balance
- Multi-body, wing+store
- multi-structural modes
- LCO analysis
  - F-16 with stores and with structural nonlinearity
  - F-18 with stores and with structural nonlinearity

ZONA Funded R&D

Commercialization

DOF = Degree-of-Freedom

Phase I

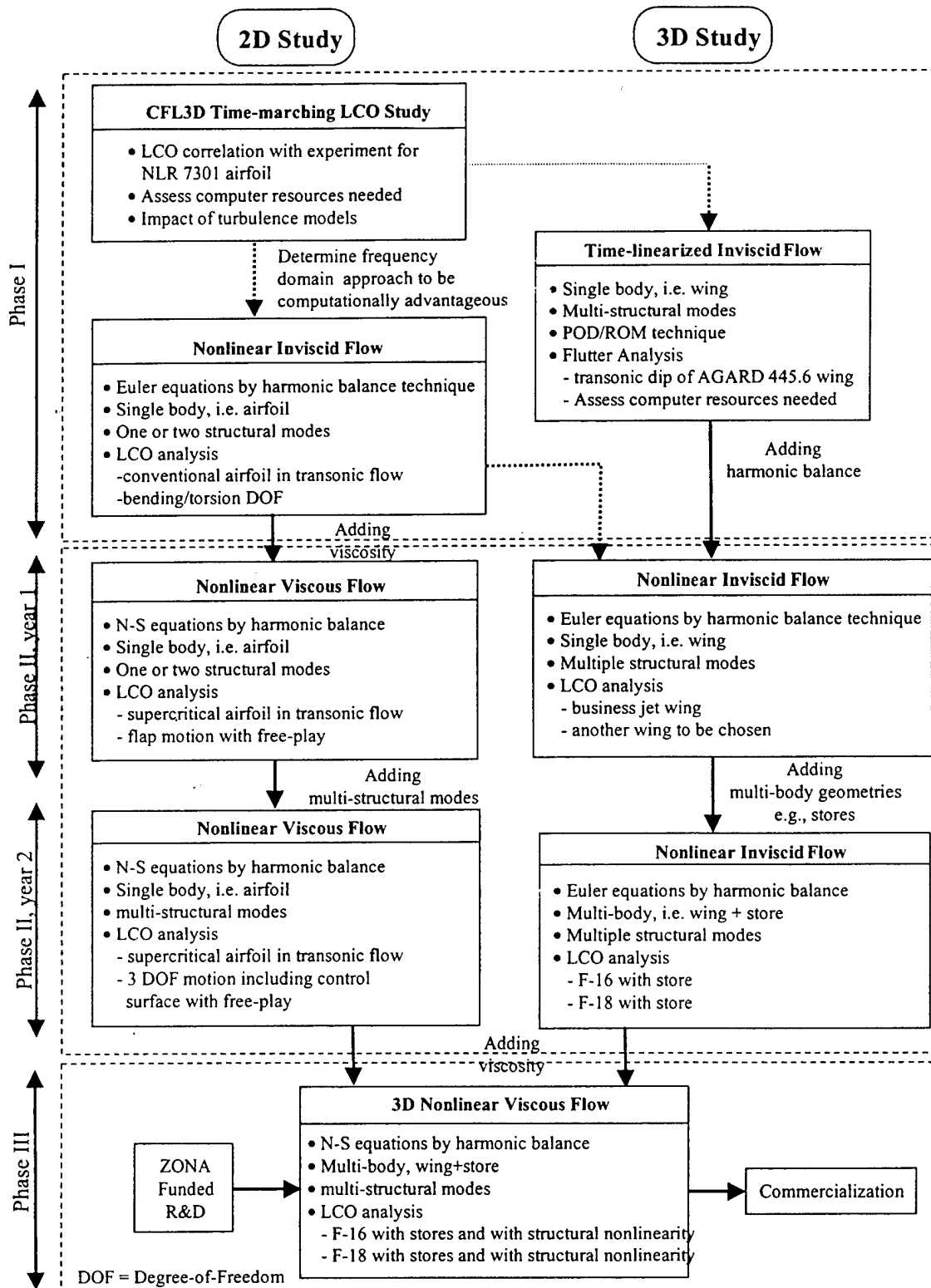Phase II, year 1

Phase II, year 2

Phase III

Figure 6.1   The Roadmap: Overall Program Approach

6.1.2 Brief Description of the Roadmap

Phase I included:
- Feasibility study of a time-marching CFD/N-S method
- Development of the frequency-domain POD/ROM EigenMode and Harmonic Balance methods including 2-D nonlinear LCO/flutter/freeplay case studies
- Development of the 3-D time-linearized frequency-domain POD/ROM EigenMode method including a flutter case study

Phase II will:
- Develop the 2-D N-S version of the above proposed approach
- Extend the geometry capability to 3-D including wing/store configurations
- Generalize the 2-D/3-D methods to include Harmonic Balance technique for nonlinear LCO analysis
- Include multiple structural mode analysis capability
- Perform case studies including F-16 and F-18 wing/store LCO and business jet wing LCO

Phase III will be funded by ZONA with the following goals:
- Accomplish the final step of the development – fully develop a nonlinear 3-D Navier-Stokes version of the proposed method for complex geometry
- Perform LCO for fighters F-16 and F-18 with stores including interaction with structural nonlinearity
- Combine computational advantages of POD/ROM and Harmonic Balance methods
- Once fully developed, a suite of computer codes will be packaged as a software product, ready for commercialization

6.1.3 Discussion of Phases I, II and III

- *Phase I*

In Phase I we have put in place two essential parts of this capability. One is that we have developed a time-linearized 3D aerodynamic model based upon a modal representation using the method of Proper Orthogonal Decomposition(POD). With this aerodynamic model we have performed a transonic flutter analysis for the AGARD 445.6 wing and compared these results to those available in the literature. Our results show good correlation with data obtained by previous investigators while reducing the computational cost for the aeroelastic analysis by several orders of magnitude over more conventional time marching CFD analyses. In this method, an accurate representation of the true aeroelastic eigenvalues and eigenvectors is obtained and thus physically accurate root loci may be obtained. This aeroelastic eigenmode information is very valuable for both improved physical understanding and for use by engineers who will be designing active control devices for aeroelastic systems with smart materials or more conventional control technology. Typically we find fewer than 50 aerodynamic states are needed and often many fewer states may be used with acceptable accuracy. The original CFD models from which the aerodynamic modes are determined have tens of thousands of states in 2D flow and hundreds of thousands or more in 3D flow.

Also in Phase I we have developed a dynamically nonlinear aerodynamic model for 2D flow based upon the harmonic balance method (a Fourier series representing the multi-harmonics of a nonlinear system). This aerodynamic model has been used to analyze LCO and takes into account both fluid and structural nonlinearities. These studies include the first systematic study of LCO due to control surface freeplay in the transonic regime and also have provided new physical insight into LCO arising from aerodynamic nonlinearities due to large shock motion for single degree of freedom flutter as well as aeroelastic divergence. Three abstracts have been prepared and submitted to the 2001 AIAA SDM conference describing the Phase I work and these are included here as appendices for the convenience of the reader.

- *Phase II*

The challenge now is to construct and follow a roadmap that will lead to the ultimate capability that is desired. To that end, consider Fig 6.1 again and now focus on the proposed Phase II effort. In Year 1 of Phase II, the 2D nonlinear aerodynamic inviscid flow model developed in Phase I will be extended to include viscous effects and LCO analyses will be done for a few structural degrees of freedom. This will lead to a significant advance toward our goal of including viscous flow, nonlinear, and multi-structural mode capabilities. In the same year our 3D, time linearized aerodynamic model will be extended to include inviscid nonlinear effects. This latter work also builds upon the achievements of Phase I where 3D and nonlinear effects were first considered separately. In general, our approach to the road map is to add a new capability (such as viscous flow effects or nonlinearities) first in a 2D model and then to use this new understanding as a basis for adding the same capability to the 3D flow models.

In year 2 of Phase II, the 2D aerodynamic model will be brought together with a multi-structural model to demonstrate the feasibility of doing LCO calculations with a many mode model for both the fluid and the structure. Harmonic balance analyses are often used with a relatively small number of modes, but this work will break new ground for models of the size typical of aeroelastic systems, i.e. 10-50 structural modes and a comparable number of aerodynamic modes. In the same year the 3D flow model will be extended to include multi-bodies, e.g. wing plus stores. Such an extension is most important in the context of 3D flows.

However this represents a larger technical risk than if we were to first do this work in 2D flow. Nevertheless we are confident that this work can and be done. LCO analyses will be performed with this code once it is available.

- *Phase III*

With the accomplishments of Phase II, years 1 and 2, in hand a strong foundation for the work of Phase III will be laid. Also the capability already developed in Phase I and the additional capability to be developed in Phase II is itself quite substantial and will represent a marked advance over current methods for LCO and other aeroelastic analyses. In the following sections are discussed two major themes of the proposed new work. The first theme is concerned with novel methods for determining LCO for multi-mode structural systems with the aerodynamic forces represented by 2D or 3D POD/ROM. The second theme addresses the question of how

we plan to add viscosity to our POD/ROM. With respect to the POD/ROM representation of more complex wing and body geometries, our initial approach will be to acquire and use existing methodologies for conventional CFD codes, e.g., the needed more complex computational grids, and then simply apply our POD/ROM methodology to those more elaborately gridded CFD models. We anticipate this approach will be successful. However, we are prepared to consider enhancements of existing CFD methods, if that proves to be needed. For the determination of LCO and the inclusion of viscosity we anticipate the need for new methodology developments and hence those are discussed in section 5.0.

6.1.4 The ZONA/Duke Team

ZONA Technology, Inc. (ZONA) and Duke University (Duke) have formed a strong team with a comprehensive background to handle this challenging project. Professor Hall (P.I.) and Professor Dowell, one of the world's leading aeroelasticians, at Duke are the originators of the proposed ROM/POD method, which has gained much attention in the aerospace community in recent years.

P.C. Chen (P.I.) and Danny D. Liu at ZONA are the small business counterpart for this project. For over a decade, ZONA continues to perfect the proven technology in aeroelastic software such as the ZONA51 code in MSC/NASTRAN (Aero Option II), now an industrial standard for supersonic aeroelastic analysis. Meanwhile, ZONA has an outstanding record in handling U.S. government contracts as evidenced by ZONA's successful performance in five ongoing contracts (since 1995): supported by AFRL/VA (on ASTROS* and VSS), by NAWC/Navy (on Missile Fin Aeroelastic Tailoring), and by NASA/Langley (on BEM Solver for CFD/CSD Interfacing), by NAVAIR/Navy (on Reconfigurable Adaptive Control of LCO and ASE instability), by NAVSEA/Navy (on ERGM Projectile Smart Structure Control). ZONA was awarded three SBIR/Phase II contracts from the above organizations in 1999. This STTR effort between ZONA and Duke is supported by Boeing as evidenced by the following endorsement letter from Mr. Rudy Yurkovich.

6.2 Phase II Objective and Anticipated Benefits

The overall Phase II technical objective is to develop a highly computationally efficient and physically accurate mathematical modeling of nonlinear aeroelastic phenomena. Such models provide substantially improved physical understanding and also more accurate prediction of nonlinear aeroelastic phenomena such as LCO.

Technical Objectives

Based on the very substantial progress made in Phase I, we will achieve the following specific objectives in Phase II:

1. Development of a 2-D viscous version of the harmonic balance technique.
2. Extension of the geometry capability to 3-D including aircraft/store configurations.
3. Generalization of the 2-D/3-D methods to include harmonic balance technique for LCO analysis involving aerodynamic and structural nonlinearities.

47

4. Inclusion of multiple structural mode capability for large finite element models of aircraft with stores.
5. Validation of the above methodologies by performing case studies including F-16 and F/A-18 wing/store LCO and a business jet wing LCO.

Anticipated Benefits

Once the Phase II technical objective is achieved, its anticipated benefits are:

1. The technical advantages of the proposed approach over the conventional time-marching CFD method are as follows:
- Computational efficiency
- Nonlinear LCO prediction capability
- True aeroelastic damping solutions can be obtained

2. Once fully developed, the proposed method will benefit the AF and the aerospace community in the following areas;
- Becomes an efficient aeroelastic/flutter tool for the industry
- Promotes an understanding in the origins of LCO, thus providing effective means to control LCO
- Prediction technique will help resolve the wing/store LCO of F-16 and F-18 aircraft, a solution urgently needed by Lockheed Martin, Boeing and AF.
- Address the transonic tail buzz problem of many next generation aerospace vehicles (e.g., F-22, JSF, X-33, X-34, etc.)
- Provides a sound foundation and efficient database in frequency-domain for effective transonic aeroservoelasticity (ASE) and MDO applications.

6.3   Phase II Work Plan

The ZONA/Duke team proposes a two-year effort to accomplish the technical objectives of Phase II. In order to clearly illustrate the Phase II work plan and its interrelationship with Phase I and Phase III, we present an overall program task chart shown in Fig 6.2. This overall program task chart is derived from the roadmap of Section 2.0 and explicitly specifies the tasks involved in the overall program

	2-D STUDY					3-D STUDY						
	TL	HB	N-S	SM	MM	TL	HB	N-S	SW	W/S	SM	MM
Phase I	●	●		●		⊖ 445.6			●			●
Phase II (yr 1)		●	⊖ DLR	◆		●	●		⊖ BIZ JET			
Phase II (yr 2)		●	●		◆	●	●			⊖ F-16/18		◆
Phase III						●	●	●	⊖ BIZ JET	⊖ F-16/18		◆

●   Yes

⊖   LCO Validation with Test

◆   Yes, plus Nonlinear Structure

TL = Time-Linearized (Euler), HB = Harmonic Balance (Nonlinear),
N-S = Navier-Stokes (Add viscosity), SM = Several Structural Modes,
MM = Multiple Structural Modes, SW = Single Wing, W/S = Wing/Store

Figure 6.2   Alternative Chart to Roadmap

The Phase II development is planned according to guidelines: (see Fig 6.1 Roadmap)

- Nonlinearities that produce LCO are of two types: aerodynamic and structural. In Phase II, we will develop models that can analyze both types of nonlinearities in a unified way. At the end of Phase II, we will have the capability to analyze cases in which the structure alone is nonlinear, and both the fluid and structure are nonlinear.

- The complexity of the aeroelastic system increases as Phase II advances:
  - *Geometry*:   2-D → 3-D/Single Wing → 3-D Wing/Store
  - *Equation Hierarchy*:   Euler → Navier-Stokes
  - *Nonlinearity*:   Time Linearized Approach → Harmonic Balance Approach
  - *Mode*:   Single Degree of Freedom → Multiple Degree of Freedom
  - *Structural Nonlinearity*:   Linear Structure → Nonlinear Structure

In this section, the theoretical formulation of the methodologies shown in Fig 6.1 will be presented in details (Sections 6.3.1 – 6.3.7). Selected test cases involving a single wing and two fighter aircraft with stores configurations are presented in Section 6.3.8. Phase II statement of work consisting of 11 main tasks are discussed in Section 6.3.9. Program Schedule and Deliverables are shown in Sections 6.3.10 and 6.3.11, respectively.

6.3.1 Three-Dimensional Navier-Stokes and Euler Equations

We start with the top-down approach:

The 3-D Reynolds-Averaged Navier-Stokes Equations read:

$$\frac{\partial U}{\partial t} + \frac{\partial(F - F_v)}{\partial x} + \frac{\partial(G - G_v)}{\partial y} + \frac{\partial(H - H_v)}{\partial z} = 0 \qquad (6.1)$$

where:

$$U = \begin{Bmatrix} \rho \\ \rho u \\ \rho v \\ \rho w \\ \rho e \end{Bmatrix}, \quad
F = \begin{Bmatrix} \rho u \\ \rho u^2 + p \\ \rho u v \\ \rho u w \\ \rho u h \end{Bmatrix}, \quad
G = \begin{Bmatrix} \rho v \\ \rho u v \\ \rho v^2 + p \\ \rho v w \\ \rho v h \end{Bmatrix}, \quad
H = \begin{Bmatrix} \rho w \\ \rho u w \\ \rho v w \\ \rho w^2 + p \\ \rho w h \end{Bmatrix}$$

$$F_v = \begin{Bmatrix} 0 \\ \tau_{xx} \\ \tau_{xy} \\ \tau_{xz} \\ \tau_{xx}u + \tau_{xy}v + \tau_{xz}w \end{Bmatrix}, \quad
G_v = \begin{Bmatrix} 0 \\ \tau_{yx} \\ \tau_{yy} \\ \tau_{yz} \\ \tau_{yx}u + \tau_{yy}v + \tau_{yz}w \end{Bmatrix}, \quad
H_v = \begin{Bmatrix} 0 \\ \tau_{zx} \\ \tau_{zy} \\ \tau_{zz} \\ \tau_{zx}u + \tau_{zy}v + \tau_{zz}w \end{Bmatrix}$$

and ρ, p, (u, v, w), e, h are the flow density, pressure, velocity, energy and enthalpy, respectively. $\tau_{xx}, \tau_{xy}, \tau_{xz}, \ldots$, etc are the Reynolds stress tensors.

In what follows, we will reduce Eq (6.1) to 3-D and 2-D Euler equations for the convenience of elucidating the frequency-domain POD/ROM approach.

6.3.2 Harmonic Balance

In Phase I, the importance of aerodynamic nonlinearities on LCO was assessed using a novel two-dimensional harmonic balance (H.B.) technique. With this approach, the unsteady flow variables can be represented by a Fourier Series in time with spatially varying coefficients. This assumption leads to a set of harmonic balance Euler equations, which can be solved efficiently using conventional CFD methods including time marching with local time stepping and multi-grid acceleration. The two-dimensional Euler equations are:

$$\frac{\partial U}{\partial t} + \frac{\partial F}{\partial x} + \frac{\partial G}{\partial y} = 0 \qquad (6.2)$$

where the flux vectors U, F and G are given by

$$U = \left\{ \begin{array}{c} \rho \\ \rho u \\ \rho v \\ \rho w \\ \rho e \end{array} \right\}, \quad F = \left\{ \begin{array}{c} \rho u \\ \rho u^2 + p \\ \rho uv \\ \rho uw \\ \rho uh \end{array} \right\}, \quad G = \left\{ \begin{array}{c} \rho v \\ \rho uv \\ \rho v^2 + p \\ \rho vw \\ \rho vh \end{array} \right\}, \quad H = \left\{ \begin{array}{c} \rho w \\ \rho uw \\ \rho vw \\ \rho w^2 + p \\ \rho wh \end{array} \right\} \tag{6.3}$$

Next, representing conservation prime variables by sum of harmonics of fundamental frequency gives:

$$\rho(x, y, t) = \sum_n R_n(x, y) e^{i\omega nt}, \quad \rho u(x, y, t) = \sum_n U_n(x, y) e^{i\omega nt}$$

$$\rho v(x, y, t) = \sum_n V_n(x, y) e^{i\omega nt}, \quad \rho e(x, y, t) = \sum_n E_n(x, y) e^{i\omega nt} \tag{6.4}$$

Requiring each frequency component to vanish independently (harmonic balance) and collecting terms of like harmonics results in

$$\frac{\partial \overline{U}(V)}{\partial t} + \frac{\partial \overline{F}(V)}{\partial x} + \frac{\partial \overline{G}(V)}{\partial y} = 0 \tag{6.5}$$

where

$$V = \left\{ \cdots R_0, \ U_0, \ V_0, \ E_0, \ R_{+1}, \ U_{+1}, \ V_{+1}, \ E_{+1} \cdots \right\}^T \text{ and}$$

$$\frac{\partial \overline{U}}{\partial t} = i\omega \left\{ \cdots 0 \cdot R_0, \ 0 \cdot U_0, \ 0 \cdot V_0, \ 0 \cdot E_0, \ +1 \cdot R_{+1}, \ +1 \cdot U_{+1}, \ +1 \cdot V_{+1}, \ +1 \cdot E_{+1} \right\}^T \tag{6.6}$$

By adding a 'pseudo-time' term, Eq (6.5) can be solved by a conventional CFD solution, i.e.,

$$\frac{\partial V}{\partial \tau} + \frac{\partial \overline{F}(V)}{\partial x} + \frac{\partial \overline{G}(V)}{\partial y} + \frac{\partial \overline{U}(V)}{\partial t} = 0 \tag{6.7}$$

Note that harmonic balance equations are similar in form to original Euler equations. Thus, existing Euler codes can be modified to solve H.B. equations. A two-step Lax-Wendroff scheme will be used. Also, since only "steady-state" solution is desired, one can use local time stepping, multiple-grid acceleration techniques and residual smoothing to speed convergence. The method is computationally very efficient, at least one to two orders-of-magnitude faster than nonlinear time-domain CFD simulations.

In Phase II, we will use the two-dimensional, nonlinear, harmonic balance aerodynamic code and add viscosity terms, i.e., we will develop a Navier-Stokes version of this analysis suitable for the analysis of oscillating airfoils. In addition, we will use this code to perform LCO analysis and prediction for simple structural models, e.g. plunge and pitch of a typical section for conventional and supercritical airfoils. In particular, we will perform correlation studies with the DLR experimental data of the NLR 7301 LCO case.

In Phase I, a three-dimensional time-linearized unsteady aerodynamic analysis was developed. In Phase II, this code will be converted to a harmonic balance analysis of three-dimensional inviscid transonic flows. We will use this three-dimensional analysis to perform LCO analyses of simple linear wing structural models. We will perform LCO correlation studies with a business jet wing or other wing to be determined.

In passing, we note the following when using aeroelastic eigenmodes for LCO prediction. The harmonic balance method has proven to be a very effective method for determining limit cycle oscillations (LCO) and other nonlinear responses of aeroelastic systems. It is often more computationally efficient and gives greater physical insight than, for example, time marching simulations. On the other hand it has some limitations, e.g. it does not allow an investigation of the possible dependence of the response on the initial conditions. Nor does it allow a precise assessment of non-periodic and chaotic motions. At best the harmonic balance method can only approximate a non-periodic motion. In practice these limitations are not often serious drawbacks; however these observations do suggest that future work may well involve a balanced consideration of both time simulations and frequency domain (harmonic balance) studies.

Another consideration is the number of harmonics to be retained in a harmonic balance analysis. If there is a dominant harmonic, a single harmonic may suffice, although it will be important to assess the effects of higher harmonics on the fundamental harmonic per se. And finally the algebraic complexity of using the method for multi-modal systems may quickly get out of hand unless special measures are taken to deal with this issue. We will return to this latter issue as, even with reduced order aerodynamic modeling of the structure and fluid, the order of the reduced model will be larger than that often encountered in classical harmonic balance analyses, i.e., on the order of several tens of states.

6.3.3 Time-Linearized Flow Three-Dimensional Flow Solver

In Phase I, we developed a three-dimensional time-linearized Euler analysis of unsteady flow about a wing. We start with the assumption that the unsteady flow $\hat{u}(x,y,z,t)$ may be expanded in a perturbation series of the form

$$\hat{u}(x,y,z,t) = U(x,y,z,t) + u(x,y,z)e^{i\omega t} \tag{6.8}$$

where $U(x,y,z,t)$ represents the steady background flow, and $u(x,y,z)$ is the complex amplitude of the unsteady small-disturbance flow arising from the wing vibration, which vibrates at frequency ω. Substituting Eq (6.8) into the nonlinear three-dimensional Euler equations, and expanding the result in a perturbation series in the small-disturbance quantities, one finds that to zeroth and first order the governing equations reads respectively

$$\frac{\partial F(U)}{\partial x} + \frac{\partial G(U)}{\partial y} + \frac{\partial H(U)}{\partial z} = 0 \tag{6.9}$$

$$i\omega\mathbf{u} + \frac{\partial}{\partial x}\left(\frac{\partial \mathbf{F}}{\partial \mathbf{U}}\mathbf{u}\right) + \frac{\partial}{\partial y}\left(\frac{\partial \mathbf{G}}{\partial \mathbf{U}}\mathbf{u}\right) + \frac{\partial}{\partial z}\left(\frac{\partial \mathbf{H}}{\partial \mathbf{U}}\mathbf{u}\right) = 0 \qquad (6.10)$$

In a conventional time-linearized analysis, Eq (6.9) and Eq (6.10) are solved using pseudo time marching and standard CFD techniques. Note that since time does not appear explicitly in either equation, they both may be solved using computational acceleration techniques such as multiple grid acceleration, local time stepping, and residual smoothing. The result is that these two equations can be solved at a fraction of the cost of solving the full nonlinear Euler equations using conventional time marching.

In Phase I, a simple clean wing model was developed. This CFD analysis used a simple grid structure that limited the approach to clean wings. In Phase II, this model will be extended to allow more complicated grid topologies, which will allow us to analyze multi-body configurations, e.g. wing/store.

6.3.4 Reduced Order Modeling of Time-Linearized Aerodynamic Models

Having developed a three-dimensional time-linearized flow solver, we next consider the reduction of that model using proper orthogonal decomposition techniques (POD). The idea behind the frequency domain proper orthogonal decomposition is a simple one. We first calculate the small-disturbance response of the aerodynamic system at M different combinations of frequency and excitation. The solutions, also called "snapshots," are denoted by $\mathbf{q}^m$ for $m=1,2,...,M$. These snapshots are then linearly combined to for a smaller number of basis vectors ϕ_k for $k=1,2,...,K$ where $K<M$. In other words,

$$\phi_k = \mathbf{Q}\mathbf{v}_k \text{ for } k = 1,2,...,K \qquad (6.11)$$

where the mth column of $\mathbf{Q}$ is just $\mathbf{q}^m$. In the proper orthogonal decomposition technique, the vectors $\mathbf{v}_k$ are found by solving a small eigenvalue problem of the form

$$\mathbf{Q}^H\mathbf{Q}\mathbf{v}_k = \lambda_k\mathbf{v}_k \qquad (6.12)$$

Only the eigenvectors $\mathbf{v}_k$ with the largest eigenvalues λ_k are used to form basis vectors defined by Eq (6.11). $\mathbf{Q}^H$ is the Hermitian of $\mathbf{Q}$.

Having computed the POD basis vectors, we assume that they will provide a useful basis for computing the unsteady solution at some other frequency and/or external excitation than was use to general the original snapshots. Thus, we let

$$\mathbf{q} = \Phi\xi \qquad (6.13)$$

where Φ is an $N \times K$ matrix whose k^{th} column is simply the basis vector ϕ_k, and ξ is a vector of aerodynamics state variables.

We note that when discretized, Eq (6.10) has the form

$$\mathbf{A}\mathbf{q} = \mathbf{A}_0\mathbf{q} + i\omega\mathbf{A}_1\mathbf{q} = \mathbf{b}_0 + i\omega\mathbf{b}_1 \qquad (6.14)$$

53

where $\mathbf{A}_0$ and $\mathbf{A}_1$ are independent of the excitation frequency ω, and are purely real, and $\mathbf{q}$ is the vector containing $\underline{u}$ at all the nodes of the CFD grid.

Substitution of Eq (6.11) into Eq (6.14), and projection of the error onto the space spanned by the basis vectors gives

$$\Phi^H \mathbf{A} \Phi \xi = \mathbf{A}_R \xi = \Phi^H \mathbf{b} \qquad (6.15)$$

Finally, the reduced-order aerodynamic matrix $\mathbf{A}_R$, which is much smaller than the original aerodynamic matrix $\mathbf{A}$, is factored using LU decomposition, and Eq (6.15) is solved for the unknown aerodynamic state variables. This step is computationally very efficient because the reduced-order aerodynamic matrix is small, sometimes as small as 10x10, but rarely larger than 100x100. The major expense in constructing the reduced-order aerodynamic model is the computation of the snapshots; the cost of finding the basis vectors and solution to Eq (6.15) is negligible by comparison.

Having described the basic reduced-order modeling technique, we next describe how to incorporate an aerodynamic reduced-order model into an aeroelastic model of flutter. Consider, for example, a two degree-of-freedom structural dynamic model of a typical section. The governing equations of motion are of the form

$$\mathbf{M}\ddot{\mathbf{h}} + \mathbf{K}\mathbf{h} = \mathbf{f} \quad \text{where} \quad \mathbf{h} = \{h, \alpha\}^T \qquad (6.16)$$

and h and α are the plunging and pitching degrees of freedom of the typical section. $\mathbf{M}$ and $\mathbf{K}$ are the mass and stiffness matrices, respectively.

Note that the aerodynamic force vector $\mathbf{f}$ is obtained from integrals involving the pressure at the surface of the airfoil. When discretized, these integrals may be expressed as

$$\mathbf{f} = \mathbf{C}q \qquad (6.17)$$

where $\mathbf{C}$ is a sparse 2xN matrix. Similarly, for the case of airfoil vibration, the vector $\mathbf{b}$ on the right-hand side of Eq (6.14) can be expressed as

$$\mathbf{b} = \mathbf{b}_0 + i\omega\mathbf{b}_1 = \mathbf{B}_0\mathbf{h} + i\omega\mathbf{B}_1\mathbf{h} \qquad (6.18)$$

where now we have made the assumption that the airfoil motion is harmonic in time although ω may be complex). For large CFD models, finding the eigenvalues is prohibitively expensive. To reduce the size of the model, we again assume that the number of aerodynamic states can be reduced using Eq (6.13). Again, projecting the error of the aerodynamic equations onto the space spanned by the aeroelastic basis vectors gives the desired reduced-order aeroelastic model, i.e.,

$$\begin{bmatrix} \mathbf{A}_{R_0} & -\Phi^H\mathbf{B}_0 & -\Phi^H\mathbf{B}_1 \\ 0 & 0 & \mathbf{I} \\ -\mathbf{C}\Phi & \mathbf{K} & 0 \end{bmatrix} \begin{Bmatrix} \xi \\ \mathbf{h} \\ \dot{\mathbf{h}} \end{Bmatrix} + i\omega \begin{bmatrix} \mathbf{A}_{R_1} & 0 & 0 \\ 0 & -\mathbf{I} & 0 \\ 0 & 0 & \mathbf{M} \end{bmatrix} \begin{Bmatrix} \xi \\ \mathbf{h} \\ \dot{\mathbf{h}} \end{Bmatrix} = 0 \qquad (6.19)$$

54

6.3.5 Reduced-Order Aeroelastic Model for Multi-Degree-Of-Freedom Structures

In Eq (6.19), we have derived a reduced-order aeroelastic model for a two degree of freedom (2 d.o.f.) structure, i.e., $\mathbf{h} = \{h, \alpha\}^T$. For multi-degree-of-freedom structures, $\mathbf{h}$ can also be interpreted as the displacements of each degree of freedom in the structural model. In this situation, the size of Eq (6.19) becomes $K+2n$, where n is the number of structural degrees of freedom. For a realistic wing structural model, n can be on the order of thousands, rendering Eq (6.19) a very large size eigenvalue problem. Solving such a large eigenvalue problem would practically be impossible.

The Modal Approach

To circumvent this problem, we introduce the so-called "*modal approach*" to Eq (6.19). The modal approach approximates $\mathbf{h}$ by the superposition of the low-order structural modes, i.e.,

$$\mathbf{h} = \Psi_a \eta \tag{6.20}$$

where Ψ_a is the modal matrix whose columns contain the modal data of the low-order structural modes and η are is the generalized coordinate vector. Since the magnitude of the modes can be arbitrary, they are usually normalized by the square root of their respective generalized masses, giving a unit generalized mass matrix. The justification for using the modal approach is based on the premise that most of the aeroelastic responses are dominated by the lower-order structural modes. Usually, for a single wing structure, the lowest ten (10) structural modes are sufficient to accurately represent $\mathbf{h}$. Substituting Eq (6.20) into Eq (6.19) and pre-multiplying the second and third rows of Eq (6.19) by Ψ_a^T yields

$$\begin{bmatrix} \mathbf{A}_{R_0} & -\Phi^H \mathbf{B}_0 \Psi_a & -\Phi^H \mathbf{B}_1 \Psi_a \\ 0 & 0 & \left[\dfrac{1}{m_i}\right] \\ -\Psi_a^T \mathbf{C}\Phi & \left[\omega_{n_i}^2\right] & \left[2\omega_{n_i}\zeta\right] \end{bmatrix} \begin{Bmatrix} \xi \\ \eta \\ \dot{\eta} \end{Bmatrix} + i\omega \begin{bmatrix} \mathbf{A}_{R_1} & 0 & 0 \\ 0 & \left[\dfrac{1}{m_i}\right] & 0 \\ 0 & 0 & \mathbf{I} \end{bmatrix} \begin{Bmatrix} \xi \\ \eta \\ \dot{\eta} \end{Bmatrix} = 0 \tag{6.21}$$

where ω_{n_i} and m_i are the natural frequency and the generalized mass of the ith structural mode, respectively. Now, the size of Eq (6.21) becomes $K+2m$, where m is the number of structural modes. Because m is much less than the number of structural d.o.f. n, the size of the aeroelastic system is substantially reduced.

The Structural/Modal Damping

Note that a structural/modal damping matrix $\begin{bmatrix} \ddots & \\ & 2\omega_{n_i}\zeta \\ & & \ddots \end{bmatrix}$ has been added to Eq (6.21). With this added matrix, Eq (6.21) will facilitate our subsequent study of LCO. In an earlier LCO study, ZONA has suggested that the structural damping could play a decisive role in LCO for a

55

wing/store system. For LCO study using the proposed method, one could alternatively use Eq (6.21) to delineate the effects with and without structural damping. Also note that the modal approach in fact increases the sparseness of the matrices in Eq (6.21). Thus, the eigenvalue problem of Eq (6.21) can be solved more efficiently by a sparse eigensolver.

6.3.6 Structural Compatible Reduced-Order Aeroelastic Model

One of the technical issues involved in the CFD aeroelastic computations is the displacement transferal from the structural finite element grid to the CFD surface grid. This technical issue arises from the problem where the CFD surface grid and the structural finite element (FEM) grid are considerably different; in their locations and densities. Solving such a displacement transferal problem of complex configuration such as whole aircraft with external stores is by no means a trivial task.

In March 1999, ZONA received a two-year contract from NASA/Langley (Ref 21) to develop a Boundary Element Method (BEM), called the BEM Solver, for the data transferal between the FEM grid and the CFD surface grid (see Section 6.1, ZONA's Related Work). By formulating the data transferal problem as an equivalent solid mechanics problem, the BEM Solver generates a universal spline matrix [S] which relates the displacements at the FEM grid to the CFD grid such that

$$\Psi_a = S \Psi_s \tag{6.22}$$

where Ψ_a and Ψ_s are, respectively, the modal matrix at the CFD grid and at the FEM grid. With the universal spline matrix [S] at hand, converting Eq (6.21) to a structural-compatible reduced-order aeroelastic model is straightforward. Substituting Eq (6.22) into Eq (6.21) gives:

$$
\begin{bmatrix}
A_{R_0} & -\Phi^H B_0 S \Psi_s & -\Phi^H B_1 S \Psi_s \\
0 & 0 & \left[\dfrac{1}{m_i}\right] \\
-\Psi_s^T S^T C \Phi & \left[\omega_{n_i}^2\right] & \left[2\omega_{n_i}\zeta\right]
\end{bmatrix}
\begin{Bmatrix} \xi \\ \eta \\ \dot{\eta} \end{Bmatrix}
+ i\omega
\begin{bmatrix}
A_{R_1} & 0 & 0 \\
0 & \left[\dfrac{1}{m_i}\right] & 0 \\
0 & 0 & I
\end{bmatrix}
\begin{Bmatrix} \xi \\ \eta \\ \dot{\eta} \end{Bmatrix} = 0 \tag{6.23}
$$

Finally, we arrive at the structural-compatible, modal-based, reduced-order aeroelastic model, Eq (6.23). The size of this model is $K+2m$, where m is the number of low-order structural modes and is usually on the order of ten for a single wing structure. Eq (6.23) contains two very sparse matrices that can be solved efficiently by a sparse eigenvalue solver.

6.3.7 Modeling LCO of High Degree-of-Freedom Nonlinear Systems

The nonlinear system that we wish to model can for the most part be modeled as quasi-linear nonlinear vector equations of the form

56

$$i\omega\mathbf{Mq} + \mathbf{N(q)} = 0 \qquad\qquad (6.24)$$

where q is a very large matrix arising containing the Fourier coefficients of the unknowns in a harmonic balance analysis, M is the a constant matrix, and N is a nonlinear vector operator arising from the harmonic balance analysis. Here q would contains the unknown flow solution in the three-dimensional harmonic balance of the three-dimensional flow field, and also the structural dynamic modes. Thus, the system may contain hundreds of thousands of degrees of freedom. This system of equations is solved using pseudo-time time marching. Thus, Eq (6.24) is solved by marching the equation

$$\frac{\partial \mathbf{q}}{\partial t} + i\omega\mathbf{Mq} + \mathbf{N(q)} = 0 \qquad\qquad (6.25)$$

in time until a steady state is reached. However, if ω is not known accurately, then Eq (6.25) will not converge, but will itself go into a mathematical limit cycle. One can show, however, that the solution q will be nearly correct. The solution can be improved by first computed a better estimate for ω using a nonlinear Rayleigh quotient, i.e.

$$\omega \approx \frac{\mathbf{q}^{H}\mathbf{N(q)}}{\mathbf{q}^{H}\mathbf{M}^{H}\mathbf{M(q)}} \qquad\qquad (6.26)$$

Eq (6.25) can then be marched again to improve the estimate of q. This process can be repeated until convergence. The result is a description of the LCO behavior of a very high dimensional system, i.e. a nonlinear CFD model coupled to a linear or nonlinear structural model. If Phase II, this technique will be applied to the harmonic balance flow solver coupled to a linear and/or nonlinear structure.

6.3.8   Selection of Test Cases

Test cases for the validation of the proposed methodology include:
- NLR 7301 supercritical airfoil transonic LCO case
- MAVRIC-I (Aeroelastic Validation Research Involving Computations) business jet wing LCO case
- Three F-16/Store LCO cases
- Five F/A-18/Store LCO cases

NLR 7301 Supercritical Airfoil Transonic LCO Case

The details of this case has already been discussed in Chapter 5. This case is selected to validate the 2-D nonlinear harmonic balance aerodynamic code using the Euler equations and the Navier-Stokes equations. The accuracy of the 2-D nonlinear harmonic balance aerodynamic code will be assessed by comparing its predicted LCO frequency and amplitude with the DLR experimental data whereas the efficiency will be assessed by comparing its computer time with the CFL3D time-marching computations.

MAVRIC-I Business Jet Wing LCO Case

MAVRIC-I business jet wing is an ongoing wind tunnel test program of NASA/Langley aeroelasticity branch. The model is constructed with a simple stepped aluminum plate providing the wing stiffness and fitted with end-grain balsa wood to provide the wing contour. Previous experiment has shown that in the 0.8 to 0.9 Mach number range, the model motions were predominantly in the first wing-bending mode and exhibited LCO.
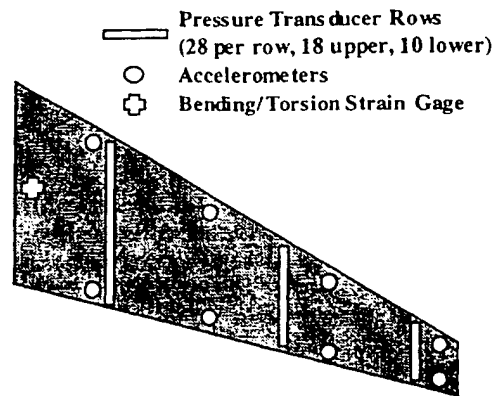

Figure 6.3   Instrumentation Layout for Refurbished MAVRIC-I Business Jet Wing Model

Currently, the model is being re-tested in the Transonic Dynamic Tunnel (TDT) as the MAVRIC-I. Fig 6.3 indicates the location of instrumentation that has been added to the model. Three chords of unsteady pressure transducers are installed at span stations 0.22, 0.63 and 0.87. Each chord has 28 upper surface and 18 lower surface close-mounted transducers. Eight accelerometers are mounted along the leading and trailing edge of the wing and bending/torsion strain gages are installed at the root. The intent of the retest is to obtain unsteady pressure and wing response data under conditions of LCO in order to validate CFD codes for such conditions. This retest program will be complete within 6-9 months.

Because of its simple finite element modeling and simple aerodynamic geometry, the MAVRIC-I business jet wing model is an ideal LCO test case for validating the 3-D harmonic balance code for single body (to be developed in the first year of Phase II). Because all harmonics of the measured time-domain unsteady pressures at LCO can be easily obtained by a Fourier series techniques, a detailed pressure distribution comparison between the measurements and the prediction by 3-D harmonic balance code in terms of frequency-domain harmonics can be performed. Of course, the comparison of LCO frequency and amplitude at various Mach numbers and dynamic pressures will also be conducted.

Three F-16/Store LCO Cases

Through a collaboration project with Lockheed Martin Tactical Aircraft System and Eglin Air Force Base (see Section 6.1, ZONA's Related Work), ZONA has established a large database of the F-16/store configurations including their finite element models and flight test LCO data. In general, the F-16 aircraft with various stores has experienced three types of LCO; (1) LCO starts from M = 0.6 and disappears at M > 1.0. This case is denoted as "F-16 LCO Type A". (2) LCO appears only in the transonic flight regime. This case is denoted as "F-16 LCO Type B". (3) LCO starts from the transonic Mach numbers and sustains into the supersonic flight regime. This case is denoted as "F-16 LCO Type C".
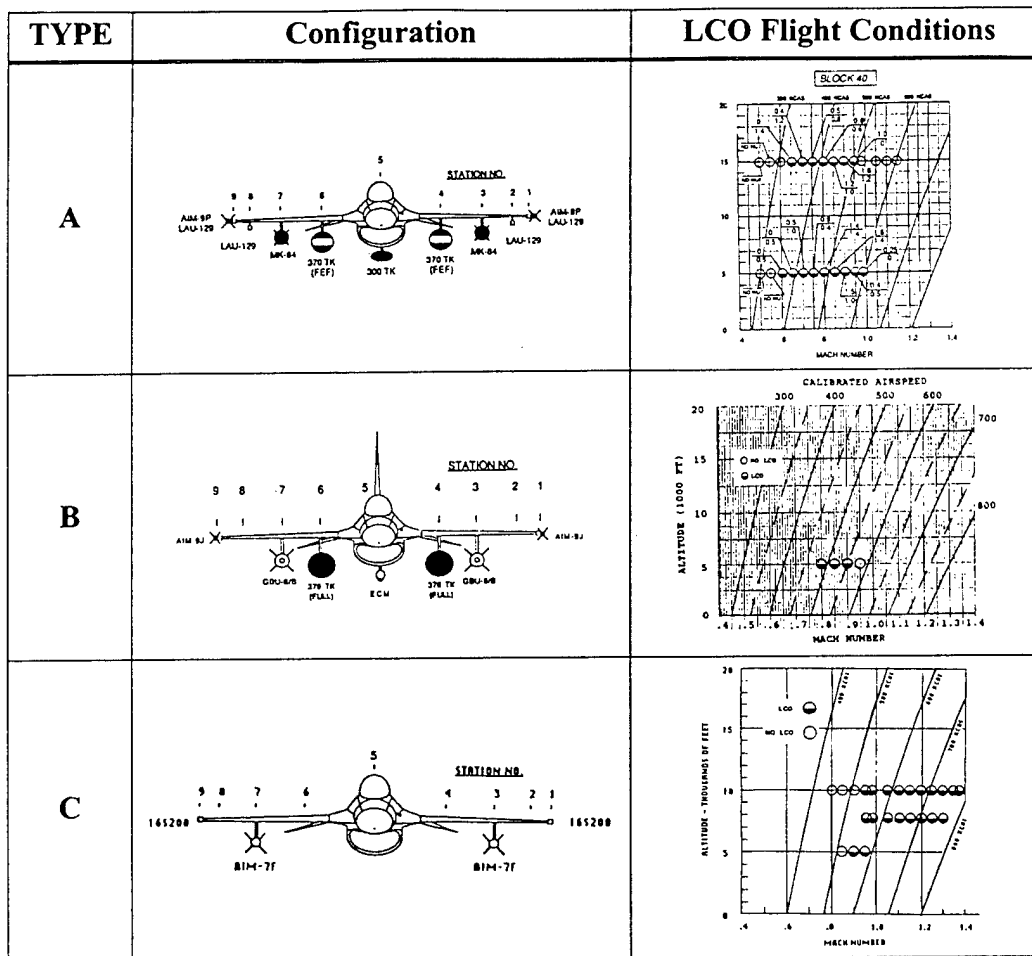
TYPE	Configuration	LCO Flight Conditions
A		
B		
C		

Figure 6.4   Three Selected F-16/Store LCO Cases

In order to validate the 3-D harmonic balance code with a multi-body capability (to be develop in the second year of Phase II), three F-16/store LCO cases are selected; each represents one type of LCO discussed above. These three F-16/store configurations and their respective LCO flight conditions are shown in Fig 6.4.

Five Selected F/A-18/Store LCO Cases

In 1999, ZONA has received a Navy SBIR Phase I contract entitled "*Adaptive Reconfigurable Control Based on a Reduced-Order System Identification for Flutter and Aeroservoelastic Instability Suppression*" (see Section 6.1, ZONA's Related Work). As one of the team members, the Boeing company, St. Louis, supplied ZONA with all the necessary data of the F/A-18 LCO configurations including the structural finite element models with various stores, the LCO flight test data and flight control system for F/A-18 LCO suppression. In general, two types of LCO frequencies were observed during the F/A-18/store flight tests: (1) Type A: LCO frequency at 5.6 Hz for cases of wing/store with tip missile, (2) Type B: LCO frequency at 8.8 Hz for cases of wing/store with tip launcher only.
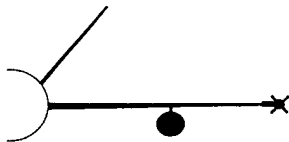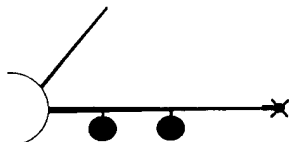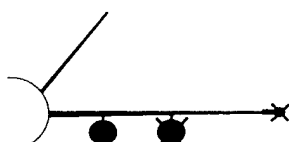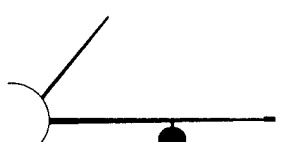
59
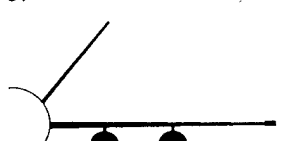
Case	Store Configuration	LCO Frequency	Flight Condition
1.	Wing Tip: Launcher + Missile Outboard Pylon: MK-84 Inboard Pylon: None	5.6 Hz	M ≈ 0.88 – 1.0
2.	Wing Tip: Launcher + Missile Outboard Pylon: MK-84 Inboard Pylon: MK-84	5.6 Hz	M ≈ 0.88 – 1.0
3.	Wing Tip: Launcher + Missile Outboard Pylon: AGM-88 Inboard Pylon: MK-84	5.6 Hz	M ≈ 0.88 – 1.0
4.	Wing Tip: Launcher Only Outboard Pylon: MK-83 Inboard Pylon: None	8.8 Hz	M > 0.9
5.	Wing Tip: Launcher Only Outboard Pylon: MK-83 Inboard Pylon: MK-83	8.8 Hz	M > 0.9

Figure 6.5   Five Selected F/A-18 / Store LCO Cases

In order to further validate the 3-D harmonic balance code with a multi-body capability, we selected five F/A-18/store LCO test cases (three for type A and two for type B) whose configuration and flight conditions are presented in Fig 6.5.

To finish the three F-16/store cases and five F/A-18/store cases within a two-year project seems to be a very ambitious plan. However, this is not the case if the POD/ROM methodology is employed. Since it is known that the underwing stores generally has little aerodynamic influence on the aeroelastic characteristics, i.e., only the inertial effects of the underwing stores impact the aeroelastic characteristics, aeroelastic analysis of wing/store configurations can exclude the underwing stores in the aerodynamic modeling but, of course, include their inertial effects in the

structural modeling. Based on this assumption, the three F-16/store and five F/A-18/store cases become the ideal test cases for the POD/ROM methodology. As already demonstrated in our Phase I achievements presented in Chapter 4, one can obtain accurate POD/ROM unsteady aerodynamics using solution snapshots unrelated to the actual structural modes. This suggests that only four sets of POD/ROM computations are required, two for F-16 with and without tip missiles and another two for F/A-18 with and without tip missiles, but using simple wing motion snapshots that are unrelated to the actual F-16 or F/A-18 structural modes. Once these snapshot solutions are at hand, the unsteady aerodynamics of the three F-16/store and five F/A-18/store cases can be obtained by using the snapshot ensemble technique described in Chapter 4, but with respect to their actual structural modes and tip missile/launcher aerodynamic configurations.

Note that excluding the underwing stores from the aerodynamic modeling is based on the assumption of their little aerodynamic influence on the whole aircraft aeroelastic characteristics. To verify this, we will conduct a flutter analysis on one of the wing/store configurations but including all underwing stores in the aerodynamic modeling. The flutter result will be used to verify the snapshot procedure discussed above. Once verified, this implies that the POD/ROM methodology can be developed as an highly efficient computational tool for massive flutter and LCO analyses of aircraft with various underwing stores.

6.3.9 Statement of Work

Tasks to be performed in Phase II are defined below. The schedule for the Phase II statement of work is shown in Section 6.7.10. Timing for related program deliverables, meeting and presentations are also noted on the schedule.

Task 1: Development of a 2-D Navier-Stokes Solver with Harmonic Balance (NSHB) Code
Take the two-dimensional, nonlinear, harmonic balance aerodynamic code using the Euler equations which was developed in Phase I and add viscosity, i.e., this becomes a Navier-Stokes code.

Task 2: Validation of the 2-D NSHB Code for Simple Structures in Transonic Flow

Use the 2-D NSHB code to perform LCO analysis and prediction for simple structural models, e.g., plunge and pitch of typical sections for conventional and supercritical airfoils in transonic flow.
- Perform flutter and LCO studies of the NACA 64010A conventional airfoil described in Chapter 3. Assess the impact of viscosity on transonic flutter dip and LCO by comparing the results of the 2-D NSHB with those of the inviscid 2-D harmonic balance code developed in Phase I.
- Perform flutter and LCO studies of the NLR 7301 supercritical airfoil described in Chapter 5. Correlate the predicted LCO frequency and amplitude with the DLR experimental results and assess the efficiency of the 2-D NSHB code by comparing its computer time with that of the time-marching CFL3D computation.

Task 3: Development of the 3-D Euler Solver with the Harmonic Balance (EHB) Code

Take the 3-D time-linearized aerodynamic code using the Euler equations developed in Phase I and convert it to a fully nonlinear dynamics code using the harmonic balance method previously developed for the 2-D code.

Task 4: Validation of the 3-D EHB Code for Simple Wing Structural Model

Use the 3-D EHB code to perform LCO analysis and prediction for simple wing structural models. Perform correlation studies with the MAVRIC-I business jet wing.
- Generate a 3-D mesh for the MAVRIC-I business jet wing.
- Use the BEM Solver to transfer the mode shapes computed at the structural finite element grid to the CFD surface mesh of the MAVRIC-I business jet wing.
- Perform LCO analysis at selected transonic Mach numbers and correlate the predicted frequency-domain pressure distribution with the NASA/Langley TDT measurements. Assess the accuracy of the predicted LCO frequency and amplitude by the comparison with the TDT measurements.

Task 5: Development of a 2-D NSHB Code with Multi-Structural Mode Capability

Take the 2-D NSHB code developed in Task 1 and add a multi-structural mode capability. This will provide the capability for LCO analysis of complex multi-mode, nonlinear structural models such as an airfoil and control surface with freeplay.

Task 6: Validation of the 2-D NSHB Code for Nonlinear Aerodynamic and Structural Models

Convert the 2 degrees of freedom NACA 64010A and NLR 7301 airfoils to a 3 degrees of freedom structure by adding a control surface motion with freeplay. Use the 2-D NSHB code with multi-structural mode capability to perform LCO studies of the 3 degrees of freedom NACA 64010A and NLR 7301 airfoils. Establish a test bed for novel and improved harmonic balance solution methods to predict LCO with nonlinear aerodynamics and structural models.

Task 7: Development of a 3-D Time-Linearized Euler Solver (TLE) Code with a Multi-Body Capability

Take the 3-D time-linearized aerodynamic code using the Euler equations developed in Phase I and add a multi-body capability. This will provide the capability to predict the transonic flutter dip of wing with stores configurations.

Task 8: Validation of the 3-D TLE Code for Multi-Body Configurations

Use the 3-D TLE code with the multi-body capability to perform flutter analysis of the three F-16/store and five F/A-18/store cases. Correlate the predicted flutter boundaries with the flutter flight test data.
- Generate the multi-block mesh systems of the F-16/store and F/A-18/store configurations with/without the tip missile.

- Use the POD/ROM methodology to obtain the snapshot solutions of the F-16/store and F/A-18/store configurations with simple wing motions that are unrelated to the actual structural modes.
- Transfer the structural mode shapes of the three F-16/store and five F/A-18/store cases from the structural finite element grid to the CFD surface grid using the BEM solver.
- Compute the unsteady aerodynamics of these F-16/store and F/A-18/store cases with respect to their actual structural modes using the snapshot ensemble technique.
- Perform flutter analysis of the three F-16/store and five F/A-18/store cases. Correlate the predicted flutter boundaries with the flutter flight test data.

Task 9: Development of a 3-D Harmonic Balance Code with Multi-Body Capability

Take the 3-D TLE code developed in Task 7 and add the harmonic balance method. This will provide the capability of LCO analysis for multi-body geometry like the wing/store configurations.

Task 10: Development of a Rayleigh Quotient Technique for LCO Prediction of High Degree-of-Freedom Nonlinear System

Apply Rayleigh Quotient technique to the codes developed in Tasks 2, 3, or 9 to demonstrate feasibility of computing LCO with high degree of freedom nonlinear system. This will give a description of the LCO behavior of a very high dimensional system, i.e., a nonlinear CFD model coupled with a nonlinear structural model.

Task 11: Validation of the 3-D Harmonic Balance Code for the Multi-Body Configurations

Use the 3-D harmonic balance code with the multi-body capability developed in Task 9 to perform LCO analysis and prediction of the three F-16/store and five F/A-18/store cases. Correlate the predicted LCO frequencies and amplitudes of these cases with their respective flight test data.

6.3.10 Planned Program Schedule

Tasks	Yr 1 Quarter				Yr 2 Quarter				Performed by
	1	2	3	4	1	2	3	4	
1. Development of a 2-D Navier-Stokes Solver with Harmonic Balance (NSHB) Code	█								Duke
2. Validation of the 2-D NSHB Code for Simple Structures in Transonic Flow									
– Perform flutter and LCO studies of the NACA 64010A conventional airfoil	█								Duke
– Perform flutter and LCO studies of the NLR 7301 supercritical airfoil		█							ZONA/Duke
3. Development of the 3-D Euler Solver with the Harmonic Balance (EHB) Code	█	█							Duke
4. Validation of the 3-D EHB Code for Simple Wing Structural Model									
– Generate a 3-D mesh for the MAVRIC-I business jet wing		█							ZONA
– Use the BEM Solver to transfer the mode shapes from the structural grid to the CFD surface grid			█						ZONA
– Perform LCO analysis at transonic Mach numbers of the MAVRIC-I business jet wing			█	█					ZONA
5. Development of a 2-D NSHB Code with Multi-Structural Mode Capability					█				Duke
6. Validation of the 2-D NSHB Code for Nonlinear Aerodynamic and Structural Models						█			Duke/ZONA
7. Development of a 3-D Time-Linearized Euler Solver (TLE) Code with a Multi-Body Capability				█	█				Duke
8. Validation of the 3-D TLE Code for Multi-Body Configurations									
– Generate the multi-block mesh systems of the F-16/store and F/A-18/store configurations					█				ZONA
– Use the POD/ROM methodology to obtain the snapshot solutions					█				Duke
– Transfer the structural mode shapes from the structural finite element grid to the CFD surface grid using the BEM solver						█			ZONA
– Compute the unsteady aerodynamics of these F-16/store and F/A-18/store cases using the snapshot ensemble technique						█			Duke/ZONA
– Perform flutter analysis of the three F-16/store and five F/A-18/store cases							█		ZONA
9. Development of a 3-D Harmonic Balance Code with Multi-Body Capability					█	█			Duke
10. Development of a Rayleigh Quotient Technique for LCO Prediction of High Degree-of-Freedom Nonlinear System							█		Duke
11. Validation of the 3-D Harmonic Balance Code for the Multi-Body Configurations							█	█	ZONA/Duke
12. Documentation									
– Interim Report	▲	▲	▲	▲	▲	▲	▲		ZONA/Duke
– Final Report								█	ZONA/Duke
Kick-Off Meeting	▲								
Final Oral Presentation								▲	

64

6.3.11 Deliverables

The deliverables and delivery cycle of Phase II are presented in Table 6.1.

Table 6.1   Deliverables of the Proposed Phase II Project

Deliverable	Delivery Cycle
Interim Reports	Quarterly
Funds & Man Hour Expenditure Reports	Quarterly
Final Report	As Required
Executable Code of the Final Program	As Required

CHAPTER 7

COMMERCIALIZATION STRATEGY

With a strong technical background, ZONA also has extensive experience in commercialization of its product. In fact, ZONA has been serving the aerospace community through consulting/contractual work and software licensing support since 1986.

- ZONA's unsteady/steady aerodynamic software in the aerospace market most notably includes ZONA51 (currently the Aero Option II in MSC/NASTRAN – an industry standard) and the ZAERO software system (covering the entire Mach range). ZONA codes have, thus far, accumulated over 120 users worldwide.
- Under an AF/STTR Phase II contract, ZONA and MSC Software are reaching a business agreement to commercialize and jointly market ASTROS* (the seamlessly integrated ZAERO module into ASTROS). ASTROS is a popular Automated STRuctural Optimization System software among aerospace industry and universities.

7.1   Next Generation Aeroelastic Software

After some 20 years of continuing R&D effort in unsteady transonic aerodynamics, high-level (3-D Euler and Navier-Stokes) unsteady CFD methods remain inadequate to handle the fixed-wing transonic aeroelastic problems encountered in industry. ZONA's recent marketing survey reveals the possible causes of such an inadequacy. These include that: (1) the current CFD methods is computationally very expensive for flutter calculations, (2) the procedures are not easily user-adaptive, (3) Structure engineers prefer to work with solutions in frequency-domain not time-domain. Industry standard methods such as the classical AIC method is lacking in the transonic regime where a reliable high-level CFD method such as CFL3D is badly needed. The proposed frequency-domain POD/ROM method originated by Hall/Dowell has a great potential to be such transonic AIC-like method which has the essence of efficiency, accuracy, modularity and could assess the key physics for nonlinear flutter/LCO. Its future applicability is far reaching which extends to areas in aeroelasticity, aeroacoustics, turbomachinery, ASE, MDO, etc. On the other hand, the ZAERO aeroelastic system exclusively adopts the AIC methodology as basis for the unified unsteady aerodynamics. Although efficient, ZAERO is incapable to provide nonlinear, viscous unsteady aerodynamics with large amplitude oscillations. Once developed, the transonic frequency-domain POD/ROM/HB (Harmonic Balance) methodology along with its Navier-Stokes option, would be an integral part of ZONA's ZAERO aeroelastic system. ZONA envisions that the production code of the frequency-domain POD/ROM/HB method should become the future industry standard for routine transonic flutter/LCO analysis.

7.2   ZONA Funded Phase III for Commercialization

Stated in Section 7.0, ZONA will fund Duke University for further R&D necessary to attain a production of aeroelastic software for commercialization. To do so, ZONA will utilize its current annual license income fund from MSC/ZONA51 and ZAERO to support the Phase III

R&D activity. Industry β-sites will be set up with Boeing/St. Louis and Lockheed Martin/Forth Worth to upgrade the code as a viable industry production software.

7.3   Commercialization of the Software with ZAERO

When the frequency-domain POD/ROM/HB code is successfully developed, ZONA will package the POD/ROM/HB/Navier-Stokes methodology (with either software option) into a well-defined commercial software product. To facilitate its sales, ZONA plans to couple the code with the unified aerodynamic module within ZAERO and jointly market for both codes.

ZONA has currently teamed up with a major FEM software house (MSC Software) for ZONA51 (in MSC/NASTRAN) and ZAERO licensing. ZONA currently supports over 120 users worldwide for the MSC/NASTRAN Aero Option II. Released in April 1999, ZAERO has already had a dozen users including Lockheed Martin/Vought Systems, Boeing/Commercial, DLR/Göttingen, SDRC, NASA/MSFC, NASA/Dryden, Scaled Composites Coleman Aerospace, etc. With ZONA's extensive aerospace contractual/software licensing experience, this software product is expected to break into the aerospace market quite readily. Prospective customers include ZONA's current clientele, other aerospace companies and DoD organization.

Other commercialization steps include advertising through magazines, the internet, and attending AIAA conventions. All these are currently being pursued by ZONA for the licensing sales of ZAERO.

CHAPTER 8

CONCLUSIONS

Phase I of our STTR effort has concluded successfully with a number of achievements attained and a clear plan developed for Phase II and III to follow upon these accomplishments. The challenge at the start of Phase I was to assess the viability of current time marching CFD codes for transonic flutter and limit cycle oscillation (LCO) analysis and design and also to develop computationally more efficient and physically accurate descriptions of aeroelastic systems including the representation of the unsteady aerodynamic forces. This has been done.

Consistent with the experience and observations of other researchers and practioners, we have found that time marching CFD codes of the conventional sort are simply too computationally intensive to be viable for aeroelastic modeling in an industrial application. (See the discussion in Chapter 5.) Moreover if such codes were to be used for the development of actively controlled smart structures, their cost would be prohibitive. Our studies were conducted with a state-of-the-art CFD code, CFL3D, made available to us by the Aeroelasticity Branch of the NASA Langley Research Center. We are most appreciative of their help in making this evaluation.

Much of our effort in Phase I has therefore been devoted to the development of alternative methods using the concept of aerodynamic modes, either eigenmodes of the flow field or the modes one can construct using the method of proper orthogonal decompostion (POD). Using a few of the most dominant modes, Reduced Order Models (ROM) can be obtained that are orders of magnitude smaller in terms of the number of degrees of freedom and computational time compare to the original CFD model. Such models are simply called POD/ROM. It is emphasized that these models retain the essential physical modeling from the CFD code from which they are obtained, e.g. Euler or Navier-Stokes equations.

A companion development has been the study of large shock motions using the method of harmonic balance (HB)to represent the dynamically nonlinear shock wave motion and aerodynamic forces due to airfoil (or wing) motion. As part of the planned work for Phase II/III we plan to combine the best features of the POD/ROM and HB methods.

Using POD/ROM and HB several studies were undertaken in Phase I to illustrate the computational efficiency and physical modeling capability of this new approach. These include

- Transonic Limit Cycle Oscillation Analysis of an Airfoil with Control Surface Freeplay (Chapter 2)

  Here the POD/ROM aerodynamic forces are combined with a nonlinear structural model to investigate LCO due to freeplay.

- Nonlinear Inviscid Aerodynamic Effects on Transonic Divergence, Flutter and Limit Cycle Oscillations (Chapter 3)

Here the harmonic balance (HB) approach is used to model the aerodynamic flow with large shock wave motions. An LCO study for an airfoil oscillating in pitch where the nonlinearity is entirely due to large shock motion has been completed.

- Three Dimensional Transonic Aeroelasticity Using Proper Orthogonal Decomposition Based Reduced Order Models (Chapter 4)

For small shock motions, the POD/ROM methodology has been extended to three dimensional flows over wings and a transonic flutter analysis has been completed.

Future plans are described in more detail in Chapter 6 and will include the addition of viscosity in both the two-dimensional and three-dimensional flow POD/ROM with the HB method to be further developed to account for large (as well as small) shock motions and also for viscous nonlinearities. A systematic plan and roadmap has been constructed for this work and a commercializtion strategy developed as well (Chapter 7).

REFERENCES

1. Denegri, C.M., "Limit Cycle Oscillation Flight Test Results of a Fighter with External Stores," AIAA-2000-1394.

2. Norton, W.J., "Limit Cycle Oscillation and Flight Flutter Testing," *Proceedings of the Society of Flight Test Engineers 21st Annual Symposium*, Aug. 1990.

3. Redd, L.T., "Flutter and Aeroservoelastic Flight Testing at the Air Force Flight Test Center," *Aerospace Flutter and Dynamics Council*, Edwards Air Force Base, CA, May 12-14, 1993.

4. Brignac, W.J., "Limit Cycle Oscillation F-16 Experience," presented at *Flutter and Dynamics Council*, Dallas, TX, May 10-11, 1989.

5. Schuster, D.M., Edwards, J.W. and Bennett, R.M., "An Overview of Unsteady Pressure Measurements in the Transonic Dynamics Tunnel," AIAA 2000-1770, *AIAA Dynamics Specialists Conference*, Atlanta, GA, Apr. 5-6, 2000.

6. Gibbons, M.D., "Aeroelastic Calculations Using CFD for a Typical Business Jet Model," NASA Contractor Report 4753, Sep. 1996.

7. Chen, P.C., Sarhaddi, D. and Liu, D.D., "Limit Cycle Oscillation Studies of a Fighter with External Stores," *39th Structures, Structural Dynamics and Materials Conference*, AIAA-98-1727, Apr. 1998.

8. Cunningham Jr., A.M. and Meijer, J.J., "Semi-Empirical Unsteady Aerodynamics for Modeling Aircraft Limit Cycle Oscillations and Other Nonlinear Aeroelastic Problems," *International Forum on Aeroelasticity and Structural Dynamics*, Manchester, U.K., Jun. 26-28, 1995.

9. Edwards, J.W., "Transonic Shock Oscillations and Wing Flutter Calculated with an Interactive Boundary Layer Coupling Method," *Euromech-Colloquium 349 Simulation of Fluid-Structure Interaction in Aeronautics*, Göttingen, Germany, Sep. 16-18, 1996.

10. Krist, S.L., Biedron, R.T. and Rumsey, C.L., "CFL3D User's Manual Version 5.0," NASA Langley Research Center, Hampton, VA, Sep. 1997.

11. Hall, K.E., Thomas, J.P. and Dowell, E.H., "Reduced-Order Modeling of Unsteady Small Disturbance Flows Using a Frequency-Domain Proper Orthogonal Decomposition Technique," *37th Aerospace Sciences Meeting and Exhibit*, AIAA 99-0655, Jan. 1999.

12. Bendiksen, O.O., "Role of Shock Dynamics in Transonic Flutter," AIAA-92-2121-CP, 1992.

13. Sheta, E.F. and Harrand, V.J., "Computational and Experimental Investigation of Limit Cycle Oscillations in Nonlinear Aeroelastic Systems," AIAA 2000-1399, *41st*

AIAA/ASME/ASCE/AHS/ASC Structures, Structural Dynamics & Materials Conference, Atlanta, GA, Apr. 3-6, 2000.

14. Dowell, E.H., Thomas, J.P. and Hall, K.C., "Transonic Limit Cycle Oscillation Analysis Using Reduced Order Modal Aerodynamic Models," extended abstract for *42nd AIAA/ASME/ASCE/AHS/ASC Structures and SDM Conference,* Seattle, WA, Apr. 16-19, 2001.

15. Thomas, J.P., Dowell, E.H. and Hall, K.C., "Nonlinear Inviscid Aerodynamic Effects on Transonic Divergence, Flutter and Limit Cycle Oscillations," extended abstract for *42nd AIAA/ASME/ASCE/AHS/ASC Structures and SDM Conference,* Seattle, WA, Apr. 16-19, 2001.

16. Thomas, J.P., Dowell, E.H. and Hall, K.C., "Three-Dimensional Transonic Aeroelasticity Using Proper Orthogonal Decomposition Based Reduced Order Models," extended abstract for *42nd AIAA/ASME/ASCE/AHS/ASC Structures and SDM Conference,* Seattle, WA, Apr. 16-19, 2001.

17. Batina, J.T., "Unsteady Transonic Small-Disturbance Theory Including Entropy and Vorticity Effects," Journal of Aircraft, Vol. 26, No. 6, June 1989, p. 531.

18. Silva, W.A., "Application of Nonlinear Systems Theory to Transonic Unsteady Aerodynamic Responses," Journal of Aircraft, Vol. 30, No. 5, Sept.-Oct. 1993, pp. 660-668.

19. Mignolet, M.P., Liu, D.D. and Chen, P.C., "On the Nonlinear Structural Damping Mechanism of the Wing/Store Limit Cycle Oscillation," AIAA-99-1459, 1999.

20. Nam, C., Chen, P.C., Liu, D.D., Yurkovich, R.M. and Urnes, J., "Adaptive Reconfigurable Control Based on a Reduced-Order System Identification for Flutter and Aeroservoelastic Instability Suppression," SBIR Phase I Final Report for Naval Air Warfare Center Aircraft Division, NAWC-TR-99, Jun. 2000.

21. Chen, P.C. and Jadic, I., "Interfacing of Fluid and Structural Models via an Innovative Structural Boundary Element Method," AIAA Journal, Vol. 36, No. 2, Feb. 1998, pp. 282-287.

22. Chen, P.C. and Hill, L.R., "A Three-Dimensional Boundary Element Method for CFD/CSD Grid Interfacing," AIAA 99-1213, 1999.

23. Tang, L., Chen, P.C., Liu, D.D. and Bartels, R.E., "Simulation of Transonic Limit Cycle Oscillations Using a CFD Time-Marching Method," an Extended Abstract for *42nd AIAA/ASME/ASCE/AHS/ASC Structures and SDM Conference,* Seattle, WA, Apr. 16-19, 2001.

24. Cunningham, A. M., Jr, "A Generic Nonlinear Aeroe-lastic Method with Semi-Empirical Nonlinear Unsteady Aerodynamics", Vol. 1 and 2, AFRL-VA-WP- TR-1999-3014, 1999.

25. Conner, M.D. , Tang, D. M. , Dowell, E. H. and Virgin, L.N., "Nonlinear Behavior of a Typical Airfoil Section with Control Surface Freeplay: A Numerical and Experimental Study," Journal of Fluids and Structures, Vol. 11, 1997, pp. 89-109.

26. Tang, D. M., Dowell, E.H. and Virgin, L. N., "Limit Cycle Behavior of an Airfoil with a Control Surface," Journal of Fluids and Structures, Vol. 12, 1998, pp. 839-858.

27. Dowell, E.H. and Hall, K.C., "Modeling of Fluid-Structure Interaction," Invited Chapter in the Annual Reviews of Fluid Mechanics, to appear, 2000.

28. Silva, W. A., "Experimental Steady and Unsteady Aerodynamic and Flutter Results for HSCT Semispan Models", presentation at the Aerospace Flutter and Dynamics Council Meeting at NASA Langley Research Center, May 24, 2000.

29. Tang, D. M., Henry, J. K. and Dowell, E. H., "Limit Cycle Oscillations of Delta Wing Models in Low Sub-sonic Flow," AIAA Journal, Vol. 37, No. 11, pp. 1355-1362,1999.

30. Ueda, T. and Dowell, E. H., "Flutter Analysis Using Nonlinear Aerodynamic Forces," Journal Aircraft, Vol. 21, No. 2, pp. 101-109, 1984.

31. Greco, P.C., Jr., Lan, C. E. and Lim, T. W., "Frequency Domain Unsteady Transonic Aerodynamics for Flutter and Limit Cycle Oscillation Prediction," AIAA Paper 97-0835, 35th Aerospace Sciences Meeting, Reno, NV, Jan. 6-10, 1997.

32. Thomas, J. T., Hall, K. C. and Dowell, E. H, "Reduced-Order Aeroelastic Modeling Using Proper Orthogonal Decompositions," *CEAS/AIAA/ICASE/NASA Langley International Forum on Aeroelasticity and Structural Dynamics*, Williamsburg, VA, June 1999.

33. Kim, T., "Frequency-Domain Karhunen-Loeve Method and Its Application to Linear Dynamic Systems," AIAA Journal , Vol. 36, No. 11, 1998, pp. 2117–2123.

34. Ni, R. H., "A Multiple-Grid Scheme for Solving the Euler Equations," AIAA Journal , Vol. 28, No. 12, 1982, pp. 2050–2058.

35. Loève, M., *Probability Theory*, D. Van Nostrand Company, Inc., NY, 1955.

36. J.L., "The Structures of Inhomogeneous Turbulent Flow," in Atmospheric Turbulence and Radio Wave Propagation, edited by A. M. Yaglom and V. I. Tatarski, Nauka, Moscow, 1967, pp. 166–178.

37. Holmes, P., Lumley, J. L., and Berkooz, G., *Turbulence, Coherent Structures, Dynamical Systems and Symmetry*, Cambridge University Press, Cambridge, 1996.

38. Yates, E. C., Jr., "AGARD Standard Aeroelastic Configurations for Dynamic Response I - Wing 445.6," NASA TM 100492, August 1987, also *Proceedings of the 61st Meeting of the Structures and Materials Panel*, Germany, AGARD-R-765, 1985, pp. 1–73.

39. Yates, E. C., Jr., Land, N. S. and Foughner, J. T. , Jr., "Measured and Calculated Subsonic and Transonic Flutter Characteristics of a 45 Deg Sweptback Wing Planform in Air and in Freon-12 in the Langley Transonic Dynamics Tunnel," NASA TN D-1616, Mar. 1963.

40. Lee-Rausch, E. M. and Batina, J. T., "Wing Flutter Boundary Prediction Using Unsteady Euler Aerodynamic Method," Journal of Aircraft, Vol. 32, No. 2, 1995, pp. 416–422.

41. Gupta, K. K., "Development of a Finite Element Aeroelastic Analysis Capability," Journal of Aircraft, Vol. 33, No. 5, 1996, pp. 95–1002.

42. Schewe, G. and Deyhle, H., "Experiments on Transonic Flutter of a Two-Dimensional Supercritical Wing with Emphasis on the Nonlinear Effects," *Proceedings of the Royal Aeronautical Society Conference on Unsteady Aerodynamics*, London, U.K., Jul. 17-18, 1996.

43. Knipfer, A. and Schewe, G., "Investigations of an Oscillation Supercritical 2-D Wing Section in a Transonic Flow," *36th Aerospace Sciences Meeting and Exhibit*, AIAA 99-0653, Jan. 1998.

44. Knipfer, A., Schewe, G. and Wendt, V., " Numerische und experimentelle Untersuchungen an einem schwingenden NLR 7301-Profil in transsonischer Stroemung, Teil 1: Flattern und erzwungene Schwingungen," DLR Bericht IB 232-98 J 05, 1998.

45. Weber, S., Jones, K.D., Ekaterinaris, J.A. and Platzer, M.F., "Transonic Flutter Computations for a 2-D Supercritical Wing," *37th AIAA Aerospace Sciences Meeting and Exhibit*, AIAA 99-0798, Reno, NV, Jan. 1999.

46. Tijdeman, H., " Investigation of the Transonic Flow around Oscillating Airfoils" NLR TR 77090U, 1977.

47. Castro, B.M., Ekaterinaris, J.A. and Platzer, M.F., "Transonic Flutter Computations for the NLR 7301 Airfoil Inside a Wind Tunnel," *38th Aerospace Sciences Meeting and Exhibit*, AIAA 2000-0984, Jan. 2000.

APPENDIX A

TRANSONIC LIMIT CYCLE OSCILLATION ANALYSIS USING REDUCED ORDER MODAL AERODYNAMIC MODELS

Earl H. Dowell, Jeffrey P. Thomas, and Kenneth C. Hall
Duke University, Durham, NC 27708–0300

TRANSONIC LIMIT CYCLE OSCILLATION ANALYSIS
USING REDUCED ORDER MODAL AERODYNAMIC MODELS

Earl H. Dowell, *   Jeffrey P. Thomas, †   and   Kenneth C. Hall ‡

Duke University

Durham, NC 27708–0300

INTRODUCTION

The principal focus of this paper is on the transonic aeroelastic behavior of an airfoil with control surface freeplay including flutter and limit cycle oscillations. In most of this work, we will assume the shock motion is sufficiently small such that it is (linearly) proportional to the airfoil motion, e.g. airfoil motions are less than the equivalent of one degree in angle of attack.

Using an Euler/CFD-based reduced order aerodynamic model, a thorough study of the flutter boundary with Mach number (M) is first presented in the absence of freeplay. Particularly noteworthy are the rapid changes of flutter modal content in the transonic range. This is attributed in part to the rapid changes of center of pressure location as the mean shock position changes with Mach number. These changes in the modal response content are also found in the limit cycle oscillations (LCO) which are encountered when control surface freeplay is present. Indeed for LCO, the modal content may change at a fixed Mach number when the dynamic pressure or flow density is varied.

Below M=0.80, the LCO and flutter oscillations are qualitatively similar to those found at low Mach number where earlier analyses and experiments have been carried out. However, the response behavior in the transonic flow regime is notably different. Of special interest is the occurrence of flutter in a narrow range of Mach number for pitch and flap (control surface) dominated motions. Moreover, beyond a certain high transonic Mach number (after the mean shock position reaches the trailing edge of the airfoil), neither flutter nor limit cycle oscillation occurs.

SIGNIFICANCE OF LCO

LCO is known to occur on various operational aerospace flight vehicles. This has been a source of serious concern since there are no analysis techniques available that have predicted LCO in an operational aircraft. There have been some semi-empirical techniques developed to correlate with LCO that have been observed in flight, and these are useful for understanding the LCO that has occurred. See Reference [1]. How-

ever these techniques are not as satisfactory for the design of a new vehicle or the substantial modification of an existing one, e.g. new stores to be carried by an aircraft.

In wind tunnel tests of flight vehicle prototypes, LCO has been notably absent for the most part. This is perhaps not altogether surprising since wind tunnel scale models have been designed based upon linear aeroelastic concepts. Such wind tunnel models and tests have been used successfully for many years to predict flutter (the onset of a dynamic linear instability). However they are inherently unable to predict a nonlinear phenomenon such as LCO.

In this regard, it should be noted that LCO may be beneficial as well as detrimental. Without the nonlinearities that lead to LCO, the onset of flutter may lead to catastrophic failure of the structure. Hence if we can understand and predict LCO, perhaps we can take advantage of these nonlinearities to shape more favorable responses of the aircraft leading to enhanced safety and performance.

TECHNICAL DISCUSSION
Sources of Nonlinearities

The principal sources of the nonlinearities essential to the LCO are a subject of current debate among the experts in the field. The candidate sources are several:

Fluid
- Shock motions
- Separated flow motions

Structure
- Free-play
- Geometric, e.g. a nonlinear relationship between strain and displacement
- Material, e.g dry friction damping

Also there is a further distinction between a static versus a dynamic nonlinearity. An important example of this is the role of a shock wave in the fluid. If a shock is present, then its creation is the result of a dynamic nonlinear process. However once a steady flow is established, and if the airfoil motion is sufficiently small, then the shock motion will also be small and proportional to the airfoil motion. Hence in this situation, the shock itself represents a nonlinear static (time independent) equilibrium and the motion may be treated as a dynamically linear perturbation about the mean shock position. In most of the following discussion, we assume a dynamically linear model of the shock motion, but also include a structural (dynamic) nonlinearity, i.e. freeplay in the connection of the control surface to the airfoil.

* J. A. Jones Professor, Department of Mechanical Engineering and Materials Science, and Dean Emeritus, School of Engineering, Fellow AIAA

† Research Assistant Professor, Department of Mechanical Engineering and Materials Science, Member AIAA

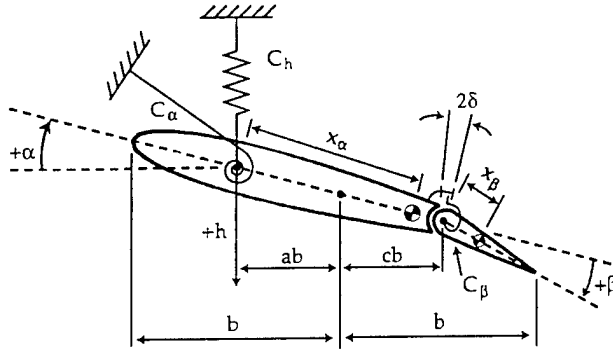‡ Associate Professor, Department of Mechanical Engineering and Materials Science, Associate Fellow AIAA

Figure 1: Airfoil with Control Surface Configuration
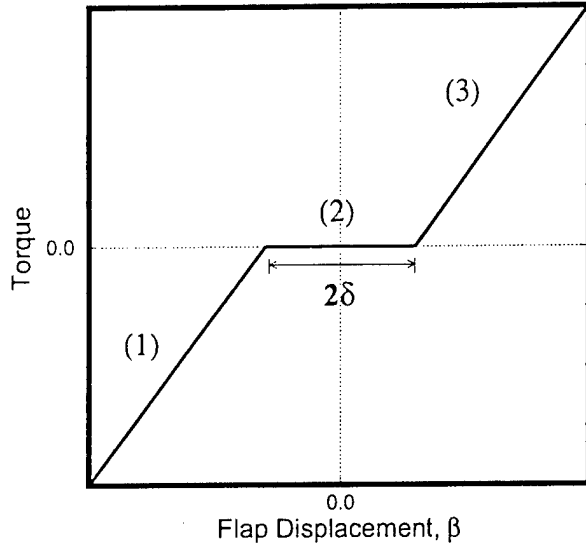
Figure 2: Restoring Moment As a Function of Control Surface or Flap Rotation Angle

Figure 3: Equivalent Nonlinear Flap Frequency Versus Flap Rotation

Airfoil with Control Surface Freeplay Model

A sketch of the configuration is shown in Figure (1). It is a conventional typical section model except that the spring that attaches the control surface to the airfoil has a nonlinear freeplay. The elastic restoring torque or moment provided by this spring is shown in Figure (2) as a function of control surface or flap rotation angle, β. The freeplay angle is δ. Note that when β is less than δ, there is zero restoring torque, while for β greater than δ, the spring stiffness is the nominal value in the absence of freeplay. The freeplay may be thought of as creating a stiffness or (uncoupled) natural frequency of the spring that varies as a function of flap amplitude. This interpretation is shown in Figure (3). Here the flap uncoupled natural frequency normalized by the nominal value in the absence of freeplay is shown as a function of flap amplitude, β, normalized by the freeplay angle, δ. Note that given a certain flap amplitude, there is a corresponding "equivalent" flap frequency. Of course for a linear system the control surface or flap frequency would have a fixed value independent of flap amplitude.

Thus conceptually and computationally one may proceed as follows. First, one determines the neutrally stable motions of the system in the absence of freeplay for various flap frequencies from zero to the nominal value. Then one determines the corresponding neutrally stable nonlinear limit cycle motion, namely the flap amplitude, from Figure (3). More details of this procedure will be given later including the construction of the linear instability or flutter boundary for this system, which serves as a basis for determining the limit cycle oscillations.

This approach has been used successfully at low Mach number and the theoretical results correlated with experiments. See References [2] and [3]. To extend these earlier calculations to transonic flow requires a substantially more sophisticated, but still computationally efficient aerodynamic model. Fortunately one is available as is described next.

Computational Fluid Dynamic (CFD) Modeling and its Modal Decomposition

A typical CFD model is very large in terms of the number of equations required to be solved. And this makes such models problematical for aeroelastic (and some other) analyses. For example, the CFD model used in the present work is based upon the Euler equations of fluid mechanics and has a spatial grid of 65 X 97 (6035) mesh points. At each grid point there are four fluid variables to be determined. Thus the CFD model per se has about 25,000 unknowns to be determined by solving 25,000 equations. This is a doable task if the structural motion is known. However if this CFD model is to be combined with a set of structural equations of motion, and solutions are to be found for many combination of structural and fluid parameters, then the calculation using the original CFD model quickly gets out of hand. Thus the search for an alternative approach.
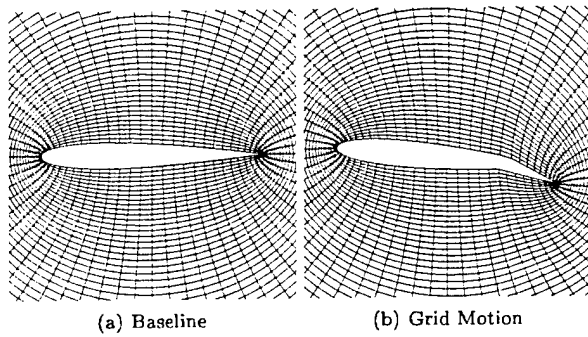
2

Figure 4: NACA 0012 Grid: 65 X 97 Computational Nodes, Outer Boundary Radius=15c

(a) Baseline   (b) Grid Motion

Figure 5: Computed NACA 0012 Steady Flow Surface Pressure Distributions: α_0 = 0.0 (deg)

Structural Parameters

Half Chord	b =	$0.127\,m$
Sectional Mass*	m =	$1.567\,kg/m$
Air Density	ρ_∞ =	$1.225\,kg/m^3$
Pitch Axis Location (e/b)	a =	-0.5
Flap Hinge Location (e_f/b)	a_f =	0.5
Mass Ratio, ($m/\rho_\infty \pi b$)	μ =	25.24
Static Unbalance, (S_α/mb)	x_α =	0.4316
Radius of Gyration, (I_α/mb^2)	r_α^2 =	0.5331
Flap Static Unbalance, (S_β/mb)	x_β =	0.01985
Flap Radius of Gyration, (I_β/mb^2)	r_β^2 =	0.01292

Uncoupled Frequencies

ω_h	=	$4.59\,Hz$
ω_α	=	$6.04\,Hz$
ω_β	=	$12.54\,Hz$

Coupled Frequencies

ω_h	=	$4.45\,Hz$
ω_α	=	$9.21\,Hz$
ω_β	=	$19.44\,Hz$

*Plunge inertia corrected for experimental support mass

$$M/m = 2.166$$

Table 1: Structural Parameters for NACA 0012 Airfoil with Control Surface

Several semi-empirical methods have been derived to address the computational feasibility issue. These as well as the method to be described and used here are discussed in more depth in Reference [4]. Among these methods are variations on the notion of a Padé approximant.

The method used here is based upon the observation that virtually all CFD models can be thought of as having a modal composition. The simplest conceptual set of modes is perhaps the fluid or aerodynamic eigenmodes of the CFD model, and these modes have been used successfully in creating reduced order models (ROM) that are computationally and conceptually attractive. See the discussion in Reference [4] and the forthcoming Reference [5].

However it turns out that determining the aerodynamic eigenmodes of a large CFD model is itself a challenging task. Hence a method called Proper Orthogonal Decomposition (POD) is employed here and in Reference [4]. The first use of this method in an Euler based aerodynamic context was by Romanowski. Again see the discussion of the literature in Reference [4]. In this method, by using a time history or frequency response of the CFD model to a known structural input, one may construct a small set of modes or basis functions, typically less than 100. Using these modes, one can reconstitute and very substantially reduce the size of the CFD model with essentially no loss in accuracy or physical content. This is the approach used here.

For the present analysis, 63 POD modes are found from the frequency responses (aerodynamic transfer functions) in flap, pitch and plunge respectively at 21 frequencies at each Mach studied using the original CFD model. Based upon previous experience, one might use an even smaller number of aerodynamic modes than this. However, even with this generous number of modes, the computations described below were all done in a few days.

The computational grid used for the CFD model is shown in Figure (4), and Figure (5) shows the chordwise steady flow pressure distributions for several Mach numbers. Note the presence of the shock at M=0.80, 0.85, and 0.90.

Linear Instability (Flutter)

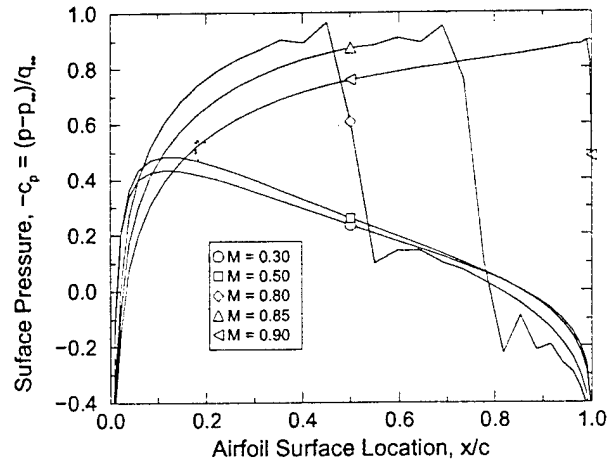First, consider the flutter behavior for this system in the absence of freeplay. The stability of this system was assessed by constructing a root locus (migration of the true aeroelastic eigenvalues) as a function of the nondimensional airspeed or dynamic pressure for each Mach number. The usual structural and flow parameters are defined in Table 1. These are typical and correspond to the theoretical and experimental model studies in References [1] and [2].

A representative root locus result is shown in Figure (6) for M=0.80. Root locus results are available for all Mach num-
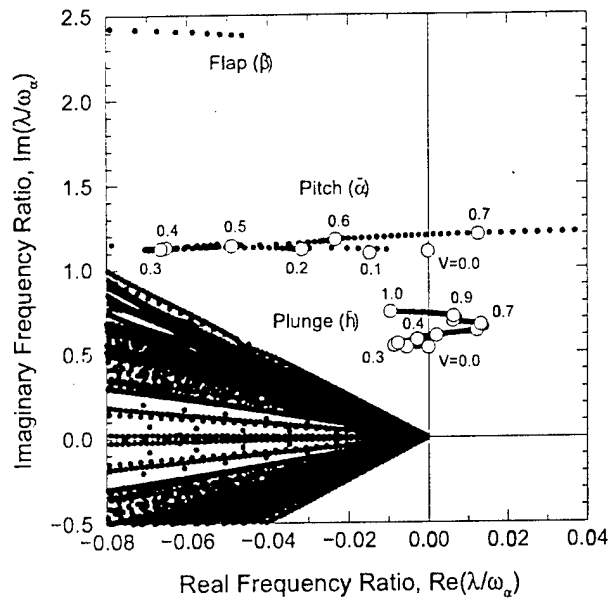
3

Figure 6: Aeroelastic System Eigenvalue Root-Loci: M = 0.80, α_0 = 0.0 (deg)

(a) Flutter Speed

(b) Flutter Frequency

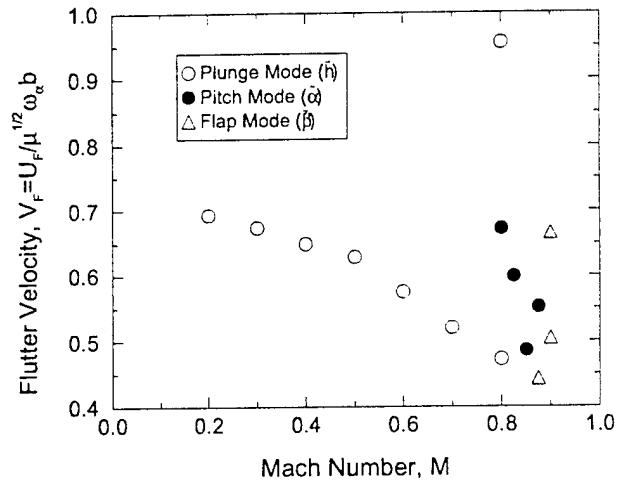Figure 7: Mach Number Flutter Trend: α_0 = 0.0 (deg)

bers used to construct the flutter boundary which is shown in Figure (7). Consider first Figure (6). The eigenvalues in this root locus are those of the coupled fluid/structural (aeroelastic) system. However the roots that originate as structural modes at low values of velocity or dynamic pressure are readily identified and labeled in the figure. The vertical axis is the imaginary part of the eigenvalue or frequency, and the horizontal axis displays the real part or rate of growth (if positive) or decay (if negative) of the oscillations associated with each root or eigenvalue.

Note especially that the "plunge" aeroelastic mode has a root that for low "gain" (or flow velocity or dynamic pressure) moves to the left and becomes more stable. But then as the flow velocity increases, it reverses direction and moves into the right half plane becoming unstable. And then at even higher velocities, it moves back into the left hand plane and becomes stable again. However by then, the pitch mode has moved into the right half plane and become unstable. Hence the aeroelastic system remains unstable once the plunge mode becomes again stable at this velocity and Mach number.

All the other roots in this figure which appear to originate from near the origin are essentially aerodynamic roots, and these roots all move off into the left half plane indicating they are always stable and increasingly so as the dynamic pressure increases. On occasion an aerodynamic root may become unstable however, though not for the parameters studied in this work.

As the Mach number becomes higher, the most critical root may change. For example, at M=0.85 the pitch root becomes unstable first, and for M=0.90, it is the flap root. At yet higher Mach numbers, no roots become unstable. For brevity these other root loci are omitted here.

Taking all of this information from the root loci at various Mach numbers, the flutter boundary trend with Mach num-

ber can be determined, and is presented in Figure (7a). There are several interesting features to this flutter boundary. Up to M=0.80, the root-loci are rather similar, and it is always the plunge root that is critical for flutter. Starting at M=0.80, the pitch root also shows instability, and at M=0.825 and 0.85, it is most critical for flutter. At M=0.875 and 0.90, the flap mode is most critical for flutter, and for M=0.925 to at least M=1.1, no flutter is observed for a non-dimensional flow velocity up to at least one. The corresponding frequencies of the flutter oscillations are shown in Figure (7b). Note that in Figure (7) when two data points are shown for say the plunge root at a fixed Mach number, the lower velocity point is when flutter begins, and the higher velocity point is when the root returns to the stable left half plane and flutter ceases in that root.

Note also the narrow range of Mach number where the change in flutter mode occurs. Results of this type have been observed in experiments where they are called "chimneys".

4

See Reference [6].

Limit Cycle Oscillations

Now the freeplay is added to the model and thus LCO may occur. As is perhaps obvious from physical intuition, when freeplay is added, the stiffness of the control surface freeplay is reduced for small motions. Hence one expects limit cycle oscillations to occur below the flutter boundary, i.e. at flow velocities less than those shown in Figure (7a). Indeed a few moments of reflection may lead one to expect that once the linear flutter boundary shown in Figure (7a) is exceeded, then exponentially explosive flutter will occur when the nonlinearity is due to freeplay. That is found to be the case as shown by the present analysis and also by the analysis and experiments of References [2] and [3].

To compute the LCO one proceeds as follows. For all other parameters fixed including Mach number, the flutter velocity is determined from a linear flutter analysis as a function of (uncoupled) flap natural frequency (or equivalently spring stiffness). Since the flap frequency (or stiffness) is known as a function of flap amplitude, see Figure (3 (or (2)), we immediately can determine from these two results (by cross-plotting), the flap amplitude for neutrally stable nonlinear motions (LCO) as a function of flow velocity. As an example for M=0.80, see Figure (8). In Figure (8a), the "flutter" or flow velocity at which neutrally stable oscillations may occur is shown as a function of flap frequency. Using Figure (3), which shows the nonlinear dependence of flap frequency as a function of flap amplitude, Figure (8b) may be constructed. This shows LCO amplitude as a function of flow velocity. The corresponding "flutter" frequency and the LCO frequency are shown in Figures (8c) and (8d) respectively.

A comment on this method is appropriate here. The reader familiar with the harmonic balance approach will recognize that a single harmonic approximation has been used to describe the freeplay nonlinearity. This approach is more fully described in the present context in Reference [3]. Of course this is a classical procedure for nonlinear systems; though it is not often used for systems with as many degrees of freedom as the present one. The results of Reference [3] confirm that the harmonic balance approach gives results in good agreement with those obtained from time marching solutions that include all harmonics, as well as the results from experiments.

The results of Figure (8) have several interesting features. First of all, the limit cycle amplitude is normalized by the freeplay angle, δ. The theory predicts and experiments agree, see Reference [3], that when the results are normalized in this manner, they are universal. That is, the limit cycle amplitude is proportional to the freeplay angle. Secondly, the lowest velocity at which LCO may occur corresponds to the minimum flutter velocity that occurs at a certain flap frequency. See Figure (8a) and then compare the lowest velocity for LCO in Figure (8b). Strictly speaking, a finite disturbance is required to generate LCO at this lowest velocity and for a small velocity range thereafter. LCO's for any disturbance, no matter how small, will only occur when the flutter velocity for a flap frequency of zero is exceeded. Again compare Figures (8a) and (8b). The unstable LCO's, which are shown along with the stable LCO's (those that are observed in an experiment), provide a measure of the level of disturbance required to ini-

tiate the LCO at the lower flow velocities. In practice such disturbances are usually present in wind tunnel experiments and flight operations.

The results of Figure (8) are typical until one reaches the higher transonic Mach numbers where linear theory predicts flutter will cease. At the highest Mach number considered here where flutter and LCO may occur, M=0.90, the LCO has a somewhat different character. See Figure (9). Again the LCO is first encountered at the minimum velocity at which flutter will occur over the range of flap frequencies. But now the corresponding flap frequency is zero. See Figure (9a). Moreover, when the flow velocity increases to higher values, there are two stable limit cycles. The nature of the disturbances to the system would determine which of these two LCO would be observed in a wind tunnel experiment or in flight. Note that the LCO branch with the larger amplitude will again move to amplitudes with very large values (to infinity according to the present theoretical model) when the flow velocity approaches the linear flutter velocity.

CONCLUSIONS

The transonic flutter and limit cycle oscillations of an airfoil with control surface freeplay have been determined using a new aerodynamic modeling technique that provides greater physical insight and understanding by tracing the true root locus of the corresponding linear aeroelastic system. This in turn enables a very computationally efficient harmonic balance technique to be used in determining the nonlinear limit cycle oscillations.

New physical insights gained include the rapid change in flutter mode that occurs in the transonic Mach number range. This phenomenon has been observed in experiments, but has not been previously predicted theoretically. With respect to LCO, these are the first results available in the transonic range for the configuration studied. The model also predicts significant changes in LCO behavior as a function of Mach number. However, these are as yet unconfirmed by experiments. Up to high subsonic Mach numbers, the flutter and LCO results are similar to those previously found at low Mach numbers.

CURRENT WORK

Current work is directed toward addressing LCO arising from large amplitude shock motions (and even in the absence of any structural nonlinearity such as freeplay). Preliminary results have now been obtained, and we have determined LCO triggered by a single degree of freedom flutter in pitch in the transonic range. For the particular configuration studied, flutter may occur below the linear flutter velocity if the disturbance is sufficiently large, say on the order of 3 degrees of pitch. These results are described in a separate abstract that is being submitted for presentation at the SDM Conference.
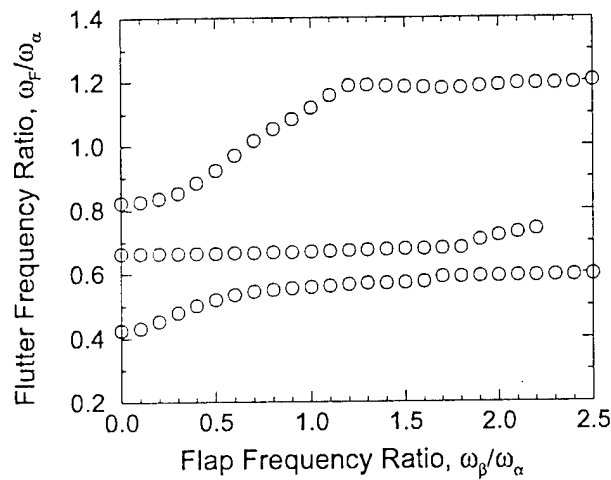
References

[1] Cunningham, A. M., Jr, "A Generic Nonlinear Aeroelastic Method with Semi-Empirical Nonlinear Unsteady Aerodynamics", Vol. 1 and 2, AFRL-VA-WP- TR-1999-3014, 1999.

[2] Conner, M.D. , Tang, D. M. , Dowell, E. H. and Virgin, L. N., "Nonlinear behavior of a typical airfoil section with control surface freeplay: a numerical and experimental
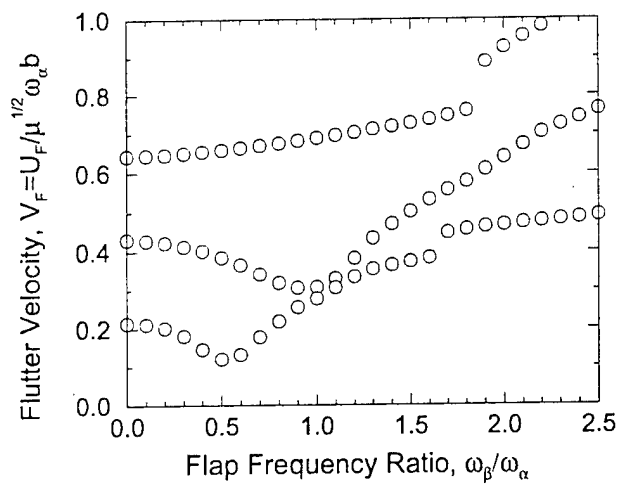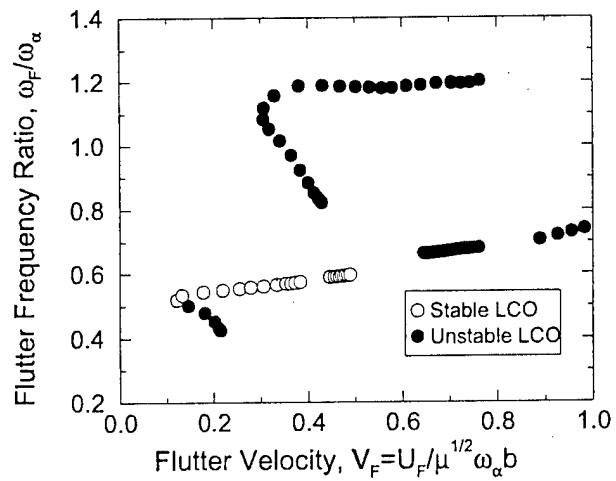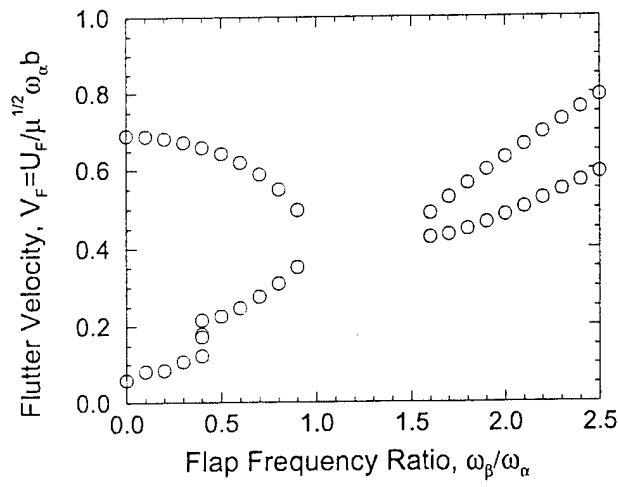
(a) Flutter Velocity
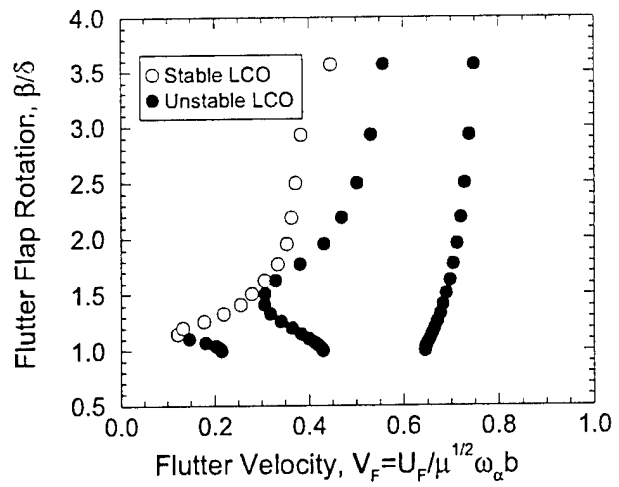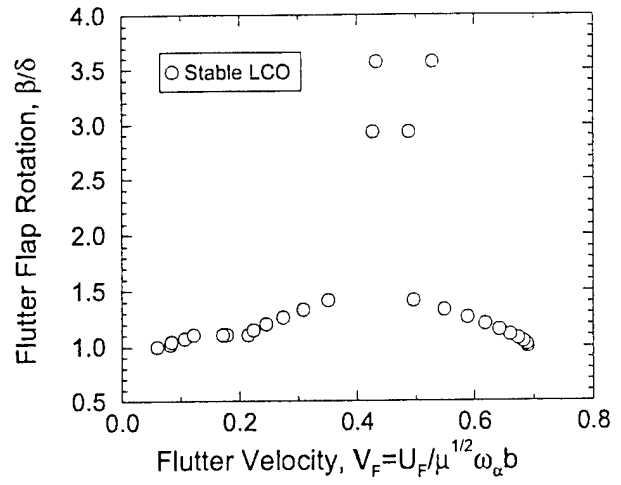
(b) LCO Flap Rotation

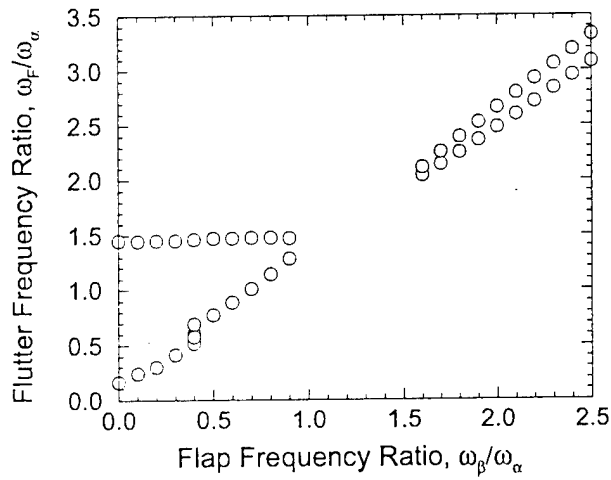(c) Flutter Frequency Ratio

(d) LCO Frequency Ratio

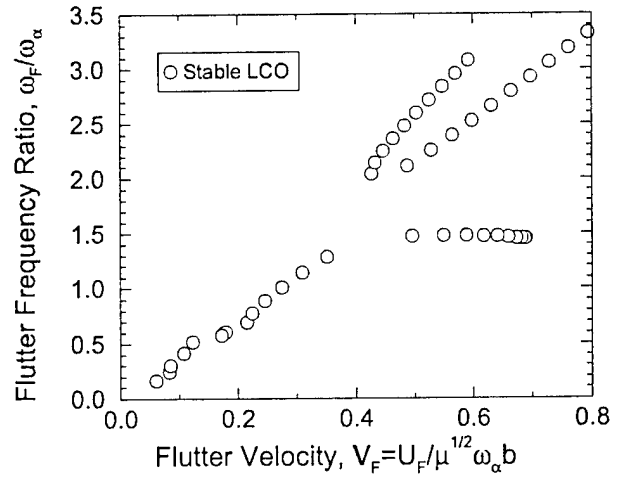**Figure 8: Limit Cycle Behavior: M = 0.80, α_0 = 0.0 (deg)**

6

(a) Flutter Velocity

(b) LCO Flap Rotation

(c) Flutter Frequency Ratio

(d) LCO Frequency Ratio

Figure 9: Limit Cycle Behavior: M = 0.90, α_0 = 0.0 (deg)

study", Journal of Fluids and Structures, Vol. 11, pp. 89-109,1997.

[3] Tang, D. M., Dowell, E.H. and Virgin, L. N., "Limit cycle behavior of an airfoil with a control surface", Journal of Fluids and Structures, Vol. 12, pp. 839-858, 1998.

[4] Hall, K. C., Thomas, J. P. and Dowell, E. H., "Reduced-Order Modeling of Unsteady Small- Disturbance Flows Using Frequency-Domain Proper Orthogonal Decomposition Technique", AIAA Paper 99- 0655, presented at the AIAA Aerospace Sciences Meeting, January, 1999; accepted for publication in the AIAA Journal.

[5] Dowell, E.H. and Hall, K.C.. "Modeling of Fluid- Structure Interaction", Invited Chapter in the Annual Reviews of Fluid Mechanics, to appear, 2000.

[6] Silva, W. A.,"Experimental Steady and Unsteady Aerodynamic and Flutter Results for HSCT Semispan Models", presentation at the Aerospace Flutter and Dynamics Council Meeting at NASA Langley Research Center, May 24, 2000.

APPENDIX B

NONLINEAR INVISCID AERODYNAMIC EFFECTS ON TRANSONIC DIVERGENCE, FLUTTER AND LIMIT CYCLE OSCILLATIONS

Jeffrey P. Thomas, Earl H. Dowell, and Kenneth C. Hall
Duke University, Durham, NC 27708-0300

NONLINEAR INVISCID AERODYNAMIC EFFECTS
ON TRANSONIC DIVERGENCE, FLUTTER AND
LIMIT CYCLE OSCILLATIONS

Jeffrey P. Thomas, *   Earl H. Dowell, †   and   Kenneth C. Hall ‡

Duke University

Durham, NC 27708–0300

INTRODUCTiON

Limit cycle oscillations (LCO) in aeroelastic systems appear to be more prevalent in transonic flow than in subsonic flow. Hence it has been thought that at least for some configurations the source of the nonlinearity that leads to LCO is in the aerodynamic flow. Of course nonlinear structural mechanisms can also lead to LCO whether the flow is transonic or not. And there have been wind tunnel experiments where the test model was designed to exhibit LCO due to a structural nonlinearity, and such test results have been successfully correlated with analysis. See References [1] and [2]. However, the present understanding of LCO induced by aerodynamic nonlinearities is less complete and as yet no systematic quantitative correlation between theory and experiment has been achieved.

This is perhaps a meaningful measure of the greater difficulty in modeling aerodynamic nonlinearities, both theoretically and experimentally, compared to modeling nonlinearities in a structure.

One of the advantages of studying theoretical models is that each of the several possible physical phenomena that may lead to LCO can be studied separately. In this paper, we consider the effects of nonlinearities arising from inviscid transonic aerodynamics. The principal physical effect of interest is the relatively large motion of the shock wave as the amplitude of say the pitch motion of the airfoil becomes sufficiently large. This in turn leads to a movement of the center of pressure with amplitude. Hence one expects to see an effect of amplitude on the neutrally stable motions that may occur. Moreover this may lead to limit cycle motions rather than the catastrophic exponentially growing oscillations predicted by time linearized models. The latter models capture the effect of the mean position of the shock and small shock motions about this mean position by assuming the shock motion is dynamically linear, i.e. the shock motion is proportional to the airfoil motion. This is not true for dynamically nonlinear aerodynamic models that allow for larger and more general shock motions including the possible appearance and disappearance

of a shock during a cycle of airfoil motion. The latter is our concern here.

TECHNICAL DISCUSSION

In this paper, we will consider two distinct aeroelastic phenomena, divergence and flutter, and their associated limit cycle oscillations. To keep the discussion focussed on the fundamental physical phenomena, and to ease the interpretation of the inherently complex phenomena, only a single structural degree of freedom will be studied. However the aerodynamic model will be a state-of-the-art computational fluid dynamics (CFD) based upon the Euler equations of nonlinear, rotational inviscid aerodynamic theory. The aerodynamic model and its spatial discretization will be discussed in the full paper.

Here we emphasize that the solution technique is for a large system of ordinary differential equations in time, which represents the time variation of the fluid unknowns at each spatial grid point in the CFD model. The unknowns are four in number at each grid point for a two-dimensional Euler flow and, for example, could be density, the two scalar components of momentum, and the total energy at each grid point. The present CFD model has about 17,000 total flow variable unknowns, and therefore an efficient solution method is imperative to carry out the studies reported here.

Harmonic Balance Solution in the Frequency Domain

The pioneering work of Ueda and Dowell [3] and Lan and his colleagues [4] should be recalled. Ueda and Dowell used a describing function technique whereby the dominant harmonic was extracted from a time marching CFD model, LTRAN2, using both indicial and harmonic motions of the airfoil. They considered a two degree of freedom typical airfoil section. Lan et. al. used the method of harmonic balance to study the unsteady transonic aerodynamics for flutter and limit cycle oscillation prediction. In their work, they used the transonic small disturbance potential flow model, as did Ueda and Dowell, and only considered a single harmonic. In the present work, we employ the Euler equations of fluid dynamics and also retain multiple harmonics in the aerodynamic model. It is found that using several harmonics improves the theoretical prediction of the aerodynamic forces. However in the aeroelastic analysis, when the fluid and structural models are coupled, only a single harmonic is used. The effects of higher harmonics on this single harmonic are retained as they are found to be significant in the fluid model.

* Research Assistant Professor, Department of Mechanical Engineering and Materials Science, Member AIAA

† J. A. Jones Professor, Department of Mechanical Engineering and Materials Science, and Dean Emeritus, School of Engineering, Fellow AIAA

‡ Associate Professor, Department of Mechanical Engineering and Materials Science, Associate Fellow AIAA

(a) Close-up (b) Overall
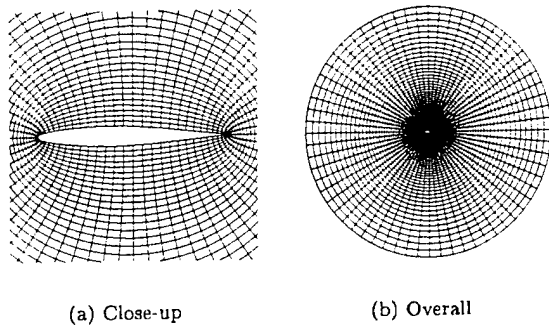
Figure 1: NACA 64A010A Computational Grid

Figure 2: Steady Flow Surface Pressure Distributions: NACA 64A010A Airfoil Section, M = 0.80

The Aeroelastic System and Its Solution

The structural equation of motion is a simple single degree of freedom model in pitch. See Figure (1) for a depiction of the airfoil and the CFD grid used in the numerical calculations. By carefully selecting the pitch axis and mass ratio, we can insure that the system will either undergo classical linear aeroelastic divergence or flutter. Divergence can occur when the aerodynamic "negative" stiffness overcomes the structural stiffness, while flutter may occur when the aerodynamic negative damping overcomes the structural damping. As will be shown, each of these classical linear aeroelastic phenomena has a distinctively different limit cycle or nonlinear behavior.

The Mach number for these studies is M=0.80 and a NACA 64A010A airfoil is considered. The NACA 64A010A is a symmetric (10.6% thickness ratio) variant of the "Ames" AGARD 156 benchmark section. The elastic axis is considered at the mid-chord. Employed for the CFD calculations is an "O"-type computational mesh with 65 × 65 radial and circumferential nodes that has an outer boundary radius of 10 chord lengths. The computed static pressure distribution for an angle of attack of 0.0 and 5.0 degrees is shown in Figure (2). Note that at 5.0 degrees, the upper surface shock wave has moved rearward and increased in strength, and on the lower surface, the shock has essentially disappeared. The center of pressure (x_{cp}) as a function of static angle of attack is shown Figure (3) where it is seen the center of pressure moves from 32% chord to 40% chord as the angle of attack varies from 0.0 to 5.0 degrees.

Linear and Nonlinear Divergence

This is perhaps the simpler of the two phenomena since by definition it is time independent, i.e. we are dealing with a static linear instability and its nonlinear counterpart. In this case, the structural equation of motion becomes an equation of static equilibrium. And for the aerodynamic model, we only need to determine the lift and moment about some appropriate axis as a function of angle of attack. For small angle of attack, we will recover the classical linear aeroelastic divergence phenomena. But the question is, what are the effects of the nonlinearity?

The equation of static equilibrium simply equates the aerodynamic and elastic restoring moments. Namely,

$$K_\alpha = q_\infty c^2 c_{m\alpha} \tag{1}$$

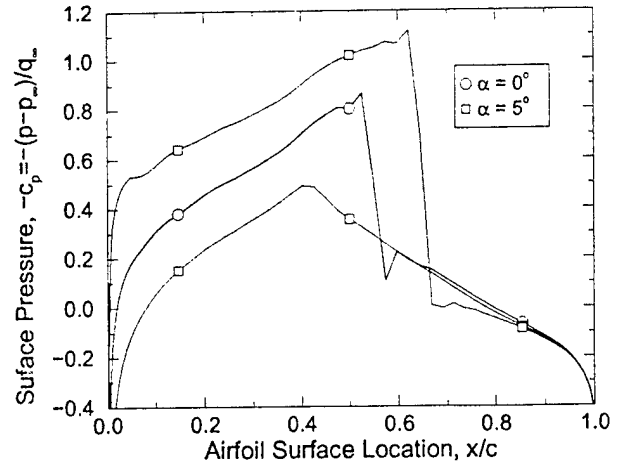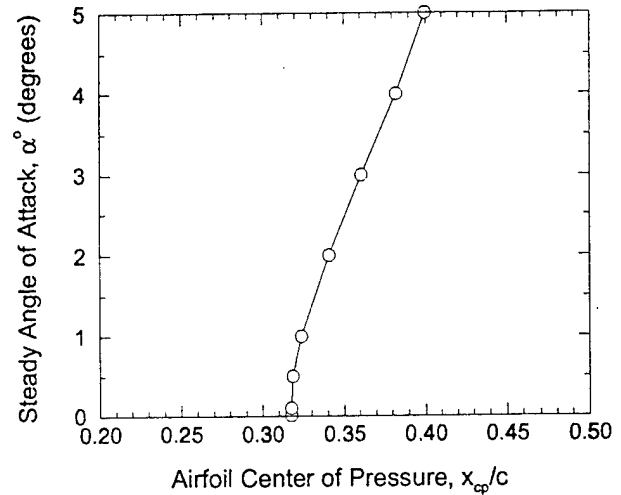**Figure 3: Center of Pressure Variation with Angle of Attack: NACA 64A010A Airfoil Section, M = 0.80**

Defining a non-dimensional dynamic pressure, λ, Equation (1) may be rewritten as

$$\lambda = \alpha/c_{m\alpha} \tag{2}$$

where λ is given by $\lambda = q_\infty c^2 /K_\alpha$, The angle of attack may have an initial angle, α_0, which is prescribed, and also an additional angle due to the torsional twist of the elastic spring, α.

Now for a linear aeroelastic model, the aerodynamic moment coefficient is simply proportional to the angle of attack. Thus for no initial angle of attack, the classical linear divergence dynamic pressure is given by Equation (2) where λ is now a fixed number.

To extend this study of divergence into the nonlinear range, we recognize that now the aerodynamic coefficient is a nonlinear function of angle of attack. For zero initial angle of attack, we may determine the twist of the torsional spring, and its de-
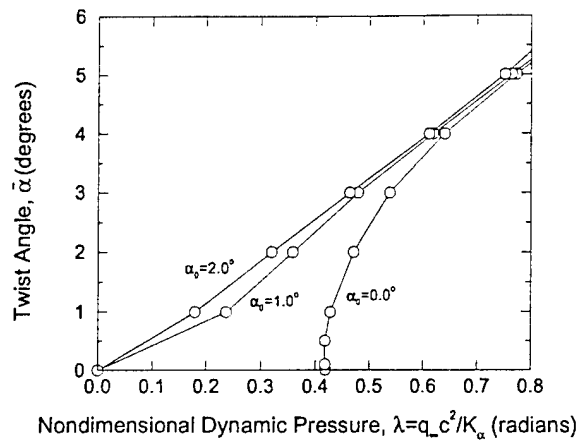
2

Figure 4: Divergence and Post-Divergence of an Airfoil Including Transonic Nonlinear Inviscid Aerodynamics: NACA 64A010A Airfoil Section, M = 0.80, Elastic Axis Location, a = e/b = 0.0

pendence on λ, by specifying the twist angle in Equation (2) and then solving for λ. This procedure is readily extended to the case with an initial angle of attack.

Qualitatively one can anticipate the effect of the aerodynamic nonlinearity by examining the aerodynamic moment variation with angle of attack. A necessary condition for divergence to occur is that the aerodynamic moment be positive in the same direction as the twist angle. Moreover, if the nonlinear aerodynamic model predicts a moment less in magnitude than that predicted by linear aerodynamic theory, the effect of the nonlinearity will be to stabilize the divergence. And vice versa if the nonlinear theory predicts an increase in aerodynamic moment over that given by linear theory. Hence by examining the slope of the moment vs. angle of attack curve with increasing angle of attack, we will know whether the effect of the nonlinearity is favorable or unfavorable.

In the example below, the effect is favorable. That is, once the divergence dynamic pressure for a small angle of attack is exceeded (this is the classical linear aeroelastic divergence dynamic pressure), then the angle of twist of the pitch spring remains finite and smoothly increases from zero beyond the divergence dynamic pressure. See Figure (4) where the angle of twist is plotted vs the non-dimensional dynamic pressure. Also shown are results with an initial angle of attack. In this latter case, there is some twist over the full range of dynamic pressure. Indeed even if the initial angle of attack is only a few degrees, it would be difficult to detect the classical divergence dynamic pressure experimentally for this example. For readers who have studied buckling of systems in the presence of imperfections (e.g. beams, plates or shells with initial curvature), this behavior will be familiar.

In this example, recall the center of pressure moves from 32% chord at low angles of attack to 40% chord at 5.0 degrees angle of attack. This is the principal reason for the stabilizing effect of nonlinear aerodynamics on the post-divergence condition.

Had the change of the slope of the aerodynamic moment curve been in the opposite direction, then the angle of twist

vs. dynamic pressure curve would have bent the other way. That is, for dynamic pressures below the classical divergence dynamic pressure, there would be non-trivial (non-zero) twist angles that represent possible static nonlinear equilibrium solutions. Intuitively one recognizes that these latter solutions would themselves be unstable, i.e. such results would be interpreted physically as the magnitude of the disturbance required to generate non-trivial twist at dynamic pressures below the classical divergence dynamic pressure. In our studies to date, only the stable nonlinear effect has been observed for statically divergent systems. However, this is not to say that unstable nonlinear divergence systems may not be encountered for some other parameter combinations.

Of course, divergence is a very special case of nonlinear aeroelasticity as it is for linear aeroelasticity, because the frequency of oscillation is zero when divergence and post-divergence occurs. Thus we now turn to an oscillatory case.

Flutter and Associated LCO

Now consider single-degree-of-freedom flutter in pitch. Here the classical flutter arises from a negative damping in the aerodynamic moment beyond a certain reduced frequency. However the reduced frequency at which the aerodynamic damping moment becomes negative increases as the angle of pitch oscillation increases. Hence the reduced velocity decreases as the angle of pitch increases, which suggests that this will lead to an unstable LCO as indeed it does.

In the example considered, we have moved the elastic axis to 20% chord to preclude divergence and to induce flutter.

It should be emphasized that in the present analysis, we are using a single harmonic to represent the pitch oscillation. However in the calculation of the aerodynamic moment, we include up to three harmonics to determine the effect of higher harmonics on the first harmonic of the aerodynamic moment. It turns out that the effect of the third harmonic is negligible. Indeed, if one only retains a single harmonic in the aerodynamic analysis, the results are qualitatively correct and have fair quantitative accuracy.

Results for the first harmonic for the lift and moment about the pitch or elastic axis are shown in Figure (5). These results are for two harmonics retained in the aerodynamic analysis. Note that the results at a reduced frequency of zero were those used in the divergence analysis discussed previously. Of course, a transformation of the pitch axis is used for the divergence analysis.
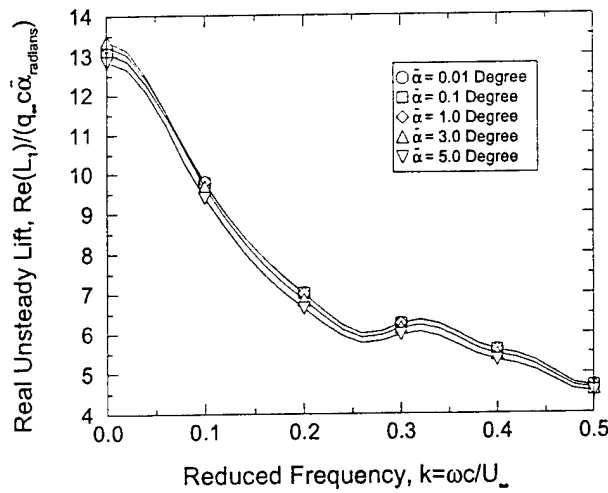
With the real and imaginary parts of the aerodynamic moment taken from Figure (5), and using the usual pitch equation of motion,

$$I_\alpha \left(\ddot{\alpha} + 2\zeta_\alpha \omega_\alpha \dot{\alpha} + \omega_\alpha^2 \alpha \right) = q_\infty c^2 c_{m_\alpha} \qquad (3)$$
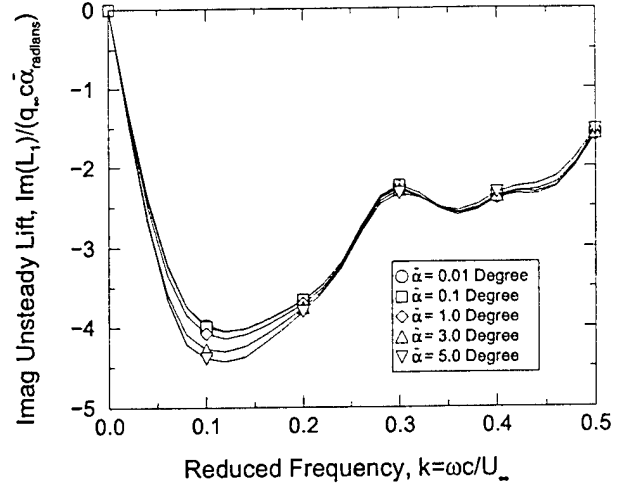
where $\omega_\alpha^2 = K_\alpha / I_\alpha$, we can convert this equation into the frequency domain, and nondimensionalize and separate it into real and imaginary parts. With some rearrangement, these two equations can be written as

$$\left(\frac{\omega_\alpha}{\omega} \right)^2 = \left[\frac{\bar{c}_{m_\alpha} \mathrm{Re}}{\bar{\alpha}} / \left(\frac{\omega c}{U} \right)^2 \right] \left(\frac{8}{\pi} \right) / \mu r_\alpha^2 \qquad (4)$$
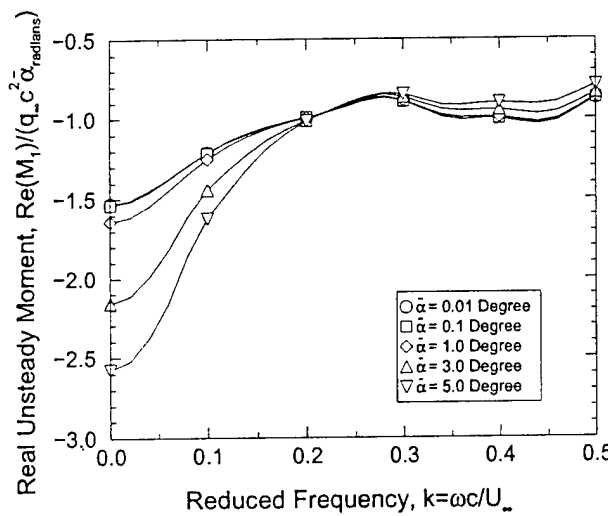
$$\zeta_\alpha = \left(\frac{\bar{c}_{m_\alpha} \mathrm{Im}}{\bar{\alpha}} \right) \left(\frac{U}{\omega_\alpha c} \right) \left(\frac{U}{\omega c} \right) \left(\frac{4}{\pi} \right) / \mu r_\alpha^2 \qquad (5)$$
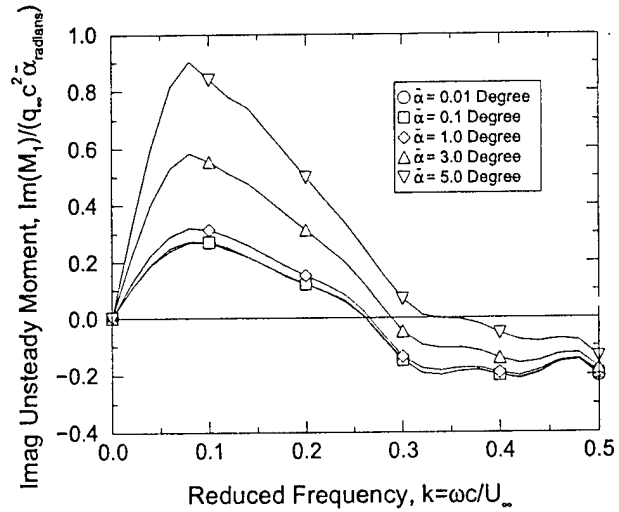
3

(a) Real Unsteady Lift

(b) Imaginary Unsteady Lift

(c) Real Unsteady Moment

(d) Imaginary Unsteady Moment

Figure 5: Unsteady Lift and Moment for Various Pitch Amplitudes: NACA 64A010A Airfoil Section, M = 0.80, α_0 = 0.0 (deg), Elastic Axis Location, a = e/b = -0.6, Two Harmonics Employed in Harmonic Balance Expansion

4

where a bar over the aerodynamic coefficient and angle of twist denotes the amplitude of the first harmonic, and Re and Im denote real and imaginary parts.

The imaginary part of the equation of motion, Equation (5), essentially determines the neutral stability condition of the system, and the real part determines the frequency of oscillation. Of course now both of these results depend on the pitch amplitude of motion.

While structural damping is readily included in the analysis, as will be seen below, it will be helpful to understand the essence of the results by first considering the solution for zero structural damping.

Zero Structural Damping

In this case, Equation (5) states that a neutrally stable oscillation will occur when the imaginary part of the aerodynamic moment becomes zero. This will occur at some reduced frequency for a particular angle of pitch oscillation (and other parameters fixed such as Mach number). Then from Equation (4), one can solve for the frequency of this neutrally stable oscillation. For sufficiently small motions, this is the flutter solution; for larger motions, we determine a limit cycle oscillation. The solution procedure then is to select an amplitude of oscillation, determine the reduced frequency at which the imaginary part of the aerodynamic moment is zero from Figure (5), and then determine the frequency of the oscillation from Equation (4). Note this is essentially the same computational procedure as for a classical flutter solution, except now the reduced frequency, the frequency of oscillation, and the reduced velocity are all functions of the pitch amplitude.

It should be noted however that just because the imaginary part of the aerodynamic moment vanishes (i.e. the aerodynamic damping becomes zero), that alone does not insure that a neutrally stable oscillation will occur. This is because the frequency determined from Equation (4) must be physically possible, i.e the right hand side of Equation (4) must be positive. It is evident that the right hand side of Equation (4) depends only on the reduced frequency (which is known by the requirement that the imaginary part of the aerodynamic moment be zero) and a non-dimensional moment of inertia. But of course these reduced frequencies themselves depend on the pitch amplitude. Thus one can determine when the right hand side of Equation (4) is positive or negative and express the result in terms of pitch amplitude and moment of inertia. This relationship is shown in Figure (6), and the regions where flutter and limit cycle oscillations are or are not possible are indicated. The value of moment of inertia that marks the boundary between no flutter or LCO possible and possible flutter or LCO is termed the "asymptotic value".

Large Pitch Moment of Inertia

Now if the mass ratio or moment of inertia is much larger than the asymptotic value, a not uncommon circumstance, then the flutter or LCO frequency is simply equal to the structural pitch natural frequency. See Equation (4). With this approximation, the results of Figure (7) are obtained for both zero and non-zero structural damping. Note that the curves bend to the left which is indicative of an unstable LCO. That is, these results are to be interpreted as the amplitude of a disturbance required to initiate explosive flutter below the classical flutter
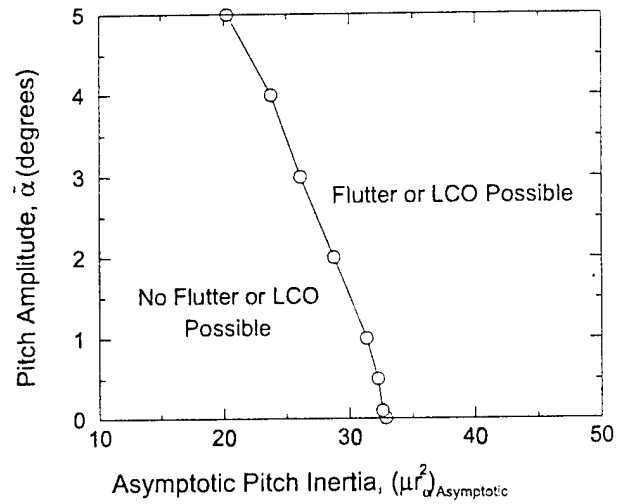

Figure 6: Asymptotic Value of Pitch Inertia For Various Pitch Amplitudes Marking Regions Where Flutter and Limit Cycle Oscillations Are or Are Not Possible: NACA 64A010A Airfoil Section, M = 0.80, α_0 = 0.0 (deg), Elastic Axis Location, a = e/b = -0.6
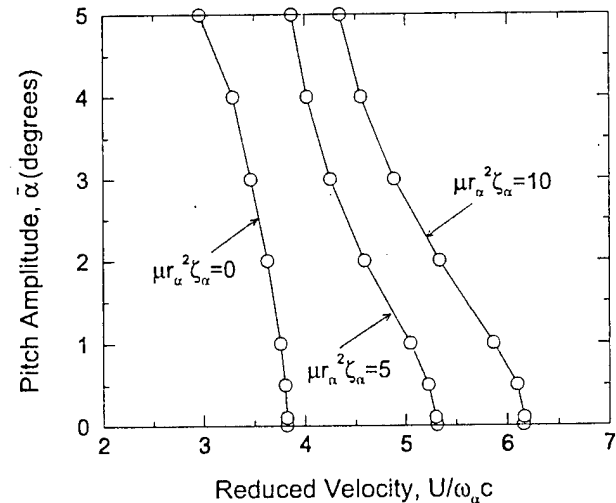

Figure 7: LCO Amplitude Versus Reduced Velocity: NACA 64A010A Airfoil Section, M = 0.80, α_0 = 0.0 (deg), Elastic Axis Location, a = e/b = -0.6

velocity for this single-degree-of-freedom pitch oscillation.

In Figure (8), shown are the values of structural damping (normalized by pitch moment of inertia) that correspond to neutrally stable limit cycle oscillations. These can be calculated from Equation (5) as a function of reduced velocity for various pitch amplitudes. A cross-plot of these data is used to construct the plots for non-zero damping values as shown in Figure (7).

5

Pitch Inertia x Damping, $\mu r_\alpha^2 \zeta_\alpha$

○ $\bar{\alpha} = 0.01°$
□ $\bar{\alpha} = 1.0°$
◇ $\bar{\alpha} = 2.0°$
△ $\bar{\alpha} = 3.0°$
◁ $\bar{\alpha} = 4.0°$
▽ $\bar{\alpha} = 5.0°$

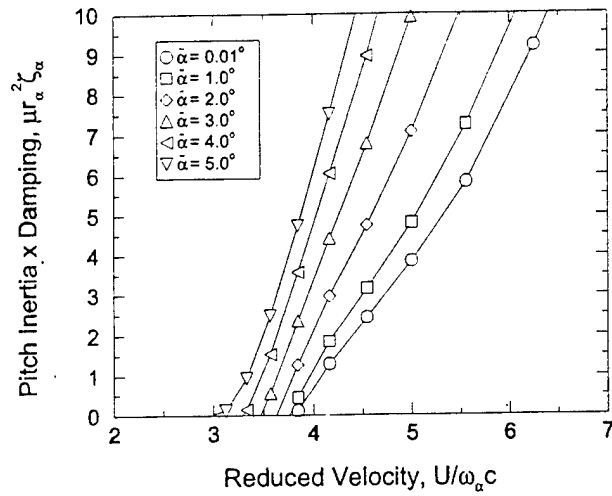Reduced Velocity, $U/\omega_\alpha c$

Figure 8: Normalized Structural Damping Corresponding to Neutrally Stable Limit Cycle Oscillations for Large Pitch Moment of Inertia: NACA 64A010A Airfoil Section, M = 0.80, α_0 = 0.0 (deg), Elastic Axis Location, a = e/b = -0.6

Pitch Amplitude, $\bar{\alpha}°$ (degrees)

$\mu r_\alpha^2 = 25$
→ ϵ ∞at $\bar{\alpha} = 3.0°$
$\mu r_\alpha^2 = 37.5$
→ 10.9 at $\bar{\alpha} = 0.0°$
Asymptote
$\mu r_\alpha^2 = 50$
$\mu r_\alpha^2 = 200$
$\mu r_\alpha^2 = 100$

Reduced Velocity, $U/\omega_\alpha c$

Figure 9: LCO Amplitude Versus Reduced Velocity for Various Pitch Inertias: NACA 64A010A Airfoil Section, M = 0.80, α_0 = 0.0 (deg), Elastic Axis Location, a = e/b = -0.6

Effects of Finite Pitch Moment of Inertia

For general values of moment of inertia and structural damping, the solution algorithm using Equations (4) and (5) proceeds as follows. First select a Mach number and pitch axis, and for a range of pitch amplitudes, determine the first harmonic of the aerodynamic moment (including higher harmonics of the aerodynamic model and their effect on the fundamental harmonic). Then for a given pitch amplitude, choose a reduced frequency and determine the flutter or LCO oscillation frequency from Equation (4). This frequency will be proportional to the pitch structural frequency, of course. With the flutter or LCO frequency determined, and the reduced frequency selected, one then knows the flow velocity corresponding to the chosen pitch amplitude. Finally from Equation (5), determine the structural damping value necessary to give a neutrally stable flutter or limit cycle oscillation. From this perspective, the flutter condition is simply the neutrally stable motion that may exist at small angles of twist, and the LCO are the neutrally stable oscillations that may exist when the pitch amplitude is finite. Of course the flutter or LCO may become unstable when it is perturbed (e.g. by perturbations in the amplitude of oscillation), and this is indeed the case in the example treated here.

Up to this point, we have assumed that the pitch moment of inertia is well above its asymptotic value. Hence the flutter frequency is the same as the structural natural pitch frequency.

Now we consider the more general case and a range of pitch inertias such that the flutter frequency is no longer precisely equal to the structural natural frequency in pitch. Results are shown for non-dimensional pitch inertias of 200,100,50,37.5 and 25 in Figures (9) and (10). These are for LCO amplitude and frequency, respectively, versus reduced velocity. The asymptotic pitch inertia results are also shown for reference.

As expected, for sufficiently large pitch inertia, say greater than 200, the asymptotic results are good approximations.
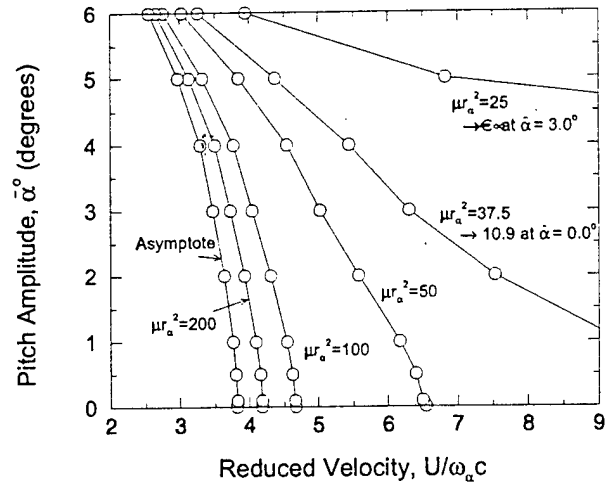
Pitch Amplitude, $\bar{\alpha}$ (degrees)

Asymptote
$\mu r_\alpha^2 = 37.5$
$\mu r_\alpha^2 = 200$
$\mu r_\alpha^2 = 100$
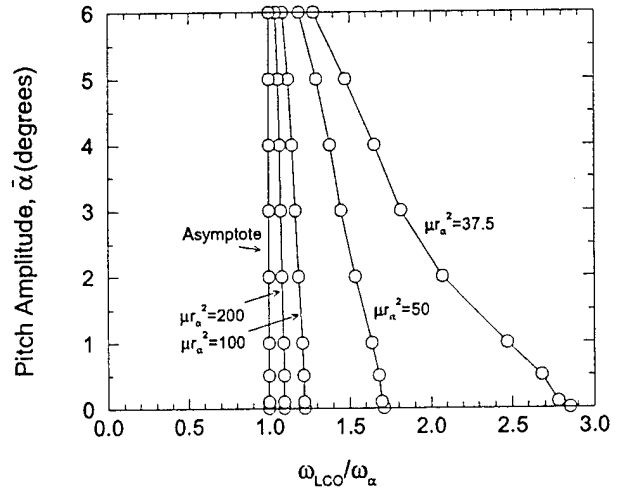$\mu r_\alpha^2 = 50$

$\omega_{LCO}/\omega_\alpha$

Figure 10: LCO Amplitude Versus LCO Frequency for Various Pitch Inertias: NACA 64A010A Airfoil Section, M = 0.80, α_0 = 0.0 (deg), Elastic Axis Location, a = e/b = -0.6

However for pitch inertias less than 100, the results show a more sensitive dependence on pitch moment of inertia. For sufficiently small pitch moment of inertia, of course, no flutter or LCO is possible.

The relationship between pitch moment of inertia and reduced velocity may be even more clearly seen by fixing the pitch amplitude and then plotting these variables as shown in Figure (11). Note in this figure, as reduced velocity decreases, the pitch moment of inertia for flutter and LCO to occur tends to infinity. Thus for sufficiently small reduced velocity no flutter or LCO will occur. Conversely as the pitch moment of inertia decreases, the reduced velocity for flutter or LCO to occur tends to infinity. Thus below some value of pitch moment of inertia, no flutter or LCO is possible. Of course, these results
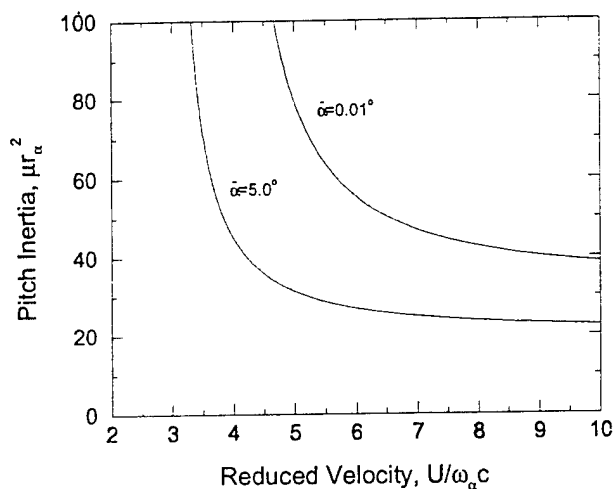
Figure 11: Pitch Inertia Versus Reduced Velocity for Fixed Pitch Amplitudes: NACA 64A010A Airfoil Section, M = 0.80, α_0 = 0.0 (deg), Elastic Axis Location, a = e/b = -0.6

are for a fixed pitch amplitude when in fact the pitch amplitude is an outcome of the analysis (not an input). However, the results are not very sensitive to pitch amplitude and the conclusions regarding asymptotic behavior hold over the full range of pitch amplitudes considered here.

CONCLUSIONS

Aerodynamic nonlinearities may be give rise to LCO, and these may be either stable (favorable) or unstable(unfavorable). An example of the former is shown here as the nonlinear counterpart of classical linear aeroelastic divergence. An example of the latter is also shown here as the nonlinear counterpart of single-degree-of-freedom pitch flutter. Future work will be directed toward the study of the nonlinear counterpart of classical bending/torsion flutter where similar methods may be used and results for the two-degree-of-freedom case will be presented in the final paper.

References

[1] Tang, D. M., Henry, J. K. and Dowell, E. H., "Limit Cycle Oscillations of Delta Wing Models in Low Subsonic Flow", AIAA Journal, Vol. 37, No. 11, pp. 1355-1362, 1999.

[2] Tang, D. M., Dowell, E. H. and Virgin, L. N., "Limit Cycle Behavior of an Airfoil with a Control Surface", Journal of Fluids and Structures, Vol. 12, No. 7, pp. 839-858, 1998.

[3] Ueda, T. and Dowell, E. H., "Flutter Analysis Using Nonlinear Aerodynamic Forces", J. Aircraft, Vol. 21, No. 2, pp. 101-109, 1984.

[4] Greco, P.C., Jr., Lan, C. E. and Lim, T. W., "Frequency Domain Unsteady Transonic Aerodynamics for Flutter and Limit Cycle Oscillation Prediction", AIAA Paper 97-0835, 35th Aerospace Sciences Meeting, Reno, Nevada, January 6-10, 1997.

APPENDIX C

**THREE-DIMENSIONAL TRANSONIC AEROELASTICITY
USING PROPER ORTHOGONAL DECOMPOSITION
BASED REDUCED ORDER MODELS**

Jeffrey P. Thomas, Earl H. Dowell, and Kenneth C. Hall
Duke University, Durham, NC 27708–0300

*An Extended Abstract for the 42nd AIAA/ASME/ASCE/AHS/ASC Structures, Structural
Dynamics, and Materials Conference, April 16-19, 2001, Seattle, WA.*

THREE-DIMENSIONAL TRANSONIC AEROELASTICITY USING
PROPER ORTHOGONAL DECOMPOSITION BASED REDUCED ORDER MODELS

Jeffrey P. Thomas, *   Earl H. Dowell, [†]   and   Kenneth C. Hall [‡]
Duke University
Durham, NC 27708-0300

INTRODUCTION

In the following extended abstract, we demonstrate how the recently devised proper orthogonal decomposition (POD) based reduced order modeling (ROM) technique (References [1] and [2]) can be used to model unsteady aerodynamic and aeroelastic characteristics of three-dimensional transonic wing configurations. Although transonic Euler flows are considered in [1] and [2], the initial demonstrations of the POD/ROM method as presented in these references are for two-dimensional flow and two structural degree-of-freedom airfoil configurations. Also in [3], an application of the POD/ROM technique to the well known vortex lattice method has been presented.

In extending the POD/ROM technique to three-dimensions, two primary issues have been of concern. First, the size of the computational fluid dynamic (CFD) model will in general be at least an order of magnitude greater than for two-dimensions. Whereas a typical CFD model for a realistic two-dimensional configuration might have on the order of 10's or even 100's of thousands of degrees of freedom (DOF), a CFD model for a three-dimensional configuration might easily have on the order of at least hundreds of thousands if not millions or more DOF's. In two-dimensions, we have found that very accurate ROM's with on the order of only a few dozen DOF's can be devised using the POD/ROM methodology. A first issue to address has thus been whether or not in three-dimensions one can also generate accurate ROM's, which require at most a few dozen DOF's.

The second concern is, for any variation of the structural properties of a given wing under consideration, will a completely new ensemble of solution vector "snapshots" have to be computed in order to devise an accurate POD/ROM. A basic aspect of the POD/ROM method is that an ensemble of solution vectors is first assembled by computing unsteady CFD solutions at a number of discrete frequencies within a frequency range of interest for the unsteady structural motions that are also of interest. In two dimensions, this step is relatively straight forward since one only has to consider a few

possible motions, e.g. pitch and plunge.

In three-dimensions however, the wing vibratory mode shapes will be different for each different structural configuration of a given wing. There can in fact be an infinite number of unsteady motions (or at least a substantial number of motions equivalent to the number of DOF's of the discrete structural model). Thus the second concern about extending the POD/ROM to three-dimensions has been whether or not it is necessary to compute a completely different ensemble of solution snapshots for every possible structural configuration. For example, say one computes solution snapshots for a given wing configuration based on the wing's particular vibratory modes shapes in order to develop a POD/ROM to model the configuration's aeroelastic characteristics. Then the question is, if the structural make-up of the wing changes, does one have to compute a whole new ensemble of solution snapshots for the same wing, but for the different set of vibratory modes shapes.

Fortunately in addressing these two issues, and as will be shown in the following, we have found that accurate POD/ROM's with just a few dozen degrees of freedom can in fact be created for a realistic transonic three-dimensional configurations. This is true even though in the model problem to be shown subsequently, the CFD model is easily an order of magnitude larger than anything we have previously studied in two-dimensions. Furthermore, we have discovered that a "fundamental" ensemble of solution snapshots, based on wing motions that need not be related to the structural modes under consideration, can be assembled as a first step. Accurate POD/ROM's for a given wing configuration can then be created by simply adding to this "fundamental" ensemble, the snapshots corresponding to actual wing structural modal motions solely at the frequencies corresponding to the end points of the frequency range of interest. In general, these two snapshots prove to be sufficient to "lock in" the conditions corresponding to the particular structural motion, and indeed the fundamental ensemble of solution snapshots is sufficient to reveal the unsteady dynamics of the fluid dynamic model. The fundamental ensemble of snapshots can be used again and again even as the structural mode change, and thus the computational cost of having to compute an entirely new snapshot ensemble for every new structural configuration is greatly reduced.

POD/ROM METHODOLOGY

In the following, we will be considering inviscid three-dimensional Euler flows. More specifically, linearized (about some nonlinear background steady flow) unsteady frequency-

1

domain CFD solutions to the Euler equations are computed. The POD/ROM procedure can be considered as a "wrapper" around any typical CFD method, and the CFD method we have employed for the present analysis is a variant of Ni's [4] approach to the standard Lax-Wendroff method. The frequency domain CFD method in effect represents a linear system formulation of the unsteady fluid dynamic model, i.e.

$$Aq = -B\zeta \qquad (1)$$

where q is an N dimensional vector (N is the number of mesh points time the number of dependent flow variables) of the unknown flow variables a each mesh point in the CFD domain, and ζ is the L dimensional vector (L is the number structural mode shapes) of modal coordinates for the structural model. A is the $N \times N$ fluid dynamic influence matrix, and B is the $N \times L$ matrix which relates the flow solver boundary conditions to each particular mode shape. Both A and B are functions of the background flow and unsteady frequency ω. The structural equations for the wing configuration being modeled within the flow can be written as

$$D\zeta = -Cq \qquad (2)$$

where D represents the $L \times L$ structural influence matrix (i.e. $D = -\omega^2 \mathcal{M} + \mathcal{K}$ where $\mathcal{M}$ and $\mathcal{K}$ are the generalized mass and stiffness matrices), and C is the $L \times M$ matrix which represents the discrete integration used to obtain the generalized forces associated with each modes shape based on the unsteady flow q. When Equations (1) and (2) are put together,

$$\begin{bmatrix} A & B \\ C & D \end{bmatrix} \begin{Bmatrix} q \\ \zeta \end{Bmatrix} = \begin{Bmatrix} 0 \\ 0 \end{Bmatrix} \qquad (3)$$

The resulting equation (3) is a fully coupled aeroelastic system of equations, which for nontrivial q and ζ, represents an eigenvalue problem with ω being the eigenvalue. Any eigenvalues with a positive real part imply the aeroelastic system is unstable.

The problem with constructing and solving this eigenvalue problem is that A is simply too large for realistic configurations. As mentioned in the introduction, N can easily be on the order of 10,000 or 100,000 for two-dimensional configurations, and on order of 100,000 to 1,000,000 or even more for three dimensional configurations. For such large cases, even attempting to set up A is well beyond the memory limits of todays largest computers.

The basic premise of the POD/ROM methodology is that we assume the unknown flowfield solution vector q can be expressed as a Ritz type expansion of the form

$$q \approx \sum_{k=1}^{K} \xi_k \phi_k \qquad K \ll N \qquad (4)$$

where ξ_k is a generalized coordinate sometimes referred to as an augmented aerodynamic state variable, and ϕ_k is the corresponding Ritz vector. Equation (4) can also be written in matrix form as

$$q = \Phi\xi, \quad \text{where} \quad \Phi = \begin{bmatrix} | & | & & | \\ \phi_1 \phi_2 & \cdots & \phi_K \\ | & | & & | \end{bmatrix} \quad \text{and} \quad \xi = \begin{Bmatrix} \xi_1 \\ \xi_2 \\ \vdots \\ \xi_K \end{Bmatrix}. \qquad (5)$$

Here, Φ is an $N \times K$ matrix whose kth column is the shape vector ϕ_k, and ξ is the K dimensional vector of augmented aerodynamic state variables ξ_k.

A reduced-order representation of the fluid dynamic and aeroelastic systems can be formulated by substituting Equation (5) into Equation (1) and/or (3) and pre-multiplying by the Hermitian transpose (Φ^H) of Φ, i.e.

$$\Phi^H A \Phi \xi = \Phi^H B \zeta \quad \text{or} \quad \mathcal{A}\xi = -\mathcal{B}\zeta \qquad (6)$$

and

$$\{\Phi^H I\} \begin{bmatrix} A & B \\ C & D \end{bmatrix} \begin{Bmatrix} \Phi\xi \\ \zeta \end{Bmatrix} = \begin{bmatrix} \mathcal{A} & \mathcal{B} \\ \mathcal{C} & \mathcal{D} \end{bmatrix} \begin{Bmatrix} \xi \\ \zeta \end{Bmatrix} = \begin{Bmatrix} 0 \\ 0 \end{Bmatrix} \qquad (7)$$

If the Ritz approximation is good one, ($K \ll N$), and Equations (6) and (7) will represent much smaller systems that can readily be solved using conventional eigenvalue techniques.

The next question becomes what are good choices for the Ritz vectors ϕ_k that will in fact result in good Ritz approximations. Previous studies as detailed in References [1] and [2] have demonstrated that shape vectors derived via the proper orthogonal decomposition technique (see for instance [5], [6], and [7]) are an excellent source. For the sake of brevity, the of details are omitted here, but a discussion of how the shapes are derived can be found in References [1] and [2]. The basic premise behind their formulation is that a number solution "snapshots" are directly computed for a number of discrete frequencies and unsteady structural motions of interest. From this ensemble of solution vectors, the POD shapes are easily derived by solving a small (the size of the number of snapshots) eigenvalue problem. The first few POD modes describe the most dominant dynamic characteristics of the fluid dynamic system, and as such, the POD shapes have proven to be an excellent set of Ritz vectors for fluid dynamic and/or aeroelastic models.
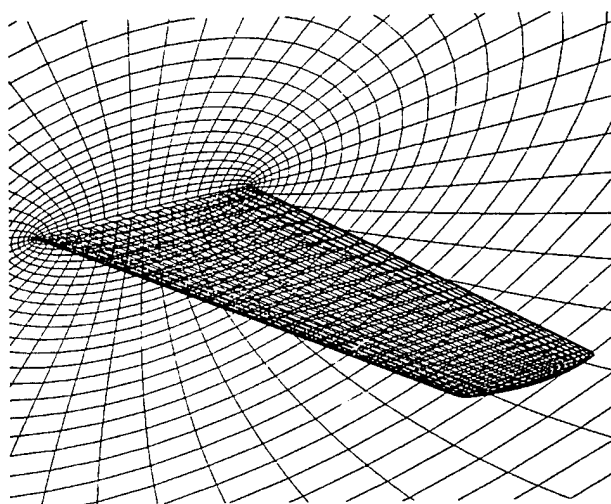
MODEL PROBLEM

The configuration under consideration is the AGARD model 445.6 wing (Reference [8] and [9]). This is a 45 degree quarter chord swept wing using the NACA 64A004 airfoil section that has an aspect ratio of 3.3 (for the full span) and a taper ratio of 2/3. Figure (1) illustrates the computational mesh employed for this configuration. The grid is an "O-O" topology that employs 49 computational nodes about each airfoil section, 33 nodes normal to the wing, and 33 nodes along the semispan. The outer boundary of the grid extends five semispans from the midchord of the wing root section. The particular structural configuration of the wing is referred to as the 2.5 ft. weakened model 3 (again see Reference [8] and [9]).
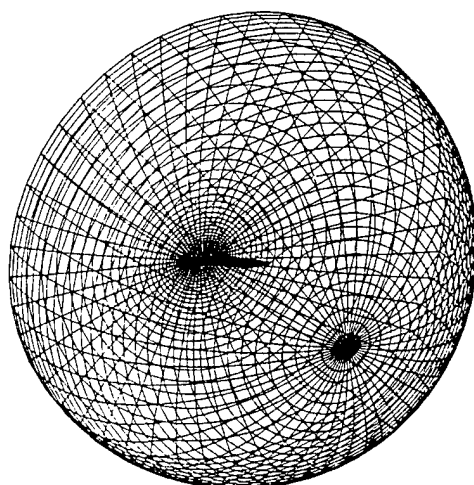
Figure (2) shows the computed wing surface and symmetry plane steady flow pressure contours for the Mach numbers of 0.960 and 1.141. A relatively weak shock can be seen at the trailing edge for M=0.960. This shock appears to get stronger at M=1.141. The wing section is quite thin (4%), so a strong shock is not really expected. Comparing contours, our flowfields look very comparable to those of Lee-Rausch and Batina [10], although they employed a much larger mesh.

FLUTTER RESULTS

Figure (3) shows the eigenvalue root-loci when sweeping through various mass ratios (to which there is a correspond-
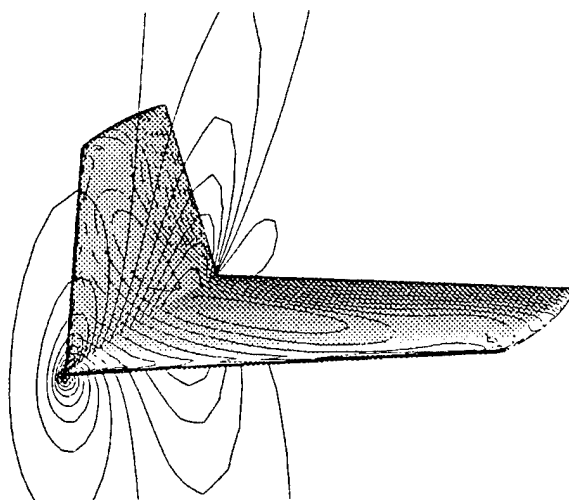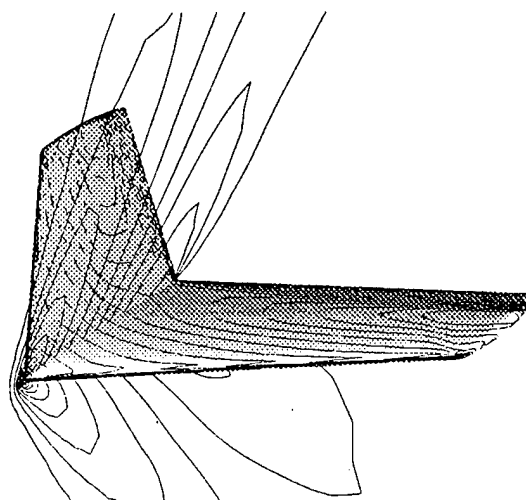
(a) Wing Surface and Symmetry Plane Grids

(b) Outer Boundary Grid

Figure 1: AGRAD 445.6 Wing Grid Topology

(a) M=0.960

(b) M=1.141

Figure 2: AGRAD 445.6 Wing Surface and Symmetry Plane Pressure Contours

ing flutter speed index) when solving the aeroelastic eigenvalue problem posed by the reduced-order aeroelastic model (Equation (7) for various Mach numbers. Solution snapshots are computed for the first five given wing mode shapes for reduced frequencies ($k = \omega b/U_\infty$) from $k = 0.0$ to $k = 0.5$ in $\Delta k = 0.1$ increments. This configuration flutters for frequencies less than 0.5, and as such, solution snapshots for $k > 0.5$ are unnecessary. This results in a total of 55 available POD shape vectors. In Figure (3), the curves represent the eigenvalues corresponding to the primarily structural natural modes as mass ratio is varied. Our method also determines the aeroelastic modes originating from the fluid dynamic modes of the POD/ROM. For the range of mass ratios ($0 \leq \mu \leq 500$) swept through in these parametric analyses, the fluid dynamic modes are very damped, and as such lie to the left and outside of the eigenspectrum range we show. As can been, for each of the Mach numbers, the first structural mode tends to be the criti-

cal flutter mode. For the highest Mach number however, the third structural mode can go unstable if the mass ratio is large enough. Also from this figure, it is evident that it is unnecessary to use all 55 of the available POD shapes. If fact, with less than one half of the POD modes (25 for instance), relatively converged results (in the sense of POD mode refinement) can be achieved.

Figure (4) shows the computed POD/ROM flutter speed and flutter frequency ratios, along with experimental data [8], and data from two other computational methods ([10] and [11]) , as a function of Mach number. As can be seen, using our methodology, we produce the well known transonic flutter speed dip, and our results are all within the same tolerance to the experimental results as the other computational methods. Gupta [11] does show better agreement with experiment at the two supersonic Mach numbers, and Gupta attributes this better agreement to better CFD grid refinement.
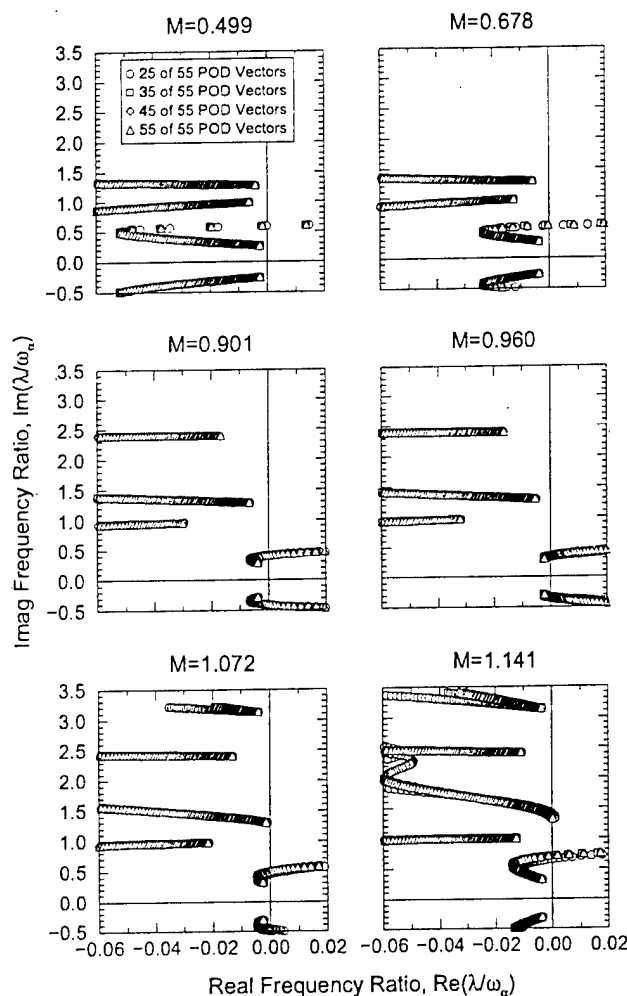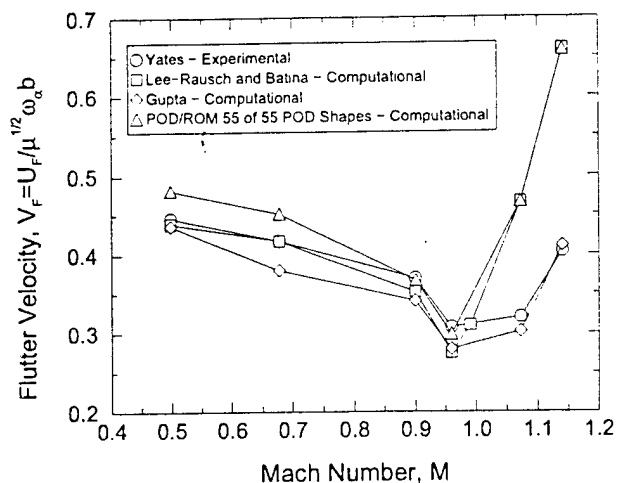
3

Figure 3: Aeroelastic Root-Loci at Various Mach Numbers for the AGRAD 445.6 Wing "Weakened" Configuration, α_0 = 0.0 (deg)

(a) Flutter Speed

(b) Flutter Frequency Ratio

Figure 4: Mach Number Flutter Trend for the AGRAD 445.6 Wing "Weakened" Configuration, α_0 = 0.0 (deg)

In the final paper, we will also address this issue.

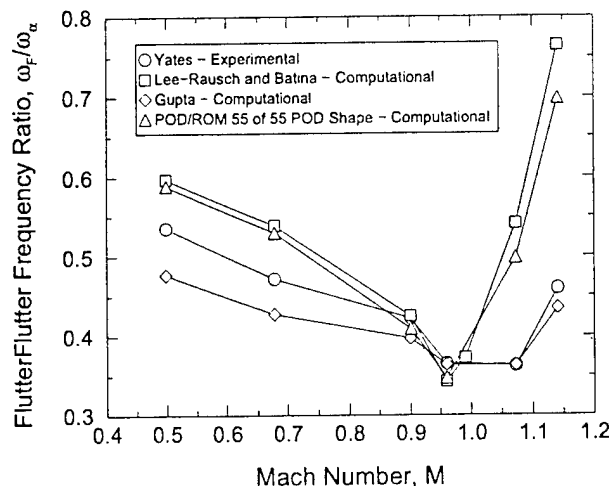Figure (5) again shows the computed POM/ROM flutter speed and flutter frequency ratios as a function of Mach number. In this instance however, the flutter results are shown for various fractions of the total available POD shapes. As can be seen, even with as few as 1/2 of the available shapes, relatively well converged results are obtained. Note however there is somewhat greater sensitivity to the number of POD/ROM modes retained at the supersonic Mach numbers.

THE USE OF ALTERNATE MODAL EXCITATIONS FOR SNAPSHOTS

One of the key concerns towards in the POD/ROM method to three-dimensional flows has been whether or not an entire set of solution snapshots must be computed for each possible structural configuration of interest. That is, say we wish to consider a similarly shaped wing that has a slightly different structural configuration, which in turn means the wing vibratory mode shapes are different. Does this mean that one has to go through and compute a whole new ensemble of solution snapshots based on these new structural motions in order to do a flutter analysis for the new wing configuration. Fortunately, as we will demonstrate in the following, although a few snapshots based on the new modal motion will need to be computed, the larger number of snapshots computed at numerous frequencies will be unnecessary. The snapshots computed from a previous wing structural configuration will still serve the purpose. That is, a couple of solution snapshots will be needed for the new structural motions, however, these will only need to be computed at the end points of the frequency range of interest. Figure (6) demonstrates how this works.

Figure (6a) shows the real and imaginary parts of the coef-

4
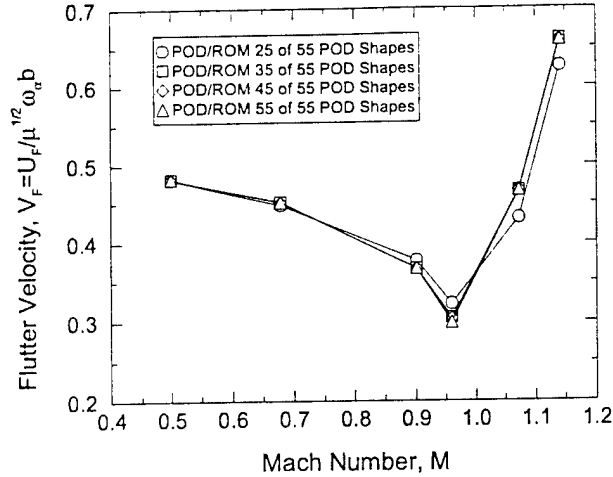
(a) Flutter Speed
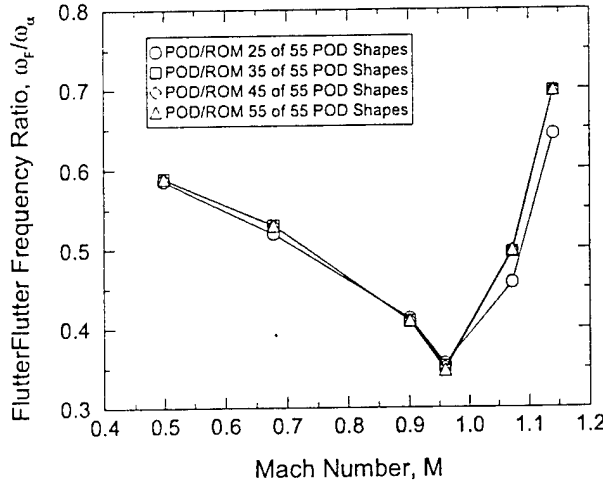
(b) Flutter Frequency Ratio

Figure 5: POD/ROM Shape Vector Refinements Characteristic for Mach Number Flutter Trend for AGRAD 445.6 Wing "Weakened" Configuration, $\alpha_0 = 0.0$ (deg)

ficient of the generalized aerodynamic force corresponding to the first mode pressure acting through the first mode shape as a function of reduced frequency at a Mach number of 0.960. The coefficient of the generalized aerodynamic force is defined as

$$C_{Q_{i,j}}(k) = \frac{1}{q_\infty c_r^2} \int \int \phi_i \, p_j(k) n_z \, dA \qquad (8)$$

where $q_\infty = \rho_\infty U_\infty^2 / 2$ is the freestream dynamic pressure and c_r is the root chord length. The integral is evaluated over the surface of the wing, and n_z is z component of the wing surface normal vector (i.e. $\hat{n} = n_x \hat{i} + n_y \hat{j} + n_z \hat{k}$ and $\hat{n}$ is oriented to point towards the wing surface). In this definition, $p_j(k)$ represents the frequency dependent unsteady pressure

resulting from a wing deformation motion of

$$\frac{z}{c_r} = \phi_j \qquad (9)$$

The curves presented in Figure (6a) are based on the actual solution snapshots and thus are what we desire the POD/ROM to model. In Figure (6b), the POD/ROM of $C_{Q_{1,1}}$ based on snapshots for each of the five structural mode shapes at frequencies of $k = 0.0$ and $k = 1.0$ (for a total of 10 snapshots) is compared against $C_{Q_{1,1}}$ for the actual snapshots for all frequencies between $k = 0.0$ and $k = 1.0$. As can be seen, the POD/ROM matches at the end points of the frequency range as is expected, however this crude POD/ROM performs rather poorly for the intermediate frequencies. Of course, if we use snapshots at all the frequencies between $k = 0.0$ and $k = 1.0$, the POD/ROM would exactly reproduce the data.

Next, in Figure (6c), a new POD/ROM for $C_{Q_{1,1}}$ now based on solution snapshots unrelated to the actual mode shapes is shown. The simple wing motion snapshots are for a full wing plunge motion (up/down), full wing pitch about the quarter chord, a first bending type of motion (wing is fixed at the root, and the z coordinate component of deflection varies linearly with span), and a first twist type of motion (wing is fixed at the root, and the pitch varies linearly with span) for frequencies from $k = 0.0$ to $k = 1.0$ at $\Delta k = 0.1$ increments for a total of 44 solution snapshots. As can be seen, the POD/ROM in this case also perform very poorly. Unbeknownst however, these solutions are in fact helping to reveal the dynamics of the system. In fact, when one uses these snapshots in combination with the actual structural mode snapshots solely at the end points of the frequency range of interest, one gets a POD/ROM which produces very accurate results to $C_{Q_{1,1}}$ as is evident from Figure (6d).

Figure (7) shows a comparison of the POD/ROM Mach number flutter trends in the case where first, the POD/ROM is based on solution snapshots corresponding to the actual modal shapes of the wing to the case where second, the POD/ROM is based on snapshots using the simple wing motion mode shapes as discussed in the previous paragraph. As for the previous Mach number flutter results (Figures (4) and (5)), the snapshot reduced frequencies range from $k = 0.0$ to $k = 0.5$ in $\Delta k = 0.1$ increments. Included in this second ensemble of solution snapshots, are the snapshots corresponding to the particular motions of the actual mode shapes at the end points of the frequency range of interest.

As can be seen in Figure (7), one can obtain accurate POD/ROM flutter results using solution snapshots unrelated to the actual wing motions (except at the end points of the frequency range of interest) that compare very well to the flutter results based on a POD/ROM model using snapshots corresponding to the actual motions. This is especially true at the lower Mach numbers. There is some difference at the highest Mach number, again suggesting supersonic flow is more sensitive for this wing.

To further illustrate the concept of being able to use solely the frequency range of interest end point snapshots, we present a few results for a simple two-dimensional configuration that first led us to the idea of the using the technique in three-dimensions. In an analogous situation of having to consider multiple structural degrees of freedom in three-dimensions, we first considered an unsteady NACA 64A010A airfoil configu-

5

ration that not only under goes typical plunge and pitch motions (see Figures (8a) and (8b), but also has motions where airfoil mean camber line distorts based on simple trigonometric functions. i.e. $z_c(x) = \bar{\delta}_1 \cos(2\pi x/c)$ (Figure 8c), $z_c(x) = \bar{\delta}_2 \sin(2\pi x/c)$ (Figure 8d), $z_c(x) = \bar{\delta}_3 \cos(4\pi x/c)$ (Figure 8e), etc. The initial question was, as one considers each subsequent motion, does one have to include a number of snapshots based on the new motion that is equal to the number of snapshots for each of the previous motions in order to produce an accurate POD/ROM.

Figure (9) illustrates how after a sufficient number of snapshots have been included in the snapshot ensemble, only the end point frequencies are required for each additional motion. In this instance, the NACA 64A010A airfoil is modeled in a M=0.5, $\alpha_0 = 0.0$ (deg) background flow, and shown on the abscissa are increments in the number of overall motions considered. Shown on the ordinate is the order in which the snapshots for each particular motion are added to the overall ensemble. The reduced frequency range of interest is $0.0 \leq k \leq 1.0$ (note, k for this airfoil problem is defined as $k = \omega c/U_\infty$), and thus the first two snapshots considered for each motion correspond the end points of this frequency range. Further snapshots added to the ensemble for a given motion are done so in a divide and conquer strategy to best model the intermediate frequencies.

Considered in Figure (9) is the accuracy of modeling the airfoil unsteady lift and moment along the paths $\bar{s} = re^{j\theta}$ (where $\theta = 90°, 60°, 120°$ and $0 \leq r \leq 1$) in the complex reduced frequency $\bar{s}$ plane. The curves illustrate the number of snapshots necessary to achieve a given level of accuracy for the nth and all previous motions. The accuracy is based on a comparison to a POD/ROM that is derived from a snapshot ensemble comprised of all the possible motions at all the possible frequencies. So for example, to achieve a 10^{-3} L_2 norm accuracy when just considering plunge motion, one needs a total of ten plunge snapshots of the frequency values indicated on the ordinate of the plot. If next considering pitch motion, one would then need to add only three pitch motion snapshots corresponding to the frequencies $k = 0.0$, $k = 1.0$, and $k = 0.5$ to the overall ensemble to get 10^{-3} L_2 norm accuracy for now both the pitch and plunge motions. Considering next the first airfoil bending motion $\bar{\delta}_1$, one would then need to add a total of seven $\bar{\delta}_1$ snapshots to achieve 10^{-3} L_2 norm accuracy for now plunge, pitch, and $\bar{\delta}_1$ motion. Three $\bar{\delta}_2$ snapshots would then be needed when also taking in account $\bar{\delta}_2$ motions, two $\bar{\delta}_3$ snapshots when considering $\bar{\delta}_3$ motions, and so on.

As can be seen, Figure (9) illustrates the interesting result that after a sufficient number of snapshots have been included in the overall ensemble, only the two end point frequency snapshots for each subsequent possible motion need be added to the ensemble to maintain a given level of accuracy. Interestingly enough, this appears to be an asymptotic limit. That is, the two end point frequency range snapshots always appear to be necessary when considering a large number of possible motions.

CONCLUSIONS

The POD/ROM method has been demonstrated for the flutter analysis of a three-dimensional transonic wing configuration. We have shown that the number of ROM DOF's neces-

sary to create accurate models is on the order of a few dozen as is the case in two-dimensions. We have also shown that it is unnecessary to compute a completely new ensemble of solution snapshots based on the vibratory mode shapes for each new structural configuration that might be under consideration. One can simply compute a set of snapshots based on some basic wing motions at a number of frequencies. Then snapshots only at the end points of the frequency range of interest need to be computed for the specific mode shapes of the configuration of interest. These end point snapshots "lock in" the unsteady fluid dynamic characteristics for the particular mode shapes, and the simple motion snapshots then act to resolve the dominant dynamics of the flow throughout the full frequency range of interest.

For the final version of the conference paper, will we include more details of the methodology along with further studies of POD/ROM refinements including mesh convergence issues.

References

[1] Hall, K. C., Thomas, J. T., and Dowell, E. H, "Reduced-Order Modeling of Unsteady Small-Disturbance Flows Using a Frequency-Domain Proper Orthogonal Decomposition Technique," AIAA Paper 99-0655, January 1999. (Recently Accepted for Publication in the *AIAA Journal*).

[2] Thomas, J. T., Hall, K. C. and Dowell, E. H, "Reduced-Order Aeroelastic Modeling Using Proper-Orthogonal Decompositions," CEAS/AIAA/ICASE/NASA Langley International Forum on Aeroelasticity and Structural Dynamics 1999, Williamsburg, Virginia, June 1999.

[3] Kim,T.,"Frequency-Domain Karhunen-Loeve Method and Its Application to Linear Dynamic Systems," *AIAA Journal*, Vol. 36, No. 11, 1998, pp. 2117–2123.

[4] Ni, R. H., "A Multiple-Grid Scheme for Solving the Euler Equations," *AIAA Journal*, Vol. 28, No. 12, 1982, pp. 2050–2058.

[5] Loève, M., *Probability Theory*, D. Van Nostrand Company, Inc., New York, 1955.

[6] Lumley, J. L., "The Structures of Inhomogeneous Turbulent Flow," in *Atmospheric Turbulence and Radio Wave Propagation*, edited by A. M. Yaglom and V. I. Tatarski, Nauka, Moscow, 1967, pp. 166–178.

[7] Holmes, P., Lumley, J. L., and Berkooz, G., *Turbulence, Coherent Structures, Dynamical Systems and Symmetry*. Cambridge University Press, Cambridge, 1996.

[8] Yates, E. C., Jr., "AGARD Standard Aeroelastic Configurations for Dynamic Response I - Wing 445.6," NASA TM 100492, August 1987; also *Proceedings of the 61st Meeting of the Structures and Materials Panel*, Germany, AGARD-R-765, 1985, pp. 1–73.

[9] Yates, E. C., Jr., Land, N. S., and Foughner, J. T. , Jr., "Measured and Calculated Subsonic and Transonic Flutter Characteristics of a 45 Deg Sweptback Wing Planform in Air and in Freon-12 in the Langley Transonic Dynamics Tunnel," NASA TN D-1616, March 1963.

[10] Lee-Rausch, E. M. and Batina, J. T., "Wing Flutter Boundary Prediction Using Unsteady Euler Aerodynamic Method," *Journal of Aircraft*, Vol. 32, No. 2, 1995, pp. 416–422.

[11] Gupta, K. K., "Development of a Finite Element Aeroelastic Analysis Capability," *Journal of Aircraft*, Vol. 33, No. 5, 1996, pp. 995–1002.
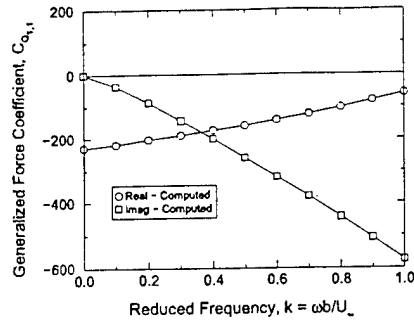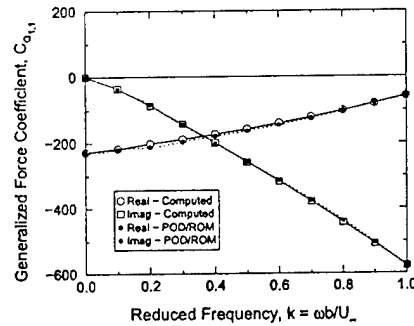
(a) Snapshots
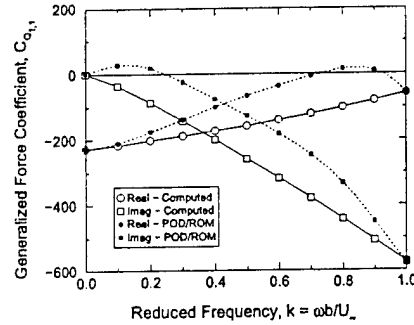
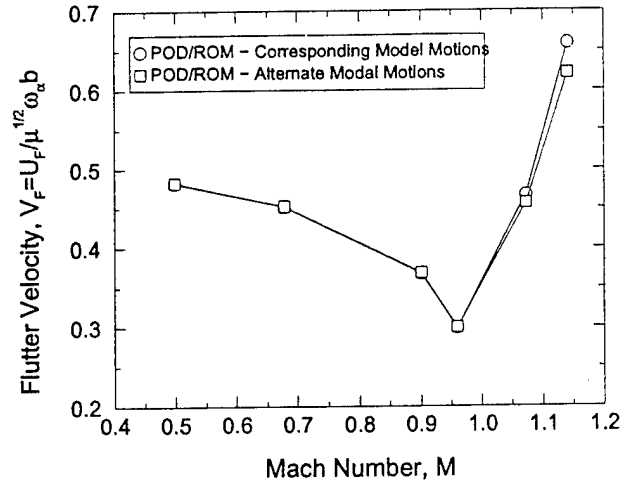(b) POD/ROM Based on $k = 0.0$ and $k = 1.0$ Modal Snapshots
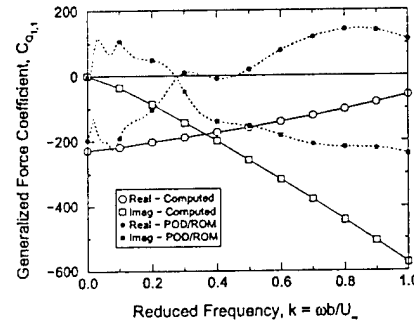
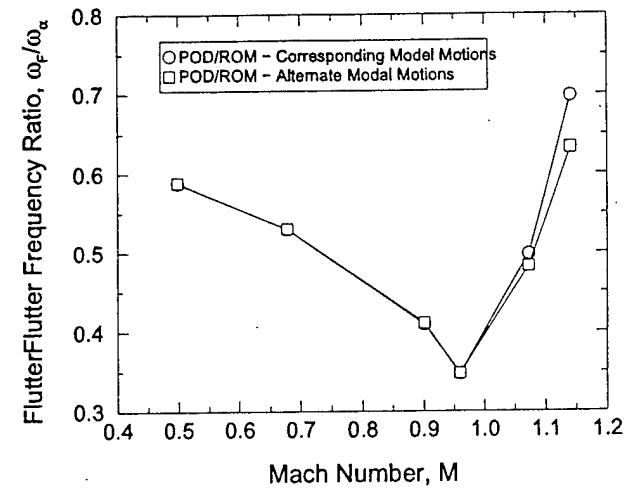(c) POD/ROM Based on "Basic" Motions Snapshots

(d) POD/ROM Based on $k = 0.0$ and $k = 1.0$ Modal Snapshots and "Basic" Motions Snapshots

Figure 6: Generalized Force Modeling with Unrelated Mode Shape Snapshots

(a) Flutter Speed

(b) Flutter Frequency Ratio

Figure 7: Mach Number Flutter Trends Using Alternate Unrelated Snapshots: AGRAD 445.6 Wing "Weakened" Configuration, $\alpha_0 = 0.0$ (deg)

(a) Plunge $\bar{h}$ (b) Pitch $\bar{h}$ (c) $\bar{\delta}_1$ (d) $\bar{\delta}_2$

(e) $\bar{\delta}_3$ (f) $\bar{\delta}_4$ (g) $\bar{\delta}_5$ (h) $\bar{\delta}_6$

(i) $\bar{\delta}_7$ (j) $\bar{\delta}_8$ (k) $\bar{\delta}_9$ (l) $\bar{\delta}_{10}$

(m) $\bar{\delta}_{11}$ (n) $\bar{\delta}_{12}$ (o) $\bar{\delta}_{13}$ (p) $\bar{\delta}_{14}$
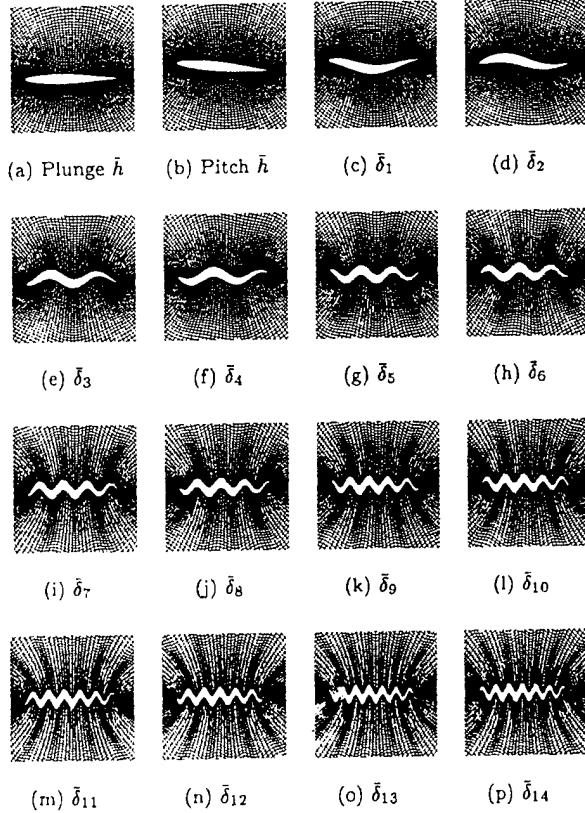
Figure 8: Airfoil Sample Motions: NACA 64A010A Airfoil Section - 129 x 65 Mesh
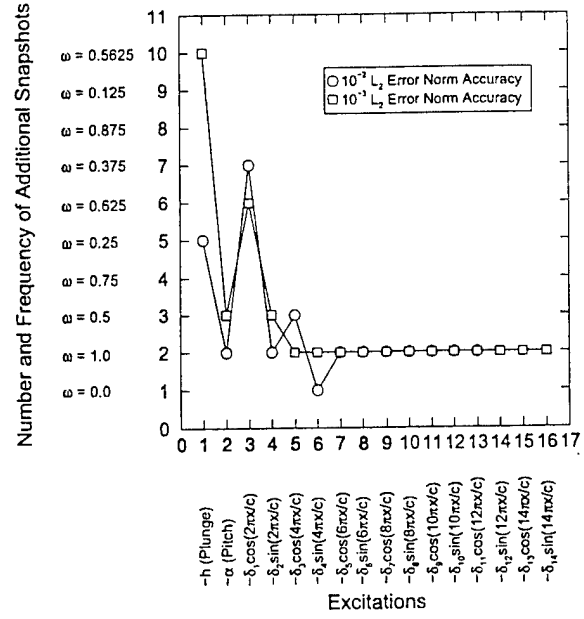

Figure 9: Additional Snapshot Requirements to Achieve Two Different Levels of Accuracy for Lift and Moment Transfer Functions Along the Paths $\bar{s} = re^{j\theta}$, where $\theta = 90°, 60°, 120°$ and $0 \leq r \leq 1$, in the Complex Reduced Frequency $\bar{s}$ Plane for n^{th} and All Previous Motions: M=0.5 α_0 = 0.0 (deg)